DOCTORAL DISSERTATION

INVESTIGATION OF ADSORPTION, UNDERPOTENTIAL DEPOSITION AND FILM FORMATION PROCESSES WITH THE ELECTROCHEMICAL QUARTZ CRYSTAL NANOBALANCE TECHNIQUE

BALÁZS B. BERKES
Master of Science

Submitted in Partial Fulfillment of the Requirements for the Degree

Doctor of Philosophy

Supervisor

Professor György Inzelt

Chemistry Doctoral School
Head of Doctoral School: Prof. Dr. György Inzelt
Analytical Chemistry, Colloid- and Environmental Chemistry, Electrochemistry Program
Head of Doctoral Program: Prof. Dr. Gyula Záray

Department of Physical Chemistry
Institute of Chemistry
Eötvös Loránd University

Budapest, May 2013

Balázs B. Berkes: *Investigation of Adsorption, Underpotential Deposition and Film Formation Processes with the Electrochemical Quartz Crystal Nanobalance Technique,*
Doctoral Dissertation, © May 2013
SUPERVISOR:
Professor György Inzelt

LOCATION:
Budapest
TIME FRAME:
2010 - 2013

PREFACE

This Thesis is a result of work carried out in the period of 2010–2013. However, as part of the final closing examinations of my education, I need to add that it is the result of learning and studying of the last 20 years. My education path was quite straightforward: starting with the elementary school via the secondary grammar school and the university, arriving to the last station (most probably for a while), to the doctoral school. The direct results summarized in this work are of course first of all to be connected to the last two stations, to the studies for a diploma and for a doctoral degree.

In 2008 I decided to graduate in electrochemistry, and joined the laboratory of Professor G y ö r g y I n z e l t. He introduced me into this discipline probably through one of the best ways: my task became the electrochemical examination of a simple but very important system, which only contained platinum, an acidic electrolyte and a reference electrode. Platinum electrode in acid media was thought to be a well-known system; however as a result of further investigations it was still possible to reveal some novel features. I got acquainted with the basic electrochemical concepts and knowledge through this system. Beyond the electrochemical methods, as their complementary technique we used the quartz crystal nanobalance to gain a deeper insight into the electrode processes. My master thesis evolved from those studies, and some part of these early experiments, the investigation of cationic adsorption on platinum, became later the topic of the doctoral research activities.

Right at the beginning of my doctoral studies I visited the reputed electrochemical research group of Professor W o l f g a n g Sch u h m a n n at the German Ruhr-Universität Bochum, for the first semester. My direct contact person and supervisor was Dr. A l i a k s a n d r B a n d a r e n k a, a junior group leader at Professor Sch u h m a n n. He introduced me a completely new field of electrochemistry, the potentiodynamic electrochemical impedance spectroscopy. I was involved in the development of a combined impedance and gravimetric measurement system, something from which I could gather a lot of knowledge again. My DAAD Fellowship came in January 2011 to an end, right at time when we could demonstrate the properties and strengths of the new technique. To the invitation of Professor Sch u h m a n n I returned in the summer of 2011 to Bochum. As a result we investigated three more system, one of which, the continuation of a former work, the influence of cationic adsorption on platinum turned to be a part of the current thesis.

After returning home, inspired by the former works of Professor I n z e l t, I began a research in organic electrochemistry. He was working on the second edition of his book about conducting polymers, as he realised that the field of electrochemistry of indoles can still offer a lot to be discovered. The main activity started with the experiments with 4-aminoindole and went on with indole. The phenomena strongly related to other fields of adsorption studies from my

past and the investigation of the initial stages of polymer layer formation are the other parts of this thesis.

I was in a lucky situation, since almost all of the results introduced here are published. Therefore their interpretation was well established earlier. The work with indole is still in progress. The present work is the compilation of these research fields.

The first chapter contains a brief description about the fundamentals of the methods and techniques. There we did not aim to give a detailed, textbook-like introduction, only those points are mentioned that were of interest to the further chapters. The thesis is composed of three individual topics that are connected through the nature of investigated phenomena. Although all of these chapters contain some experimental description, relevant for better understanding, a collective experimental part is written, and can be found in the second chapter. The following three parts discuss respectively the development of the combined potentiodynamic electrochemical impedance spectroscopy and quartz crystal nanobalance method, the investigation of the influence of cations on platinum and the adsorption and electropolymerization studies of indole and 4-aminoindole. Each of these chapters contains an introduction comprising the motivation and the survey of the relevant literature. Furthermore the results are demonstrated, discussed and concluded in the individual chapters, too.

Balázs B. Berkes
May 2013
Budapest

"I will praise thee, O Lord my God,
with all my heart:
and I will glorify thy name for evermore."

— Psalm 86:12

ACKNOWLEDGEMENTS

I would like to express my appreciation to all those who brought me closer to the completion of this dissertation. Since it happened by so many people in so many ways, it is impossible to mention here them all.

First off all I would like to acknowledge with much appreciation the crucial role of my supervisor Professor György Inzelt. The continuous discussions, his conscientious guidance, his endless patience, the pleasant conferences and the lot of personal conversations.

Special thanks go to my supervisors in Germany, to Professor Wolfgang Schuhmann and to Dr. Aliaksandr Bandarenka. They provided me a stimulating, friendly atmosphere. Many thanks for their help and support. Here I would like to thank every help to all my colleagues at the Ruhr-Universität Bochum, to everyone who made my stay to an unforgettable, nice memory. Thanks to the Plassmann family for the housing and their support during my 2nd stay. Vielen Dank dafür!

I wish to thank to Professor Juan M. Feliu, inviting me to Alicante and making possible to spend a month in his group. I was happy to meet his nice colleagues. Furthermore I am grateful to Professor Robert F. Savinell, who allowed me to work in his group, at the Case Western Reserve University during the summer of 2012, and to the group members for their support. I would emphasise my great 'land-lady' Carol, who did not allow me to 'get lost' in the U.S.

Of course my deep gratitude is to my colleagues, here at home with whom I worked and/or learned together, who served for the good atmosphere: to former PhD student Ákos Kriston, to Ákos Nemes, to Szilvia Kasek ...

Special thanks to my best friend Soma Veßtergom, whose name I can only write with a worthy font type. I really consider it an honour that I could work with him, that we could (and can) have our every day lunch together accompanied with never ending conversations. I appreciate him for his lot of help and suggestions, plentiful advice ...

I am thankful to my chemistry teachers (to Mrs. Katalin Reinhardt Kazsoki and to Mrs. Julianna Miklós *née* Vig) by whom the love of chemistry was given to me.

This thesis would not have been possible without having my lovely family. They support was the most necessary condition to be able to study and even to complete a PhD programme! And when I mention family, I obviously think also on my loving wife, Adél, whit whom every day is a present, and who was

plentiful of patience and created always the calm conditions when I worked on this thesis!

I am thanful to the German Academic Exchange Service (Deutscher Akademischer Austauschdienst, DAAD) for their Scholarship, enabling me to spend a semester in Germany, and to The Electrochemical Society (ECS) awarding me to the Joseph W. Right Summer Fellowship in 2012, allowing me the visit to the USA.

Mindenki segítségét nagyon köszönöm!

CONTENTS

ACRONYMS

AC	Alternating Current
AFM	Atomic Force Microscopy
APM	Acoustic Plate Mode
BNC	Bayonet Neill–Concelman
CE	Counter Electrode
CNLS	Complex Non-linear Least Squares
CPE	Constant Phase Element
CV	Cyclic Voltammogram
DC	Direct Current
DFT	Density Functional Theory
EEC	Equivalent Electrical Circuit
EIS	Electrochemical Impedance Spectroscopy
EQCM	Electrochemical Quartz Crystal Microbalance
EQCN	Electrochemical Quartz Crystal Nanobalance
FPW	Flexural Plate Wave
HER	Hydrogen Evolution Reaction
HOR	Hydrogen Oxidation Reaction
IS	Impedance Spectroscopy
ML	Monolayer
MMS	Mercury - Mercury Sulfate Electrode
OCP	Open Circuit Potential
ORR	Oxygen Reduction Reaction
QCM	Quartz Crystal Microbalance
RE	Reference Electrode
SAW	Surface Acoustic Wave
SCE	Saturated Calomel Electrode

SHE Standard Hydrogen Electrode

SRS Stanford Research Systems

TSM Thickness-Shear Mode

UPD Underpotential Deposition

WE Working Electrode

Part I

FUNDAMENTALS

This chapter provides a short survey to the fundamentals of applied methods, based on the state-of-the-art of the electrochemical textbooks and review papers. The theory and application of cyclic voltammetry, electrochemical impedance spectroscopy and electrochemical quartz crystal nanobalance techniques are briefly outlined. The most important relationships to serve for the further chapters are summarized.

1

FUNDAMENTALS OF THE APPLIED METHODS

1.1 INTRODUCTION

In this chapter the main techniques employed in the experiments are described in a nutshell. They are not reviewed, only the most important relationships are given to serve the understanding of the further calculations or the measurements. The theories and the derivations of the mathematical expressions from basic assumptions are also absent, since they can found in the cited articles or textbooks. We do not intend to elaborate long on none of the methods; their relevant elements are included at the discussion of the results at the appropriate sections.

The analysis of the theory of cyclic voltammetry together with the discussion of the countless reaction types because of their complexity is far beyond the scope of this chapter. Furthermore the qualitative understanding of our relatively simple systems do not require them. The case with electrochemical impedance spectroscopy is similar: only the essentials are written here. The special, system dependent theories are detailed at the results and discussion section of the measurements. The quartz crystal nanobalance occurs everywhere, being the complementary part of electrochemical methods, therefore the most comprehensive description is given about it.

1.2 DIRECT CURRENT TECHNIQUES

Under the name direct current techniques we understand the basic potential step and sweep methods, pulsed voltammetry and controlled current techniques. In the experiments serving as basis for the present dissertation the mainly applied method was the cyclic voltammetry and its advanced versions (that allow the scan rate, $\mathrm{d}E/\mathrm{d}t$ (where E is the applied potential and t is time), to be zero for certain periods during cycling). Here we give a brief summary about the technique and do not want to surmount very well written electrochemical textbooks [1–8] or simply repeat them too much.

When the main properties of an unknown electrochemical system need to be surveyed the most often applied technique is cyclic voltammetry. It serves with a wealth of information about the kinetic and thermodynamic details of a system. It rapidly provides the first understanding of the processes, like electron-transfer and chemical reactions or adsorption processes. It offers the ability to locate redox potentials of electrochemical reactions and to evaluate the effect of media.

During cyclic voltammetry the potential of the working electrode is swept linearly according to a triangular waveform and the potentiostat measures the resulting current. The obtained current vs. potential curve is termed as the Cyclic

Voltammogram (CV). It is a complicated, time dependent function of many physical and chemical parameters.

For the sake of brevity we just mention some ground-breaking articles from the history of the technique which made possible a deeper understanding or simpler interpretation of measured data or the ability to measure data at all. These are the work of Randles [9], Ševčik [10], Nicholson [11], Reinmuth [12], Hickling [13]. Without citing his works, there is no doubt that linear sweep voltammetry – the closest relative of cyclic voltammetry – originated in a technique invented by Jaroslav Heyrovský in 1922.

1.2.1 *The shape of cyclic voltammograms*

In the following we introduce the interpretation of the shape of a typical CV through a simulation for the reaction

$$\mathrm{O} + \mathrm{e}^- \rightleftharpoons \mathrm{R} \tag{1.1}$$

where O and R represent the chemical formula of an oxidized and reduced species respectively.

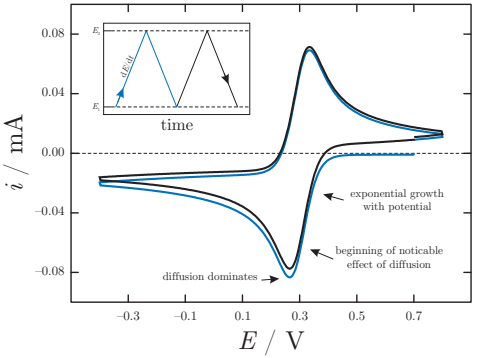

Figure 1.1: First 2 cycles of a simulated CV. The first cycle is marked with the blue line. Concentration of O and R was initially $0.01\,\mathrm{mol\,dm^{-3}}$ and 0, respectively. $\mathrm{d}E/\mathrm{d}t = 100\,\mathrm{mV\,s^{-1}}$, $R_\Omega = 15\,\Omega$, $D_\mathrm{O} = D_\mathrm{R} = 1 \times 10^{-5}\,\mathrm{cm^2\,s^{-1}}$, $k_0 = 0.033\,\mathrm{cm\,s^{-1}}$, $E^0 = 0.3\,\mathrm{V}$, $\alpha = 0.5$, $A = 0.0314\,\mathrm{cm^2}$, $C_\mathrm{DL} = 10\,\mu\mathrm{F}$, $T = 298.15\,\mathrm{K}$. The names of the symbols are listed in the text.

Figure 1.1 shows the simulated cyclic voltammogram. In the figure caption R_Ω denotes the resistance in the system (mainly solution resistance); D_O and D_R are the diffusion coefficient of the species O and R, respectively; k_0 is the rate constant of the reaction in Equation 1.1; E^0 is the equilibrium potential of the same reaction; α is the charge transfer coefficient; A is the electrode surface area; C_DL is the double layer capacitance and T stands for temperature. The three main parameters of the applied triangular shaped potential-time function

are the sweep rate (i.e. the slope of the $E(t)$ curve, $\mathrm{d}E/\mathrm{d}t$) and the two switching potentials. In our case these parameters had the values of $\mathrm{d}E/\mathrm{d}t = 100\,\mathrm{mV\,s^{-1}}$, $E_1 = -0.4\,\mathrm{V}$ and $E_2 = 0.6\,\mathrm{V}$ where E_1 and E_2 are the lower and upper switching potentials respectively (see the inset of Figure 1.1). Advanced methods allow to keep the potential at certain values during cycling. The characteristic parameters of the voltammogram are the peak currents of oxidation or reduction, the corresponding peak potentials, the midpoint potential which is the average of the two peak potentials and from which the thermodynamically defined formal potential can be calculated. For a fully reversible reaction the values of these last two parameters are approximately the same. The separation between the anodic and cathodic peaks expressed in mV is another important parameter for kinetic informations. It refers to the reversibility of the process at low scan rates (where the ohmic resistance is negligible).

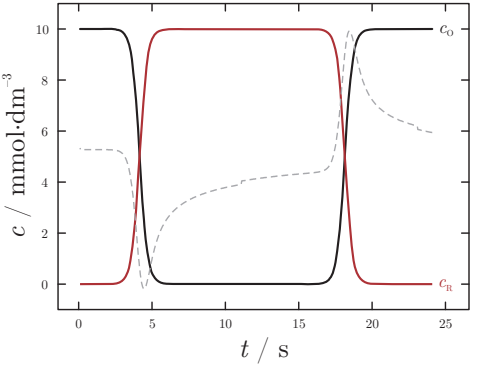

Figure 1.2: Variation of concentration of O (c_O) and R (c_R) with time at the electrode surface during the cyclic voltammetric measurement. For the sake of clarity the first cyclic voltammogram is also shown with the dashed line. Concentration of O and R was initially 0.01 mol dm^{-3} and 0, respectively. The other simulation parameters are listed in the caption of Figure 1.1.

The variation of the concentrations at the electrode surface of the constituents of Equation 1.1 are seen in Figure 1.2. Initially there was no reduced species present in the solution, its concentration started to increase along with the beginning of the reduction of O. When O was being reduced, at potentials more negative than the equilibrium potential of the process, its concentration at the surface was zero (diffusion limited reaction), and its concentration remained zero until the oxidation of R started. The shape of the shown, simple, reversible voltammograms and that of the concentration profiles are determined by only two laws: *i*) Fick's law of diffusion for the case of a planar electrode, and *ii*) Erdey-Grúz–Volmer's law on electrode kinetics (which can be simplified to Nernst's law at big values of k_0).

At the end of the 1940's a theoretical expression for the peak current for a reversible cyclic voltammogram was derived as a function of the scan rate to

give the Randles–Ševčik expression. According to this relationship, the dependence of the peak currents on scan rate follows a characteristic square-root law.

Cyclic voltammograms are not always governed by diffusion controlled processes. For example, the cases of a redox reagent adsorbed onto an electrode surface or confined to a thin layer of solution adjacent to the electrode surface are also of considerable importance. In contrast to cyclic voltammetric responses for solution systems with semi-infinite planar diffusion, for redox processes for confined or thin layer systems close to the electrode or adsorbed molecules at the electrode surface, the peak current expression becomes linear with respect to the scan rate [8].

In this work both type of voltammograms will be presented, and even if they are not so ideal, there can be unambiguously categorized into these two types.

1.3 ELECTROCHEMICAL IMPEDANCE SPECTROSCOPY

The method of impedance measurements is widely used in many fields of electrochemistry, e.g. electrode kinetics, double-layer studies, batteries, corrosion, solid-state electrochemistry, bioelectrochemistry (especially membranes). It is one of the linear response methods, which means that the system is perturbed by a sine wave current or potential of such a small amplitude that the response contains only the first-order terms of the Taylor-expanded non-linear current-voltage(-concentration) relationship [14].

Impedance spectroscopy is a powerful method of characterizing electrochemical systems, electrode | electrolyte interfaces, investigating the dynamics of electrode reactions, adsorption-desorption processes, underpotential and bulk phase depositions, conducting polymers just to mention a few phenomena of our interest. Impedance measurements are, however, not sufficient alone: additional observations are required to gain confidence in the model of a certain system.

The technique with its theoretical background and with a multitude of applications is very well summarized in the work of Barsoukov and Macdonald [15], Orazem and Tribollet [16], Lasia [17], Sluyters-Rehbach and Sluyters [18] and Inzelt and Láng [19]. The fact that the Commission on Electrochemistry of the Physical Chemistry Division of The International Union of Pure and Applied Chemistry reported its recommendations about the terminology, nomenclature and representation of the field [14] also emphasizes the relevance and importance of impedance measurements in electrochemical experiments.

A flow diagram of a general characterization procedure using impedance spectroscopy is presented in Figure 1.3. Here CNLS stands for complex nonlinear least squares fitting. Experimentally obtained impedance data for a given electrode-materials system may be analysed by using an exact mathematical model based on a plausible physical theory that predicts theoretical impedance $Z_t(\omega)$ or by a relatively empirical equivalent circuit whose impedance predictions may be denoted by $Z_{es}(\omega)$. In either the case of the relatively empirical equivalent circuit or of the exact mathematical model, the parameters can be

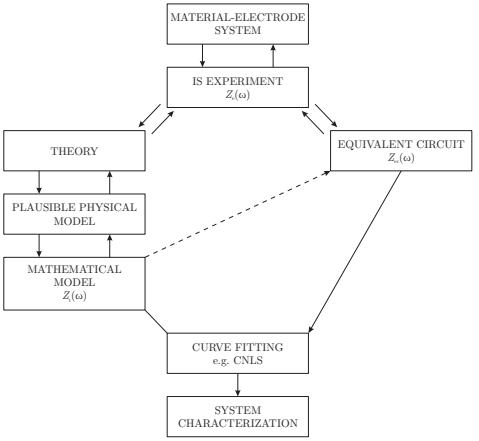

Figure 1.3: Flow diagram for the measurement and characterization of a material-electrode system. Figure is reprinted from [15].

estimated and the experimental $Z_e(\omega)$ data compared to either the predicted equivalent circuit impedance $Z_{ec}(\omega)$ or to the theoretical impedance $Z_t(\omega)$ [15].

A usual way to interpret impedance data is in the form of Equivalent Electrical Circuits (EECs). The experimental impedance data is approximated by the impedance of and electrical circuit made up of ideal circuit elements (resistors, capacitors, inductances, various distributed elements etc.). These correspond in the real system to real conductive paths, like charge transfer of conductivity of a bulk phase, to double layer or adsorption capacitances, to space charge polarization regions. The distributed elements are of two type: either associated with non local processes, like diffusion, or are originated from local distributions of microscopic properties, like the Constant Phase Element (CPE).

In our data elucidation we use equivalent electrical circuits. The choice of the particular physical model is based on an *a priori* knowledge about the system and on the measurement results. Additional independent information from the EQCN measurements is assumed to be helpful in acquiring relevant preknowledge and hence support the modelling process.

The detailed description of impedance models used by us, together with their interpretation are introduced at the chapters where the physical problems, the system to be described appear.

1.4 THE ELECTROCHEMICAL QUARTZ CRYSTAL NANOBALANCE

The Quartz Crystal Microbalance (QCM) is a piezoelectric device capable of extremely sensitive mass measurements. It oscillates in a mechanically resonant shear mode by application of an alternating, high frequency electric field us-

ing electrodes which are usually deposited on both sides of the disk [20]. This is how Daniel A. Buttry gave a concise description on the technique. To distinguish between electrochemical uses of QCM we use the term Electrochemical Quartz Crystal Microbalance (EQCM) which is often referred to as a nanobalance (EQCN) since it is capable to detect mass changes in the nanogram range. Both names are used and accepted by chemists. However, there are views not agreeing with the nomenclature:

"The term "quartz crystal microbalance" is an unfortunate name for this device for several reasons: (1) The word "crystal" is redundant when it follows "quartz", a crystalline material; (2) the devices do not invariably act exclusively as microbalances, being subject to a number of other physical perturbations as well; (3) the name could also correspond to a SAW, APM, or FPW device fabricated from quartz. The term thickness-shear mode (TSM) resonator follows the convention used for the SAW, SH-APM, and FPW notations in that it describes the nature of the acoustic mode upon which the device is based." [21]

A general categorization of devices based on the use of piezoelectric crystals for sensor applications and material characterization can be given as follows:

— Thickness-Shear Mode (TSM) resonators

— Surface Acoustic Wave (SAW) devices

— Acoustic Plate Mode (APM) devices, and

— Flexural Plate Wave (FPW) devices.

QCM and EQCN belong to the TSM resonators, typically incorporated in an oscillator circuit, where the oscillation frequency tracks the crystal resonance and indicates mass changes on the crystal surface.

1.4.1 *Background of operation*

The thorough understanding of the operation requires an in-depth knowledge of the theory of elasticity, piezoelectricity and electricity. There are numerous excellent text books on these disciplines [21–26]. Here we merely mention some milestones from the development of the device.

The discovery of the piezoelectric effect is ascribed to the brothers Pierre Curie and Jacques Curie [27]. Cady [24] defined piezoelectricity as "...electric polarization produced by mechanical strain in crystals belonging to certain classes, the polarization being proportional to the strain and changing sign with it." This is the so called *direct piezoelectric effect*. To the operation of the QCM, however, the existence of the reverse process is the necessary condition. That is called the *reverse piezoelectric effect* by which the application of an electric field causes deformation in certain materials. The reverse effect was predicted by Lippmann [28] and experimentally verified by the Curie brothers. That is, if two facets of a piezoelectric material (e.g. quartz) are covered with a conducting material (electrodes in a non-electrochemical sense) and a potential difference is applied between the facets the crystal becomes deformed. This

way electrical energy can be transformed to mechanical one. Applying an appropriate, periodically varying potential difference to the crystal will cause it to resonate with a given frequency value.

For thickness-shear mode resonators quartz is used as the piezoelectric material, because of its advantageous mechanical properties. The first quartz crystal oscillator was developed by Walter Gouyton Cady in 1918 to control the frequency of radio broadcasting stations.

Since that time piezoelectic quartz crystals are used in great numbers for controlling frequency in communication equipment, and are widely used as selective filters in electrical networks. Special quartz crystals, are available which can control frequencies to 1 part in 10^9 (or even better) and very accurate clocks can be run from this signal [29].

The resonant frequency of the crystal is extremely sensitive to the mass on its surface. Günter Sauerbrey was credited to be the first who established a quantitative connection between the deposited mass and the resonant frequency change [30]. The relation was a simple proportionality between the change in resonant frequency (Δf) and deposited mass (Δm) on the surface with area A:

$$\Delta f = -C_f \Delta m \tag{1.2}$$

where C_f is the integral sensitivity of the crystal ("integrale Schichtwägeempfindlichkeit"). In his derivation Sauerbrey used the crystal properties (thickness (d), fundamental frequency (f_0) and density of the quartz (ρ_Q)) to obtain a value for the integral sensitivity. It can be further transformed introducing the shear modulus (μ_Q) into the expression:

$$C_f = \frac{f_0}{d\rho_Q} = \frac{2f_0^2}{(\mu_Q \rho_Q)^{1/2}} \tag{1.3}$$

Without going into details the most appropriate type of quartz is the so called AT-cut quartz resonating in thickness shear mode. An alternating potential across the crystal causes a vibrational motion with amplitude parallel to the surface of the crystal. QCM was originally used in vacuo to measure metal deposition rates, thickness of evaporated metal films, dew point and adsorption of gases. It was thought for long that presence of a contacting liquid would prevent the oscillation. Later it has been shown to operate in contact with liquids [31], enabling its use as a solution-phase microbalance.

The first electrochemical use was reported by Bruckenstein and Swathirajan [32] who examined the surface coverages of underpotentially deposited species at immersed electrodes. The same year results on the mechanism of oxide layer formation were published from the same laboratory. The Electrochemical Quartz Crystal Nanobalance (EQCN) technique is well suited to the study of the mechanism of the formation and dissolution of monolayer and thicker films at solid electrodes [33].

The applicability of the simple Sauerbrey equation (Equation 1.3), and the inexpensiveness of the measuring system made the technique increasingly popular and numerous studies appear every year using EQCN as a complement to other electrochemical techniques. The main fields are the study of mono-and

multilayer deposition processes, dissolution of metals, mass transport in conducting polymer layers, corrosion studies, underpotential deposition of metals, adsorption-desorption studies, electrovalency measurements of anion adsorption, bubble formation, self assembled monolayers etc. [34]. The already large and steadily increasing number of papers dedicated to the application of QCM methods reveals their power for characterizing interfacial processes.

1.4.2 *The use of some relations for measurement interpretations*

There were several attempts to receive more general mass-frequency relationships then the Sauerbrey equation. These are usually derived from fundamental considerations about acoustic wave propagation in the crystal and deposited material and about crystal properties [35–38]. Since we did not take advantage of these expressions during the discussions of problems in the present dissertation we skip their detailed description.

In many cases Equation 1.3 is valid; however mass change is not the only process influencing the frequency response of the EQCN. It is also sensitive, inter alia, to the changes of the density and viscosity of the contacting liquid, pressure and temperature variation, electrode roughness, surface stress changes. Therefore interpretation of EQCN data requires careful account for these possible changes to be able to obtain correct results.

Some further limits of Equation 1.3 need to be taken into account, which are as follows:

1. When deriving the mass-frequency relationship the film deposited on the surface is handled as an extension of the quartz crystal. This is a good approximation only if the layer is rigidly attached to the crystal and simultaneously moves with it. This condition is fulfilled in case of adsorption of small molecules or thin deposited metal layers.

2. The added mass should be much less then the mass of the crystal itself. Usually the condition is that the mass of the film should not exceed 2% of the mass of the crystal.

3. The integral sensitivity (C_f) of the crystal is obtained within the frame of the assumption that the deposited mass is uniformly distributed over the active area. However, the sensitivity of the crystal depends on the position. A local sensitivity so called differential sensitivity can be defined which varies from point to point. Its radial dependence (the used crystals are always disc shaped with well defined thickness and radius) was determined with a sophisticated method by the application of scanning electrochemical microscopy to deposit tiny but known amount of copper to the different surface positions [39]. The sensitivity vs. position function could be fitted with a Gaussian curve, resulting in a maximum sensitivity at the center of the crystal. Therefore only in the case of evenly distributed films is the condition for the use of Equation 1.3 is met.

4. The active area must be completely covered. This condition is a consequence of the former one.

5. The covered are must be known precisely. The QCM does not actually measures the mass; it measures the areal density of the deposited material only.

Knowledge on the influence of liquid properties on the frequency response is the most relevant for electrochemical uses. The QCM is immersed into the electrolyte that causes a frequency decrease compared to the frequency measured in air. The effect was first quantitatively described by K a n a z a w a and G o r d o n [40] who proposed the following equation to calculate the frequency change (Δf) when immersing an electrode into a liquid with a viscosity of η and density of ρ:

$$\Delta f = f_0^{3/2} \left(\frac{\eta \rho}{\pi \mu_Q \rho_Q} \right)^{1/2} \tag{1.4}$$

where f_0 is the the resonant frequency of the unloaded resonator, ρ_Q and μ_Q are the density and shear modulus of quartz, respectively.

1.4.3 *Deviations from ideal behaviour*

Ideal behaviour means in our context the applicability of Equation 1.3 for the correct obtaining of the electrode mass change. Several further effect interfere with each other causing deviations from the ideal cases. Below a list of such factors is given.

1.4.3.1 *Surface roughness*

Trapping of liquid in surface cavities will result in an additional mass component whose magnitude will depend upon the amount of trapped liquid and the size of the cavities [34]. Since we used platinized platinum electrodes to our investigations as well, it was of utmost importance to study of the effect of platinization on the EQCN response.

We have carried out systematic studies by electrodes starting with a smooth one (vacuum-deposited and polished platinum) which has been gradually platinized, and the electrode with different amounts of Pt deposited and surface roughness have been tested after each deposition. It has been found that the frequency change (measured in dry state) was proportional with the amount of the deposited platinum calculated by the charge used for the deposition. The immersion in water or different acids practically gave the theoretical response calculated from the density and viscosity data. The only exception found was observed in Cs^+ containing solutions when the frequency decrease was somewhat higher than that expected from the viscosity and density variation. The frequency change has been measured in the different potential regions in order to control the state of the surface. The cyclic EQCN responses showed the same characteristics up to a roughness factor, $f_r \approx 70$, and the frequency responses were proportional to the roughness factor. The only effect observed was that for electrodes of high roughness factor, $f_r \gtrapprox 25$ the immersion into a solution caused a higher than theoretical frequency response by 30 Hz to 250 Hz;

however, the frequency response during a cyclic voltammetric or chronoamperometric perturbation remained proportional to the surface roughness calculated from the hydrogen UPD charge, therefore the liquid occluded in the pores did not influence the frequency responses [41].

Others carried out experiments with polycrystalline gold electrode to demonstrate the effect of liquid confined in surface cavities [42]. They determined the amount of liquid from the frequency change and related it to the mean cavity size which makes up the roughness pattern.

1.4.3.2 *Viscoelastic effects*

One of the uses of EQCN is the determination of the apparent molar masses. An example is the determination of molar masses of exchanged species when conducting polymers undergo redox transformations. Conducting polymer films may change their viscoelasticity as a result of swelling or changing morphology with potential. It is therefore important to check the linearity between the deposited amount of polymer obtained from the frequency measurements and the related charge calculated from current measurements. The linearity is a necessary condition for the use of the Sauerbrey equation.

Sophisticated methods to explore the phenomena involve the impedance analysis of the quartz [43] or ac-electrogravimetry [44].

1.4.3.3 *Effect of pressure*

The resonant frequency depends on the depth of immersion of the crystal into the liquid. This change with hydrostatic pressure is parabolic [45]; however, the magnitude of the change is very small at depths applied in electrochemical cells. On the other hand this is not very important since the pressure generally will be constant throughout a typical experiment.

1.4.4 *Calculating apparent molar masses*

Application of EQCN with electrochemical techniques in which the current is detected enables the calculation of molar masses of species connected to the cause of the frequency change. From Equation 1.3 the mass change can be calculated. On the other hand the measured current values are useful to calculate the charges passed to a system from Faraday's law. The apparent molar masses can be calculted from the independently obtained informations according to the following equation:

$$M = -\frac{zF}{C_f} \times \frac{\Delta f}{Q} \tag{1.5}$$

where z is the number of electrons involved in the reaction, F is the Faraday constant, Δf is the frequency change, Q is the charge passes to the system.

The use of Equation 1.5 assumes that the charge, calculated from the measured currents serves in 100% for the mass change, i.e. if the currents are not related directly to processes causing mass change the apparent molar masses cannot be connected to any species. An example is double layer charging where

even though the change in population of ions causes considerable mass change, usually it cannot be directly related to one type of ion. Another assumption is that the charging efficiency is 100% which is usually not the case in many systems, like in those, that will be shown in Chapter 5.

Apparent molar masses during a whole process can be estimated from the slope of the $\Delta f(Q)$ function, i.e. the derivative of the curve is proportional to the molar mass (see Equation 1.5).

We will demonstrate the usefulness of the technique in the examination of adsorption processes, characterisation of electrode | electrolyte interfaces, underpotential deposition of metals and finally on the adsorption of organic molecules and electropolymerization.

REFERENCES

[1] A. J. Bard, L. R. Faulkner, Electrochemical Methods: Fundamentals and Applications, Wiley, 2001.

[2] C. G. Zoski (Ed.), Handbook of Electrochemistry, Elsevier, 2007.

[3] C. M. A. Brett, A. M. O. Brett, Electrochemistry: Principles, Methods and Applications, Oxford University Press, Inc., 1993.

[4] J. O'M. Bockris, A. K. N. Reddy, M. Gamboa-Aldeco, Modern Electrochemistry 2A: Fundamentals of Electrodics, volume 2A of *Modern electrochemistry*, Kluwer Academic Publishers, 2000.

[5] V. S. Bagotsky, Fundamentals of Electrochemistry, John Wiley & Sons, Inc., 2nd edition, 2005.

[6] E. Gileadi, Electrode Kinetics for Chemists, Chemical Engineers and Materials Scientists, Wiley, 1993.

[7] J. Wang, Analytical Electrochemistry, Wiley, 2nd edition, 2001.

[8] F. Scholz (Ed.), Electroanalytical Methods: Guide to Experiments and Applications, Springer, 2nd edition, 2010.

[9] J. E. B. Randles, A cathode ray polarograph. Part II. – The current-voltage curves, Transactions of the Faraday Society 44 (1948) 327–338.

[10] A. Ševčik, Oscillographic polarography with periodic triangular voltage, Collection of Czechoslovak Chemical Communications 13 (1948) 349–377.

[11] R. S. Nicholson, I. Shain, Theory of stationary electrode polarography. Single scan and cyclic methods applied to reversible, irreversible, and kinetic systems., Analytical Chemistry 36 (1964) 706–723.

[12] W. H. Reinmuth, Three-dimensional representation of voltammetric processes, Analytical Chemistry 32 (1960) 1509–1512.

[13] A. Hickling, Studies in electrode polarisation. Part IV. – The automatic control of the potential of a working electrode, Transactions of the Faraday Society 38 (1942) 27–33.

[14] M. Sluyters-Rehbach, Impedances of electrochemical systems: Terminology, nomenclature and representation - Part I: Cells with metal electrodes and liquid solutions (IUPAC Recommendations 1994), Pure and Applied Chemistry 66 (1994) 1831–1891.

[15] E. Barsoukov, J. R. Macdonald (Eds.), Impedance Spectroscopy – Theory, Experiment, and Applications, John Wiley & Sons, Inc., 2nd edition, 2005.

[16] M. E. Orazem, B. Tribollet, Electrochemical Impedance Spectroscopy, The ECS Series of Texts and Monographs, John Wiley & Sons, Inc., 2008.

[17] A. Lasia, Electrochemical impedance spectroscopy and its applications, in: B. E. Conway (Ed.), Modern Aspects of Electrochemistry, volume 32, Kluwer Academic Publishers, 2002, pp. 143–249.

[18] M. Sluyters-Rehbach, J. H. Sluyters, Sine wave methods in the study of electrode processes, in: Electroanalytical Chemistry, volume 4, Marcel Dekker, Inc., 1970, pp. 3–128.

[19] G. Inzelt, G. Láng, Electrochemical impedance spectroscopy (EIS) for polymer characterization, in: S. Cosnier, A. Karyakin (Eds.), Electropolymerization, Wiley-VCH, Weinheim, Germany, 2010, pp. 51–76.

[20] D. A. Buttry, Applications of the quartz crystal microbalance to electrochemistry, in: A. J. Bard (Ed.), Electroanalytical Chemistry: A series of advances, volume 17, Marcel Dekker, Inc., 1991.

[21] D. S. Ballantine, Jr, R. M. White, S. J. Martin, A. J. Ricco, G. C. Frye, E. T. Zellars, H. Wohltjen, Acoustic Wave Sensors – Theory, Design, and Physico-Chemical Applications, Elsevier, 2007.

[22] L. D. Landau, E. M. Lifshitz, Theory of eleasticity, in: Course of Theoretical Physics, volume 7, Pergamon Press, 1970.

[23] A. A. Vives (Ed.), Piezoelectric Transducers and Applications, Springer-Verlag Berlin Heidelberg, 2nd edition, 2008.

[24] W. G. Cady, Piezoelectricity, volume 1, Dover Publications Inc., 1964.

[25] R. P. Feynman, R. B. Leighton, M. Sands, The Feynman Lectrures on Physics, volume 2, Addison-Wesley Publishing Company, Inc., 1964.

[26] G. Inzelt, Electroanalytical Methods: Guide to Experiments and Applications, Springer, 2nd edition, pp. 257–270.

[27] P. Curie, J. Curie, Développement par compression de l'électricité polaire dans les cristaux hémièdres à faces inclinées, Bulletin de la minérologique de France 3 (1880) 90–93.

[28] G. Lippmann, Principe de conservation de l'électricité, Annales de Physique et de Chimie 5 (1881) 145–178.

[29] W. H. King, Piezoelectric sorption detector, Analytical Chemistry 36 (1964) 1735–1739.

[30] G. Sauerbrey, Verwendung von Schwingquarzen zur Wägung dünner Schichten und zur Mikrowägung, Zeitschrift für Physik 155 (1959) 206–222.

[31] P. L. Konash, G. J. Bastiaans, Piezoelectric crystals as detectors in liquid chromatography, Analytical Chemistry 52 (1980) 1929–1931.

[32] S. Bruckenstein, S. Swathirajan, Potential dependence of lead and silver underpotential coverages in acetonitrile using a piezoelectric crystal oscillator method, Electrochimica Acta 30 (1985) 851–855.

[33] S. Bruckenstein, M. Shay, An in situ weighing study of the mechanism for the formation of the adsorbed oxygen monolayer at a gold electrode, Journal of Electroanalytical Chemistry and Interfacial Electrochemistry 188 (1985) 131–136.

[34] D. A. Buttry, M. D. Ward, Measurement of interfacial processes at electrode surfaces with the electrochemical quartz crystal microbalance, Chemical Reviews 92 (1992) 1355–1379.

[35] J. G. Miller, D. I. Bolef, Acoustic wave analysis of the operation of quartz-crystal film-thickness monitors, Journal of Applied Physics 39 (1968) 5815–5816.

[36] J. G. Miller, D. I. Bolef, Sensitivity enhancement by the use of acoustic resonators in cw ultrasonic spectroscopy, Journal of Applied Physics 39 (1968) 4589–4593.

[37] C.-S. Lu, O. Lewis, Investigation of film-thickness determination by oscillating quartz resonators with large mass load, Journal of Applied Physics 43 (1972) 4385–4390.

[38] C. Lu, Applications of piezoelectric quartz crystal microbalances, in: A. W. Czanderna, C. Lu (Eds.), Methods and Phenomena – Their Application in Science and Technology, volume 7, Elsevier Science Publishers B.V., 1984.

[39] A. C. Hillier, M. D. Ward, Scanning electrochemical mass sensitivity mapping of the quartz crystal microbalance in liquid media, Analytical Chemistry 64 (1992) 2539–2554.

[40] K. K. Kanazawa, J. G. Gordon, Frequency of a quartz microbalance in contact with liquid, Analytical Chemistry 57 (1985) 1770–1771.

[41] G. Inzelt, B. B. Berkes, Á. Kriston, A. Székely, Electrochemical nanogravimetric studies of platinum in acid media, Journal of Solid State Electrochemistry 15 (2011) 901–915.

[42] R. Schumacher, The quartz microbalance: A novel approach to the in-situ investigation of interfacial phenomena at the solid/liquid junction, Angewandte Chemie International Edition in English 29 (1990) 329–343.

[43] H. L. Bandey, M. Gonsalves, A. R. Hillman, A. Glidle, S. Bruckenstein, Dynamic quartz crystal impedance measurements of polyvinylferrocene film deposition, Journal of Electroanalytical Chemistry 410 (1996) 219–227.

[44] C. Gabrielli, M. Keddam, N. Nadi, H. Perrot, Ions and solvent transport across conducting polymers investigated by ac electrogravimetry. application to polyaniline, Journal of Electroanalytical Chemistry 485 (2000) 101–113.

[45] K. E. Heusler, A. Grzegorzewski, L. Jäckel, J. Pietrucha, Measurement of mass and surface stress at one electrode of a quartz oscillator, Berichte der Bunsengesellschaft für physikalische Chemie 92 (1988) 1218–1225.

Part II

EXPERIMENTAL

2

GENERAL DESCRIPTION OF THE EXPERIMENTS

In the following a general description about the experimental conditions applied during the measurements will be given. Each chapter contains however a more concise experimental part summarizing the most relevant information about the measurements related to that chapter.

2.1 ELECTROCHEMICAL INSTRUMENTATION

2.1.1 *The Electrochemical Quartz Crystal Nanobalance*

2.1.1.1 *Frequency and Resistance Measurements*

The nanogravimetric measurements were carried out using either the QCM100 or QCM200 Quartz Crystal Microbalance Controller with a QCM25 5 MHz Crystal Oscillator products of the Stanford Research Systems, Inc. The QCM200 system is shown in Figure 2.1.

Figure 2.1: Complete QCM setup consisting of QCM200 Digital Controller, QCM25 Crystal Oscillator, Crystal Holder and three quartz crystal sensors. The QCM25 and QCM200 units are connected together through a Category 5 patch cable. The picture was taken from the operation and service manual of the device.

The use of the QCM100–QCM25 system requires an external frequency counter. The Frequency Output port (BNC) on the front panel is for the direct connection of the devices. The measured data can be transferred directly from the frequency counter to the computer. Our system consists of a Universal Frequency Counter PM 6685 (Philips/Fluka) besides the QCM100.

The QCM200 system is a stand-alone instrument with a built-in frequency counter and resistance meter. Series resonance resistance and frequency are

measured and displayed directly on the front panel without the need for an external frequency counter or precision voltmeter. There is also an analog output proportional to the relative frequency which can be used to interface with potentiostats. We transferred the frequency and resistance data via an RS232 serial port to a computer. In some cases we collected the frequency data in an additional way too: by connecting the QCM200 via its frequency output port to the analog input port of the potentiostat.

2.1.1.2 *Sensor Crystals*

We used sensor crystals with both systems consisting of a thin disk of 5 MHz, 1 inch in diameter, AT-cut, α-quartz with circular electrodes patterned on both sides.

AT-cut quartz crystals are commonly used as thickness-shear mode sensors because of their superior mechanical and piezoelectric properties, and nearly zero temperature coefficients at room temperature [1].

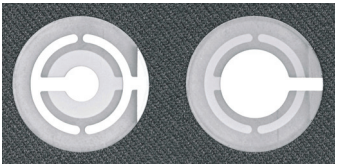

Figure 2.2: Quartz crystal nanobalance crystals of the SRS Company. On the left side the contact surface, on the right side the liquid surface of the crystal is shown.

The nominal frequency of oscillation of all crystals is 5 MHz (fundamental mode). The unperturbed crystals will normally be within ± 1000 ppm of their nominal frequency. For shear mode oscillation there are several frequencies that correspond to resonant conditions. The 5 MHz is regarded as optimal for laboratory use since it provides *i*) acceptable (submonolayer) sensitivity, *ii*) robustness (331 µm crystal thickness), and *iii*) stable oscillation in most viscous media.

The exposed area of the crystals to the liquid (often referred to as electrochemically active surface area) is 1.37 cm^2. The piezoelectrically active area, i.e. which determines the electrode oscillation area is 0.4 cm^2.

2.1.1.3 *Electrode Materials*

Gold or platinum coated crystals were used to our experiments. Aid of better adhesion a thin (2-20 nm) Ti layer is deposited directly onto the quartz surface.

In our rather extensive practice of using quartz crystals it happened that the assembly (composed of the quartz and the deposited metal layers) delaminated into layers. This rendered the crystal useless. In other cases the electrode material close to the perimeter became discontinuous most probably due to melting when applying higher currents.

2.1.1.4 *Surface Finish*

According to the producers certificate the crystals are polished and their average surface roughness is ~ 5 nm. We performed experiments examining the surfaces

of our electrodes. Atomic Force Microscopy (AFM) data for the corresponding Au and Pt WEs are shown in Figure 2.3. The average roughness of the Au and Pt electrodes was estimated to be about 4.6 nm and 4.0 nm, respectively.

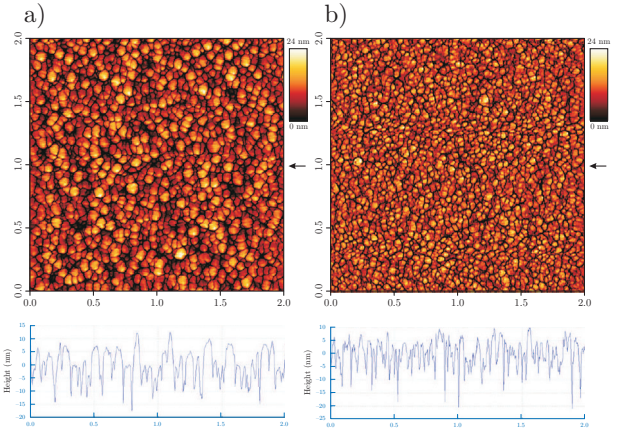

Figure 2.3: AFM amplitude images (2 µm × 2 µm area shown) of (a) Au and (b) Pt working electrodes. Corresponding topography cross sections (shown below) are taken along the directions marked with arrows.

2.1.1.5 *Calibration*

The calibration of the nanobalance under electrochemical conditions is the prerequisite to obtain a reliable relationship between the frequency shift and the corresponding mass change. We used the same method that was reported in the literature by Gabrielli et al. [2]. It is the first article dealing with electrochemical calibration.

The calibration is based on the deposition of silver on platinum from $AgNO_3$ solution by the means of chronoamperometry applying a wide range of current densities. We performed cyclic voltammetric deposition/dissolution of Ag on Pt EQCN electrodes under different conditions (i.e. with varying scan rates and potential limits), too. The deposited amount of silver can be determined from the measured current values, using Faraday's law of electrolysis assuming 100% of charge efficiency:

$$m = \frac{Q}{zF} M_{\mathrm{Ag}} \tag{2.1}$$

where m is the deposited mass, Q is the charge consumed during the deposition, z is the number of electrons involved in the reaction, F is the Faraday constant, M_{Ag} is the molar mass of silver ($M_{\mathrm{Ag}} = 107.87\,\mathrm{g\,mol^{-1}}$). If these current values are from cyclic voltammetric measurements a correction for the double layer capacitance before calculating the charge is needed. On the other hand

the deposited mass is directly related to the frequency variation according to the Sauerbrey equation (see Equation 1.3). From Equation 2.1 and Equation 1.3 it follows:

$$C_f = \frac{\Delta f}{Q}\frac{zF}{M_{Ag}}A \tag{2.2}$$

where A is the electrochemically active surface area of the quartz crystal. As Equation 2.2 shows the determination of C_f follows the determination of the slope of the Δf vs Q curve. In the case of metal deposition this curve is linear with a well defined slope.

Obtaining a value for C_f enables us to relate the frequency change to the mass change occurring at the electrode surface. In our systems a simple proportionality relation – the Sauerbrey equation – was always applicable. To the further calculations if nothing else is indicated $C_f = 56.6\,\mathrm{Hz\,cm^2\,\mu g^{-1}}$ was used.

2.1.1.6 *Immersion test*

When installing a new crystal into the holder it is reasonable to carry out a so called immersion test of the crystal before the electrochemical experiments. This means a complete immersion of the crystal into a solution with know viscosity and density (usually water). A theoretical prediction on the magnitude of the frequency decrease can be done using the Kanazawa–Gordon equation (Equation 1.4 in Chapter 1). For a 5 MHz polished crystal $\sim$ 715 Hz frequency decrease is expected in distilled water. This is a fast and reliable check whether the crystal installation was successfully done.

2.1.1.7 *Cleaning of the Crystal and the Holder*

The crystals were cleaned either in their special commercial cleaning basket unit or together with the holder. First of all both polar and apolar organic solvents were used to remove organic residues from the surface. This was followed by a thorough rinsing with deionized distilled water.

The crystal holder is made of Kynar®, a highly non-reactive, chemically resistive, pure thermoplastic fluoropolymer (polyvinylidene fluoride). With the help of a dummy crystal it could be cleaned in piranha solution.

2.1.2 *The Potentiostats*

There were three different kinds of potentiostats used to the measurements. These were as follows:

— Elektroflex 453 Computer Controlled Potentiostat (Szeged, Hungary)

— VSP – Modular 5 Channels Potentiostat/Galvanostat/EIS (Bio-Logic SAS)

— SP-300 – State-of-the-art Research Grade Potentiostat/Galvanostat/EIS (Bio-Logic SAS)

The VSP multichannel potentiostat is show in Figure 2.4.

Figure 2.4: VSP multi potentiostat with the built in current booster and the low current options. The picture was taken from http://www.bio-logic.info/potentiostat/products.html.

The Elektroflex 453 was exclusively employed in this work for the measurement of cyclic voltammograms shown in Figure 4.2 and Figure 4.3. The combined electrochemical impedance spectroscopy – quartz crystal nanobalance technique was developed using the SP-300 potentiostat. The related measurements (Ag UPD on Au and Cu UPD on Pt) were carried out with that device. The adsorption and electropolymerization studies of indole and 4-aminoindole were realized with help of a VSP potentiostat. The frequency ranges applied during impedance spectroscopy ($\sim$ 0.1 Hz – $\sim$ 10 kHz) were amply within the capability of the devices (10 µHz to 7 MHz in the case of the SP-300 and 10 µHz to 1 MHz in the case of the VSP potentiostat [3]). The magnitude of the lowest current was in the order of $\sim$ 10 µA, which could be measured even without the additional low current option to the Biologic potentiostats.

2.2 ELECTROCHEMICAL CELLS

Special electrochemical cells were designed to ensure *i*) stable circumstances for the nanogravimetric measurements *ii*) optimal arrangement of the electrodes for reproducible impedance measurements *iii*) an inert atmosphere for most of the measurements *iv*) long-term cleanliness of the system for the long-time measurements and *v*) the ease for a relatively fast assembling.

2.2.0.1 *Cleaning of the Electrochemical Cells*

Cleanliness in electrochemical surface science is a key factor to be able to unambiguously analyse experimental data and reproduce results. The employed Pt and Au electrodes are extremely sensitive to all kinds of contaminations. Usu-

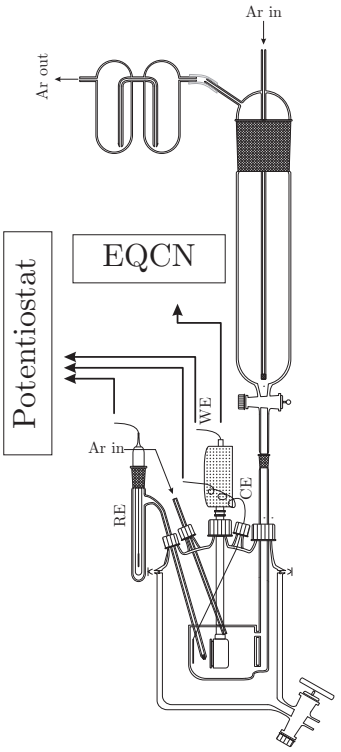

Figure 2.5: Schematic drawing of the EIS-EQCN set-up. RE, WE, and CE denote reference, working, and counter electrodes, respectively.

ally it is not enough to use clean gases and chemicals but a great care must be taken to clean all the electrodes the electrochemical cell.

Two methods were suitable for our purposes.

— The first one is based on the oxidative destruction of organic contaminants by hydrogen peroxide. The glassware is soaked overnight in a mixture of concentrated sulfuric acid (Suprapur®(Merck)) and concentrated hydrogen peroxide (Suprapur®(Merck)) – in the so called piranha solution. After careful removal of the etcher the glassware is thoroughly rinsed with deionized distilled water (see Section 2.4) and subjected to multiple boiling–water exchange cycles. When the aim is the complete removal of sulfate ions, the heating is made in an ultasonic bath under constant sonication and water exchange.

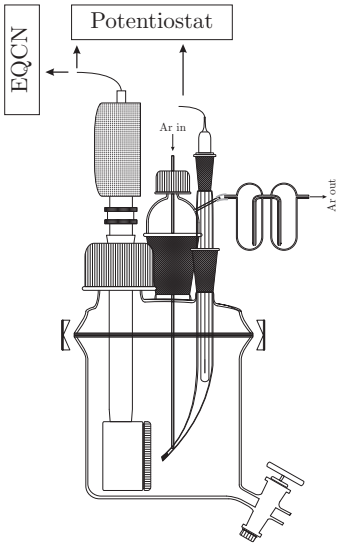

Figure 2.6: Schematic drawing of one of the electrochemical cells, used in Budapest. This cell was deployed for the organic electrochemical studies.

— The second method applies an aqueous solution of $KMnO_4$ to oxidise impurities. The glassware is set for ∼12 hours in the $KMnO_4$ solution. After the cell is taken out from the bath it is rinsed with deionized distilled water, a dilute solution of sulfuric acid and hydrogen peroxide and finally with deionized distilled water again. Then it is heated and boiled in a large beaker exchanging water 2-4 times.

2.3 ELECTRODES

The electrochemical cells used in this work were (classical) three electrode cells. They consisted of *i*) a working electrode, that was either gold or platinum coated EQCN electrode (Stanford Research Systems (SRS)); *ii*) a counter or auxiliary electrode, that was always chosen appropriately to the working electrode (i.e. a platinum wire or plate/foil was used to platinum and a gold wire or plate/foil to a gold working electrode, respectively); *iii*) a reference electrode. The reference electrode was either a sodium chloride saturated calomel electrode (SCE) or a potassium sulfate saturated mercury – mercury sulfate electrode (MMS). In both cases the electrode was separated from the solution with a ceramic frit. A detailed description about the working electrodes (cleaning, surface finish etc.) is given in Section 2.1.1. The metal counter electrode plates used at the Ruhr-Universität Bochum were ordered from Goodfellow.

2.4 CHEMICALS

The necessity for ultrapure water in electrode-kinetic and electrosorption studies has been recognized for many years [4]. Therefore further treatment of distilled water is inevitable for electrochemical objects. To this end distilled water was always deionized, the organic contaminants were removed either with Millipore or Siemens water purification systems before any kind of use. Both system provide water with a resistivity of 18 MΩ cm, and a total organic carbon content < 1 ppb.

List of the chemicals and their purity grade (if available):

1. Liquids
   a) Sulfuric acid, 96%, Suprapur®, Merck
   b) Sulfuric acid, 96%, analytical grade (p.a.), Merck
   c) Sulfuric acid, 96%, reagent grade, Sigma-Aldrich
   d) Perchloric acid, 70-72%, *Trace*SELECT®Ultra, Sigma-Aldrich
   e) Perchloric acid, 70-72%, analytical grade (p.a.), Sigma-Aldrich
   f) Hydrogen peroxide, 30%, Suprapur®, Merck
   g) Hydrogen peroxide, 30%, analytical grade (p.a.), Merck
   h) Hydrochloric acid, 38%, puriss, Riedel-de Haën
2. Solids
   a) Silver(I) oxide, 99,99+%, metal basis, Sigma-Aldrich
   b) Copper(II) oxide, 99,9999%, metal basis, Sigma-Aldrich
   c) Caesium sulfate, 99,99+%, trace metal basis, Sigma-Aldrich
   d) Caesium sulfate, $\geq$ 99.5%, analytical grade (p.a.), Sigma-Aldrich
   e) Sodium sulfate, 99,99+%, trace metal basis, Sigma-Aldrich
   f) Sodium sulfate, $\geq$ 99.0%, reagent grade, Sigma-Aldrich
   g) Indole,$\geq$ 99%, Sigma-Aldrich
   h) 4-aminoindole, 97%, Sigma-Aldrich
   i) Potassium permanganate, Reanal
3. Gases
   a) Argon, 5.0, Air-Liquid
   b) Argon, 5.0, Linde

REFERENCES

[1] D. S. Ballantine, Jr, R. M. White, S. J. Martin, A. J. Ricco, G. C. Frye, E. T. Zellars, H. Wohltjen, Acoustic Wave Sensors – Theory, Design, and Physico-Chemical Applications, Elsevier, 2007.

[2] C. Gabrielli, M. Keddam, R. Torresi, Calibration of the electrochemical quartz crystal microbalance, Journal of The Electrochemical Society 138 (1991) 2657–2660.

[3] Bio-Logic Science Instruments, Product catalogue, 2013.

[4] B. E. Conway, H. Angerstein-Kozlowska, W. B. A. Sharp, E. E. Criddle, Ultrapurification of water for electrochemical and surface chemical work by catalytic pyrodistillation, Analytical Chemistry 45 (1973) 1331–1336.

Part III

ON THE WAY TO SIMULTANEOUSLY ACQUISITE IMPEDANCE AND GRAVIMETRIC DATA IN A CYCLIC POTENTIAL SCAN

Simultaneous acquisition of Electrochemical Impedance Spectroscopy (EIS) and Electrochemical Quartz Crystal Nanobalance (EQCN) data in cyclic electrode potential scans was used to characterize nonstationary Underpotential Deposition (UPD) of atomic layers of Ag on Au and Cu on Pt. Both EIS and EQCN data sets complemented each other in the elucidation of interface models and the investigation of different aspects of the interfacial dynamics. EIS-EQCN provided an opportunity to monitor coadsorption and competitive adsorption of anions during the Ag and Cu UPD using *i*) the electrode mass change, *ii*) adsorption capacitances, and *iii*) double-layer capacitances. Kinetic information is available in the EIS-EQCN through the charge transfer resistances and apparent rate coefficients. The EIS-EQCN appeared to be a promising tool for an improved characterization and understanding of nonstationary electrochemical interfaces.

The chapter is based on the following articles:

— B. B. Berkes, A. Maljusch, W. Schuhmann, A. S. Bondarenko, *The Journal of Physical Chemistry C* **115** (2011) 9122-9130.

— M. Huang, J. B. Henry, B. B. Berkes, A. Maljusch, W. Schuhmann, A. S. Bondarenko, *Lecture Notes on Impedance Spectroscopy: Measurement, Modeling and Applications* **3** (2012) 35-39.

3

DEVELOPMENT OF COMBINED IMPEDANCE AND GRAVIMETRIC TECHNIQUE

3.1 INTRODUCTION

The in situ characterization of boundaries between electrodes and liquid electrolytes plays a key role in physical chemistry and electrochemistry [1–4]. This characterization is critical to control a number of processes, especially those in which the surface status and kinetic parameters can change at different stages or with time [1]. Typical examples of these processes include electrodeposition of thin films, adsorption, intercalation, and electropolymerization.

Nowadays, the investigation of the electrode | electrolyte boundary is routinely performed using a wide arsenal of electrochemical and nonelectrochemical techniques [5]. However, so called direct current (DC) techniques, such as voltammetric techniques, remain the main source of information. In these techniques, a DC current is recorded and analysed as a function of the electrode potential. Voltammetric techniques are robust in obtaining a first understanding of the system under investigation, as the electrode potential is one of the fundamental parameters which controls the status of the electrode | electrolyte interface.

Application of voltammetric techniques often requires multiple cycling of the electrode potential to distinguish different constituents contributing to the DC current, like the double-layer charging, electron transfer processes, diffusion, or specific adsorption. However, multiple cycling is not always acceptable for nonstationary systems and particularly for surfaces which irreversibly change their properties from cycle to cycle. Nonstationarity in this context would complicate data acquisition and interpretation: the system does not demonstrate the same properties in the forward and backward potential scans and also in cycle-to-cycle sequences. Possible reasons for this kind of behaviour include surface alloying, dielectric film growth, lateral interactions in adsorbate layers, electrode surface oxidation, and intercalation. Therefore, other in situ techniques need to be concurrently applied to complement voltammetric techniques for an extended characterization of these systems in a single potential scan [6]. The choice of the techniques in this case is not trivial as multiparameter measurements can be unacceptably long, and the response analysis could become ambiguous. The optimal combination would obviously require acquisition of a maximum amount of independent and self-consistent data from a minimal number of measurements.

In this work, we demonstrate that simultaneous acquisition and analysis of impedance and gravimetric data in one cyclic potential scan is advantageous for a detailed electrochemical characterization of nonstationary electrode | electrolyte interfaces. Scanning the potential is necessary to compare the surface status and continuously monitor changes at different stages of the electrode process.

On the other hand, by combining EIS and EQCN, it is possible to elucidate self-consistent physical models of the interface at various electrode potentials providing deeper physical insight into the system under investigation.

Here, we use EIS-EQCN to characterize two model processes: the electrochemical UPD [7] of atomic layers of *i*) Ag on Au and *ii*) Cu on Pt. In these systems, the deposition of monolayer amounts of Ag and Cu occurs at potentials more positive than those for the bulk phase deposition. Both processes, however, are difficult to investigate using conventional voltammetric techniques due to their high nonstationarity. An additional reason to select these model systems was that there were no EIS studies which characterize Cu UPD on Pt or Ag UPD on Au.

UPD of Ag on Au is fast and coupled with a strong coadsorption of perchlorate anions [7]. Moreover, Ag deposition induces spontaneous surface alloying which irreversibly changes the Au substrate [8, 9]. It should be noted that Ag UPD on Au has been studied extensively using different electrochemical and non-electrochemical techniques [8–18]. It was the first system where the UPD phenomenon was found [19]. However, there is still a controversy in the literature even on the voltammetry and the charges for the Ag UPD on Au. The reported charges range from $108\,\mu C\,cm^{-2}$ (which corresponds to 0.5 Monolayer (ML) of Ag) [11] to $380\,\mu C\,cm^{-2}$ ($\sim$ 1.7 ML) [14]. Nevertheless, electrochemical scanning tunnelling microscopy studies confirmed the formation of a compact (1×1) Ag monolayer [7, 20].

The difference in the Ag UPD voltammetry data can be caused by both anion coadsorption and surface alloying of Ag adatoms with Au [8]. Snyder and Erlebacher [9] found that a significant atom exchange occurs during the alloying on Au(111) terraces. This suggests that a multiparameter characterization of the Ag UPD on Au should be performed within a single cyclic potential scan since the electrode surface irreversibly changes within one cycle.

In contrast to Ag UPD on Au, deposition of Cu atomic layers on Pt is slow [7, 21, 22]. Ex situ and in situ measurements confirm that a complete Cu monolayer is formed prior to bulk phase deposition [7]. Cu UPD on Pt is used as a model reaction not only in fundamental studies [23] but also in applied research, for example, to estimate the real surface area of Pt catalysts [24]. Early stages of the UPD can be influenced by a competitive adsorption of OH^- [21, 22, 24, 25]. Anion adsorption and slow kinetics, however, drastically complicate the electrochemical investigation of this system because of its nonstationary characteristics. For example, in the case of voltammetry, for a Cu coverage higher than 0.5 ML, the coulometrically determined Cu coverage was too low by up to 30% as compared to that determined using ultrahigh vacuum measurements [26]. For a Cu coverage smaller than 0.5 ML, the coulometry overestimates it by up to 50% [26].

Therefore, our goal is to use the proposed combined EIS-EQCN approach for the characterization of these complex nonstationary systems and compare the results for both the slow Cu UPD on Pt and fast Ag UPD on Au.

3.2 RATIONALE FOR A COMBINED eis!-eqcn! TECHNIQUE

As DC techniques alone are not always appropriate to fully characterize non-stationary systems, it is necessary to consider the applicability of other techniques. The EIS technique involves measuring the response of the electrode interface to an alternating current (AC) probing signal with varying frequency at a range of electrode potentials [27, 28]. Analysis of the EIS data then enables decomposition of the AC response in to components related to the simultaneous processes occurring at the electrode | electrolyte interface (e.g. double layer capacitance, charge transfer resistance and diffusional properties of the system). While EIS has been shown to allow characterization of non-stationary systems [27, 29], some complex electrochemical systems can introduce ambiguities that hinder the analysis process. It becomes vital to employ other complementary techniques in conjunction with EIS to extract further information about the status of the interface and, hence, allow characterization.

With the ability to sense changes in electrode mass within the nanogram range, EQCN allows electrochemical studies to become more comprehensive, as it is now possible to detect mass changes on the electrode surface which do not contribute to the voltammetric response [30]. Additionally, DC techniques, such as voltammetric techniques, can still quantify the total charge which passes through the interface. The combination of key elements of impedance spectroscopy, electrogravimetry and direct current techniques therefore unlocks the ability to characterize complex electrochemical interfaces.

To maximize the effectiveness of such a complementary approach the data acquisition should take place in a single cyclic (staircase) potential scan. This method holds promise for the characterization of nonstationary systems, as was demonstrated previously [27–29, 31–38]. The multidimensional data acquired in such a combined EIS-EQCN scan, once analysed, can provide a more accurate and detailed model for characterization of the interface. This provides a deeper physical insight into the electrode | electrolyte interface.

Following acquisition and validation of the EIS data (Kramers-Kronig tests), EQCN, and DC data, a suitable physical model which is completely consistent with all of the complementary data is elucidated. Subsequent fitting of the EIS data to this physical model and further analysis of the available EIS-EQCN datasets enables the identification of a number of important parameters characterizing the electrode dynamics, such as: *i*) the electrode mass variation, $\Delta m\,(\Delta f)$; *ii*) the resonance resistance, ΔR, corresponding to the dissipation of the oscillation energy due to growing structures and the nature of the medium at the interface; *iii*) the double layer capacitance of the interface; *iv*) the adsorption capacitances and *v*) the apparent rate coefficients of adsorption ($k_a f_a(\theta)$) (will be discussed later).

3.3 EXPERIMENTAL

A general description of the experiments is given in the main experimental chapter. Here we only summarize the specific points to these measurements.

A Biologic SP-300 potentiostat and a QCM 200 quartz crystal microbalance (SRS, USA) were used to control the EIS and EQCN measurements.

Before each experiment, all the glassware used in this work was cleaned in a "piranha" solution (can be explosive, strong oxidizer) consisting of a mixture of 96% H_2SO_4 (Merck, Suprapur) and 30% H_2O_2 (3:1, Merck Suprapur) for 12 h. To remove sulfate ions we used multiple heating, ultrasonic treatment, and rinsing with Siemens UltraClear water (0.055 μS cm^{-1}, TOC content <1 ppb). Silver(I) oxide (Aldrich, 99,99+%, metal basis) and copper(II) oxide (Aldrich, 99,9999%, metal basis) were used to prepare Ag^+- and Cu^{2+}-containing solutions.

Either Pt or Au foil (GoodFellow) counter electrodes (CEs) of high surface area and a mercury–mercury sulfate (MMSs) reference electrode (RE) were used (Schott, kept in a separate compartment and separated from the working solution with a ceramic insert). In this chapters all potentials refer to the mercury–mercury sulfate reference electrode.

AFM data for the corresponding Au and Pt WEs are shown in Figure 2.3. The average roughness of the Au and Pt electrodes was estimated to be about 4.6 nm and 4.0 nm, respectively.

AFM images were acquired using a NanoWizard 3 AFM controlled by a JPK SPMControl Station III (JPK Instruments AG, Germany) mounted on a vibration damping table Vario Control Micro 40 (Halcyonics GmbH, Germany). Cantilevers were made of doped single crystal silicone (type ACTA, Applied Nanostructures, USA), had tip-radius < 10 nm, offered spring constant ~ 40 N m^{-1} and had Al coating on a reflex side. All images were acquired ex situ using tapping mode under ambient laboratory conditions with scanning speed of 1 μm s^{-1}.

3.4 RESULTS AND DISCUSSION

3.4.1 *Measurement Scheme*

The potentiodynamic EIS-EQCN measurements were organized as follows. The electrode potential was scanned stepwise (see Figure 3.1), similar to the measurements described in references [39, 40]. At each potential step, an EIS spectrum was taken within AC frequency range from 30 kHz to 10 Hz. The lower frequencies were avoided to keep a reasonable potential scan rate and minimize unwanted contaminations during the measurements. The gravimetric data were acquired simultaneously with the EIS.

To minimize artefacts in impedance data acquisition at high frequencies, a shunt with the capacitance connected between the RE and CE was used. The value of the capacitance was empirically selected in a series of calibration experiments.

The EIS spectra analysis and Kramers-Kronig tests were performed with the EIS Spectrum Analyzer software [41]. The quality of the fitting and modelling was controlled by the root-mean-square deviation and individual parameter uncertainties (see Section 3.6 for further details).

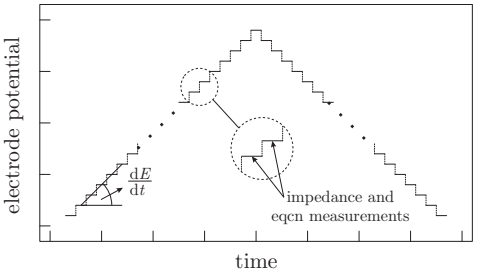

Figure 3.1: Schematic representation of the EIS-EQCN measurement program.

3.4.2 *Theoretical Considerations about EQCN and EIS*

A description about the electrochemical quartz crystal nanobalance method, about electrochemical impedance spectroscopy and the corresponding theories is given in Chapter 1. Here we summarize only the main points.

EQCN is based on the analysis of changes in the resonance frequency, Δf, of the quartz crystal. The Δf depends linearly on the surface mass change Δm at the working electrode

$$\Delta f = -C_f \Delta m \tag{3.1}$$

where C_f is the sensitivity factor which is a fundamental property of the EQCN crystal. The EQCN also measures the series resonance resistance ΔR which corresponds to the oscillation energy dissipation from the growing structures and from the medium in contact with the crystal. ΔR also changes with the viscosity or elasticity of the material (film or liquid) in contact with the crystal surface. Therefore, both Δf and ΔR can be used as independent indicators of mass loading and viscosity at the electrode | electrolyte interface during the electrochemical deposition.

On the other hand, EIS acquires and analyzes frequency dependencies of the impedance of a system. It normally uses small ($\leq 10\,\mathrm{mV}$) AC probing signals within a frequency range between a few megahertz to millihertz depending on system properties. The EIS analysis involves the finding of a physical model (expressed as an equivalent circuit) and identifying its parameters by fitting the impedance spectra to the model. Elucidating the equivalent circuits in EIS is not always straightforward, as complex systems can cause an ambiguity in the modelling. Therefore, additional independent information from for example EQCN or other techniques becomes essential to prove the selected model.

In the following, we present theoretical considerations on EIS of the UPD of metal atomic layers, which are selected as model systems in this study.

When a small AC perturbation signal is applied to a system where a single-stage UPD is possible, the Faradaic current i, the adatom coverage θ, and surface concentrations C_s of the electroactive particles can oscillate around quasi-steady-

state values. A linear part of the response which is assigned to the UPD can be written as follows [42]

$$\Delta i = \left(\frac{\partial i}{\partial E}\right)\Delta E + \left(\frac{\partial i}{\partial \theta}\right)\Delta\theta + \left(\frac{\partial i}{\partial C_s}\right)\Delta C_s \tag{3.2}$$

where the symbol Δ corresponds to a parameter, which oscillates during AC probing. Solving Equation 3.2 with the assumption of the additivity of the UPD current and the double-layer charging current leads to an adsorption model (Figure 3.2a) with the interfacial impedance Z [43, 44]

$$Z(j\omega) = R_s + \left((j\omega)^n C'_{DL} + \frac{1}{R_{ct} + (j\omega C_a)^{-1} + Z_T(j\omega)}\right)^{-1} \tag{3.3}$$

where ω is the angular frequency; C'_{DL} and the exponent n describe the response of the double layer (see Section 3.6 for further details); $R_{ct} = 1/(\partial i/\partial E)$ is the charge transfer resistance; $C_a = -q_a(\partial\theta/\partial E)$ is the adsorption capacitance; q_a is the charge necessary to form an adsorbate layer; Z_T is a mass transport impedance, which is usually represented by the Warburg impedance, $Z_{\mathfrak{W}} = A_{\mathfrak{W}}(j\omega)^{-1/2}$; $A_{\mathfrak{W}}$ is the Warburg coefficient; R_s is the electrolyte resistance; and j is the imaginary unit.

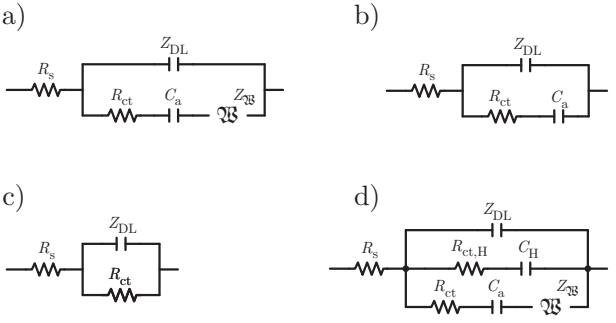

Figure 3.2: Equivalent circuits of: (a,b) a reversible UPD (a) with and (b) without diffusion limitations; (c) a slow irreversible UPD; (d) two reversible adsorption processes (where one has diffusion limitations) which occur simultaneously. Z_{DL}, impedance of the double layer; R_{ct}, charge transfer resistance; C_a, capacitance of adsorption; $Z_{\mathfrak{W}}$, diffusional Warburg impedance; R_s, the electrolyte resistance.

The adsorption model in Figure 3.2a does not show any continuous pathways for the DC current at $\omega \to 0$, which agrees with the fact that the DC current of the UPD at steady state is zero [42, 45, 46]. This model, however, allows a DC current to flow at unsteady state conditions, for example, in a potentiodynamic scan, enabling the adsorption capacitance to charge.

In the absence of diffusion limitations, the analysis of Equation 3.2 leads to the model shown in Figure 3.2b [42, 44–46]. In this particular case, the ability to

distinguish between contributions of the double layer and the adsorption capacitance C_a will depend on the R_{ct}. For a very fast adsorption, R_{ct} is small, and Z_{DL} will effectively incorporate C_a. On the other hand, for a slow irreversible adsorption, contributions of the $\Delta\theta$ and ΔC_s in Equation 3.2 can be small, and a simplified model as shown in Figure 3.2c is applicable [27, 28]. Finally, if two adsorption processes (one of them, for example, without diffusion limitations) with different time constants occur simultaneously, they can be described by the model shown in Figure 3.2d (see also references [36, 37] and [42, 45, 46]).

The choice of the particular physical model is based on an *a priori* knowledge about the system and on the measurement results. Additional independent information from the EQCN measurements is assumed to be helpful in acquiring relevant preknowledge and hence support the modelling process.

Using an approach developed by Kerner and Pajkossy [47], one can extract information about variations in the electrode potential of kinetic parameters. The ratio between the Warburg coefficient, $A_{\mathfrak{W}}$, extracted from the EIS spectra and the charge transfer resistance gives the apparent rate coefficient of the adsorption $k_a f_a(\theta)$ [47]

$$\sqrt{2D}\frac{A_{\mathfrak{W}}}{R_{ct}} = k_a f_a(\theta) \tag{3.4}$$

where D is the diffusion coefficient of the electroactive ions and $f_a(\theta)$ is a coverage related factor, which is a monotonously changing function of θ (for example, in the case of the Langmuir isotherm $f_a(\theta) = 1 - \theta$ [47]. The apparent rate coefficient $k_a f_a(\theta)$ expresses the rate by which the ad-atoms deposit onto the partially covered electrode surface, and k_a is the rate of UPD in which the ad-atoms deposit onto a free surface. The convenience of this approach in kinetic investigations is the elimination of the electrode surface area and the surface concentrations from the calculations.

In summary, several important parameters can be derived from the EIS-EQCN measurements and analysis. These include: *i*) the electrode mass variation $\Delta m\ (\Delta f)$; *ii*) the resonance resistance ΔR which corresponds to the dissipation of the oscillation energy due to the growing structures and from the medium at the interface; *iii*) the parameters characterizing the double layer; *iv*) the adsorption capacitances and *v*) the apparent rate coefficients of adsorption $k_a f_a(\theta)$.

3.4.3 *Deposition of Atomic Layers of Ag on Au*

Figure 3.3 shows the cyclic voltammogram (CV) of Ag UPD on a polycrystalline Au working electrode in 0.1 mol dm^{-3} $HClO_4$ recorded in the potential range between 0.55 V and 0.03 V. A series of broad adsorption-desorption peaks are observed before the bulk Ag phase deposition occurs. At potentials more positive than 0.5 V, the UPD current overlaps with the onset of OH and O adsorption at the Au electrode (Figure 3.3) [48]. Significant cathodic and anodic currents are observed as a result of the UPD [7] just prior to the potentials of the 3D Ag phase formation. In general, the CV displays the reversible nature of the Ag UPD.

It should be noted here that there is a certain degree of diversity in the voltammetric data reported from different laboratories. Rooryck [49] summarized a number of significantly different cyclic voltammograms obtained for

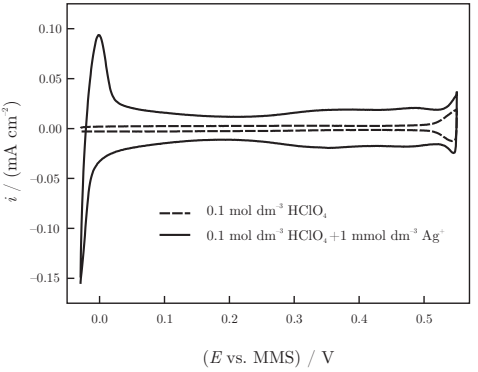

Figure 3.3: Cyclic voltammogram of Ag UPD on Au in 1 mmol dm^{-3} Ag^+ containing 0.1 mol dm^{-3} $HClO_4$. A reference cyclic voltammogram characteristic of Au in clean $HClO_4$ solution is also depicted in the figure. $dE/dt = 50\,mV\,s^{-1}$.

the Ag UPD on Au(111) from various investigators. This difference is explained by the surface status of the single crystals. Well-ordered Au(111) single crystals show sharp reversible UPD peaks [20], while in the case of defective polycrystalline Au surfaces the peaks of Ag UPD are significantly less intense and much broader [50]. The Au electrode surface status will likely also contribute to the charge measured from cyclic voltammograms. While electrochemical scanning tunneling microscopy studies confirmed the formation of a compact (1×1) Ag monolayer on well-ordered Au(111) crystals [7, 20], the measured charge for the Ag UPD varies from 108 µC cm^{-2} (which corresponds to 0.5 ML of Ag) [11] to 380 µC cm^{-2} [14].

The charge calculated from the anodic part of the voltammogram shown in Figure 3.3 was about 225 µC cm^{-2} which was close to the theoretical values for the Au(100)–(1×1)Ag and Au(111)–(1×1)Ag ML (192 µC cm^{-2} and 222 µC cm^{-2}, respectively). However, broad UPD peaks are likely due to polycrystallinity of the Au electrode used in this study. To ensure that the potential range selected for this study covers the whole UPD range, we performed additional experiments (see Figure 3.4): the cathodic potentials were selected just before the potentials where the 3D phase formation starts. The latter can be unambiguously observed by the corresponding anodic peak growing when the electrode potential is held more negative than 0.03 V.

Figure 3.6 summarizes the results of the in situ investigation of Ag UPD on Au using EIS-EQCN. The Ag adsorption and desorption change the Au-electrode weight constantly during the cyclic potential scan (Figure 3.6a). Apart from a general reversibility of the process, a difference can be seen between the $\Delta f(E)$ curves in the cathodic and anodic scans. Taking the theoretical charge for the Ag monolayer (222 µC cm^{-2}) and the corresponding mass change at 0.03 V, the calculated adsorbate molar weight was around 160 g mol^{-1}. This value is significantly bigger than that expected for Ag (107.9 g mol^{-1}). Clearly, ClO_4^- coad-

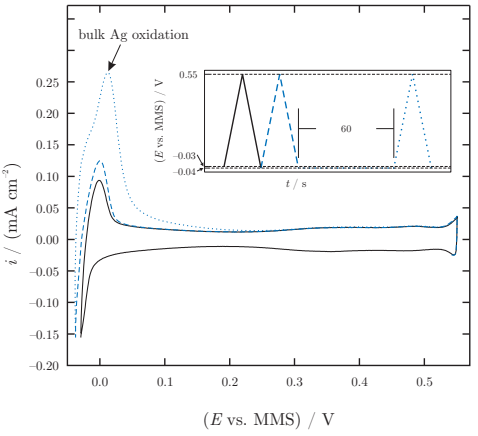

Figure 3.4: Cyclic voltammogram of polycrystalline Au in 1 mmol dm^{-3} Ag^+ containing 0.1 mol dm^{-3} $HClO_4$. The UPD potential range was selected downto 0.03 V.

sorption contributes to the apparent molar weight which is consistent with previously reported data [7, 18, 20, 48]. Notably, a weak adsorption of perchlorate anions is also possible at the bare Au surface [48, 51] and evident from the $\Delta f(E)$ curves taken in 0.1 mol dm^{-3} $HClO_4$ (Figure 3.6a). However, the latter cannot explain the excessive molar weight calculated at 0.03 V as the perchlorate anions desorb from the Au surface at this potential. Therefore, specific coadsorption of ClO_4^- should be considered for further Ag UPD data analysis.

Cycling the Au electrode in pure 0.1 mol dm^{-3} $HClO_4$ does not significantly change the resonance resistance ΔR (Figure 3.6b). Remarkably, addition of Ag^+ ions leads to a reproducible increase of the resistance in both the cathodic and anodic scans. This increase in ΔR, however, is difficult to explain by a simple effect of Ag^+ adsorption. We hypothesise that this irreversible change is caused by an increased disorder of the Au surface as a result of surface alloying of Ag with Au [8, 9].

Figure 3.6c-e shows the results of the EIS data analysis (see Section 3.6 for the complete set of data and details related to the fitting process). The parameters presented in the figures are the results of fitting the impedance data to the following models: *i*) shown in Figure 3.2b for the Au electrode in 0.1 mol dm^{-3} $HClO_4$ and *ii*) shown in Figure 3.2d for the Au electrode in 0.1 mol dm^{-3} $HClO_4$ + 1 mmol dm^{-3} Ag^+. These models demonstrated the best fit to the EIS data from all the physical models shown in Figure 3.2. Additionally, these models are consistent with the CVs and EQCN data.

A set of impedance data characterizing the electrochemical interface during Ag UPD on Au is shown in Figure 3.5. This impedance dataset is the collection of 2D impedance spectra taken at different electrode potentials during the staircase potential scan together with the EQCN data. Each of these 2D spectra were analysed in order to elucidate the physical model of the electrode | electrolyte

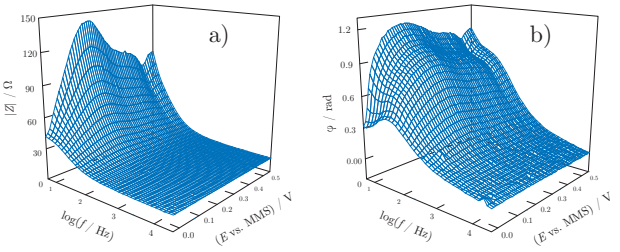

Figure 3.5: Extended Bode plots of the impedance spectra ($|\ Z\ |$ and the phase shift φ as a function of frequency f and the electrode potential E) characterizing the Ag UPD on a polycrystalline Au electrode in the examined potential region. $\mathrm{d}E/\mathrm{d}t = 0.3\,\mathrm{mV\,s^{-1}}$ (cathodic scan). Electrolyte: $0.1\,\mathrm{mol\,dm^{-3}}$ $HClO_4$ + $1\,\mathrm{mmol\,dm^{-3}}$ Ag^+.

interface. Models as shown in Figure 3.2 were used in this analysis. The model shown in Figure 3.2b demonstrated the best fit for the Au-electrode in $0.1\,\mathrm{mol\,dm^{-3}}$ $HClO_4$. The model shown in Figure 3.2d demonstrated the best fit in case of $1\,\mathrm{mmol\,dm^{-3}}$ Ag^+ containing $0.1\,\mathrm{mol\,dm^{-3}}$ $HClO_4$ solution.

One of the most important parameters which characterizes the electrode | electrolyte boundary and becomes available from the EIS analysis is the $C'_{DL}(E)$. The C'_{DL} is proportional to the double-layer capacitance and sensitive to adsorption as well as surface H_2O molecule reorientations, 2D phase transitions, and new phase growth (see Section 3.4.2 and Section 3.6 for further details) [42]. Variations of the C'_{DL} with the potential of the Au electrode in $0.1\,\mathrm{mol\,dm^{-3}}$ $HClO_4$ and in $0.1\,\mathrm{mol\,dm^{-3}}$ $HClO_4$ + $1\,\mathrm{mmol\,dm^{-3}}$ Ag^+ are shown in Figure 3.6. Weak adsorption of perchlorate anions at the bare Au surface in $0.1\,\mathrm{mol\,dm^{-3}}$ $HClO_4$ reveals itself with the peak in the $C'_{DL}(E)$ dependence at $\sim 0.1\,\mathrm{V}$. The peak position is consistent with the corresponding $\Delta f(E)$ curves (Figure 3.6a) which also detect an adsorption process. Adsorption of OH at the potentials more positive than $0.5\,\mathrm{V}$ leads to an increase in the apparent C'_{DL} values. Notably, cathodic and anodic parts of the $C'_{DL}(E)$ taken in $0.1\,\mathrm{mol\,dm^{-3}}$ $HClO_4$ do not coincide with each other. We propose that this is due to Au surface oxidation above a potential of $0.5\,\mathrm{V}$.

The $C'_{DL}(E)$ curves recorded in the presence of Ag^+ show almost perfect reversibility in the cyclic potential scan. Early stages of Ag deposition have almost no effect on the $C'_{DL}(E)$, which decreases slightly between $0.55\,\mathrm{V}$ and $0.2\,\mathrm{V}$. Completion of the Ag deposition leads to a 1.5-fold increase in the C'_{DL} values, as probably a more compact double layer is formed.

As discussed previously, the adsorption of ClO_4^- plays a significant role in the Ag UPD on Au. This is also confirmed by our EIS analysis. Fitting the corresponding spectra to the model shown in Figure 3.2d gives the best fit within the whole potential range examined, with acceptably small relative errors of the individual parameters. In this particular case, EIS is probably able to resolve two simultaneous adsorption processes because of a difference in their time con-

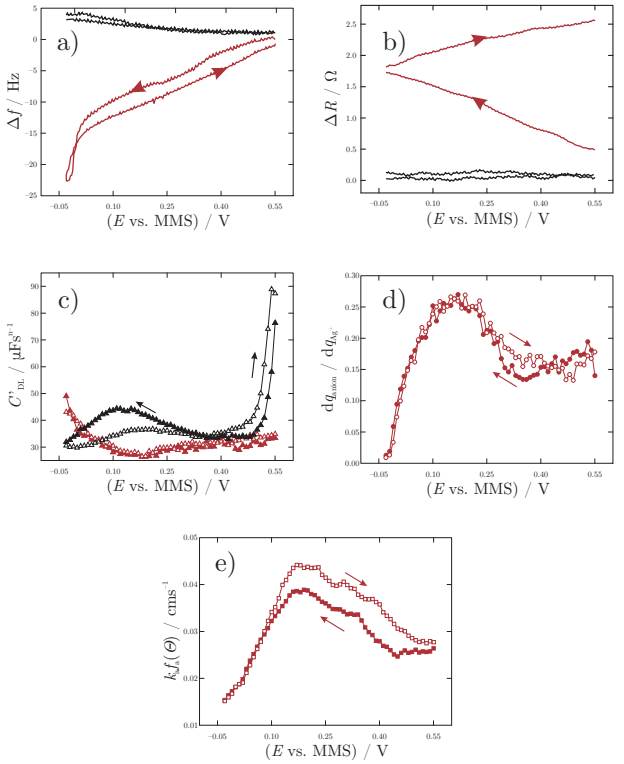

Figure 3.6: EIS-EQCN data for Ag UPD on Au. The red and black curves show the results obtained for the measurements in 1 mmol dm^{-3} Ag^+ containing 0.1 mol dm^{-3} $HClO_4$ and in 0.1 mol dm^{-3} $HClO_4$ solutions, respectively. $dE/dt = 0.3\,mV\,s^{-1}$.

stants, similar to other UPD systems [36, 37, 39, 45, 46]. These two adsorption processes are characterized by two different adsorption capacitances $C_a(E)$ and $C_a^{'}(E)$ for the Ag UPD and perchlorate anions, respectively.

Recalling the meaning of the adsorption capacitances $C_a(E)$ and $C_a^{'}(E)$ suggests that their ratio $C_a^{'}(E)/C_a(E)$ is roughly equivalent to the ratio of $dq_a^{'}/dq_a$ between the apparent anion and cation charges. Figure 3.6d shows the dependence of the ratio vs the electrode potential. Using this plot, it is possible to follow the dynamics of the specific ClO_4^- adsorption as the result of the Ag UPD. Early stages of Ag deposition between 0.55 V and 0.3 V are associated with the adsorption of one perchlorate anion per six Ag ad-atoms, assuming one electron transfer per anion or cation (Figure 3.6d). At $\sim$ 0.15 V, $dq_a^{'}/dq_a$ reaches

its maximum of around one anion per four adsorbed Ag atoms. Further Ag deposition decreases the dq_a'/dq_a ratio suggesting that additional perchlorate adsorption probably meets some steric difficulties. An alternative explanation of the observed behaviour of the dq_a'/dq_a with the change of potential includes a noninteger effective electron transfer. However, this is outside the scope of this work and needs further investigations.

Additionally, kinetic information about the Ag UPD can be obtained through the apparent rate coefficient $k_a f_a(\theta)$ available from the EIS analysis (see Equation 3.4). The $k_a f_a(\theta)$ slowly increases (Figure 3.6e) between 0.55 V and 0.2 V. Formation of a compact Ag layer at more negative potentials decreases the apparent rate coefficient due to the coverage related factor $f_a(\theta)$ which becomes dominating. Additional contribution to the variation of the $k_a f_a(\theta)$ comes from different UPD kinetics at steps, kinks, Au terraces, and also point defects which appear as a result of surface alloying, as was demonstrated in reference [52] for Pb UPD on Ag(111) and Ag(100).

The measured Ag UPD apparent rate coefficients from 0.15 cm s^{-1} to 0.45 cm s^{-1} (Figure 3.6e) are reasonably close to the standard rate constants k_0 of Ag bulk deposition on Ag. The latter can be estimated from the reported standard exchange current densities and ranges from $\sim 6.25 \times 10^{-4}$ cm s^{-1} for Ag(100) surfaces to ~ 0.25 cm s^{-1} for polycrystalline Ag and up to ~ 13.5 cm s^{-1} for Ag deposition at growing atomic Ag steps [53]. Remarkably, the $k_a f_a(\theta)$ dependencies do not coincide in the cathodic and anodic scans disclosing a "memory effect" which can be also seen from the dependencies of $\Delta R(E)$ (Figure 3.6b).

3.4.4 *Deposition of Atomic Layers of Cu on Pt*

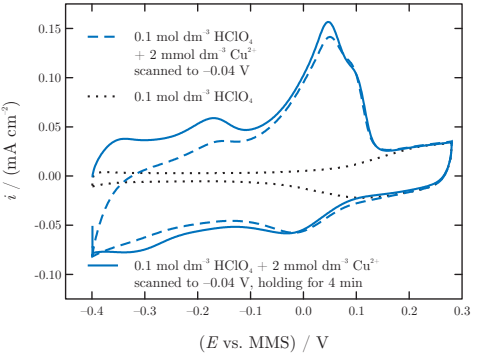

Figure 3.7: Cyclic voltammogram of Cu UPD on Pt in 2 mmol dm^{-3} Cu^{2+} containing 0.1 mol dm^{-3} $HClO_4$. A reference cyclic voltammogram characteristic of Pt in clean $HClO_4$ solution is also depicted in the figure. $dE/dt = 50$ mV s^{-1}.

Cyclic voltammograms characterizing Cu UPD on a polycrystalline Pt electrode are presented in Figure 3.7. Deposition of an atomic Cu layer starts at $\sim 0.1\,\mathrm{V}$ and shows two broad cathodic peaks before Cu bulk phase deposition starts at potentials more negative than $-0.4\,\mathrm{V}$. The anodic part of the CV shows a large peak at $\sim 0.05\,\mathrm{V}$ and a prepeak at around $-0.15\,\mathrm{V}$. The measured anodic charge corrected for the background current for the underpotentially deposited Cu depends on conditions of the CV experiment [24, 26]. The anodic charge $\sim 360\,\mu\mathrm{C\,cm^{-2}}$ can be calculated from the voltammogram if a continuous potential cycling is used. Notably, if the potential is held at $-0.4\,\mathrm{V}$ for 4 min or longer, a stable anodic charge of $\sim 440\,\mu\mathrm{C\,cm^{-2}}$ is determined, which is lower than the theoretical value for a full Cu monolayer on Pt(111) ($480\,\mu\mathrm{C\,cm^{-2}}$). This difference can be explained by a slow Cu UPD kinetics and the possible influence of anion coadsorption [7].

Another voltammetric observation which is important for the further analysis is that early stages of atomic Cu layer deposition are overlapping with the OH adsorption/desorption at the Pt surface (Figure 3.7).

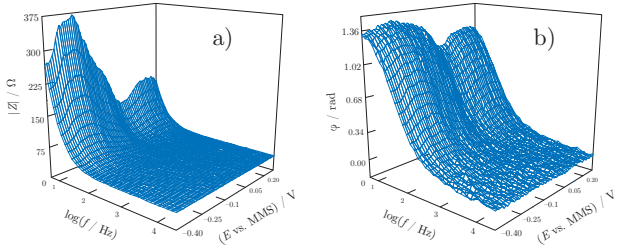

Figure 3.8: Extended Bode plots of the impedance spectra ($|\,Z\,|$ and the phase shift φ as a function of frequency f and the electrode potential E) characterizing the Cu UPD on a polycrystalline Pt electrode in the examined potential region. $\mathrm{d}E/\mathrm{d}t = 0.3\,\mathrm{mV\,s^{-1}}$ (cathodic scan). Electrolyte: $0.1\,\mathrm{mol\,dm^{-3}}$ $HClO_4$ + $2\,\mathrm{mmol\,dm^{-3}}$ Cu^{2+}.

A set of impedance data characterizing the electrochemical interface during Cu UPD on Pt is shown in Figure 3.8. This impedance dataset as we discussed in conjunction with Figure 3.5 is the collection of 2D impedance spectra taken at different electrode potentials during the staircase potential scan. These 2D spectra were analysed in order to elucidate the physical models, shown in Figure 3.2. The simple adsorption model shown in Figure 3.2c was found to give the best fit to the impedance data. Additional elements did not improve fitting and increased the relative calculated errors for the parameters.

Figure 3.9 shows the results of EIS-EQCN investigation of Cu UPD on Pt. Deposition of a Cu monolayer and its following oxidation manifest themselves in the cyclic $\Delta f(E)$ variation with the potential (Figure 3.9a). Taking the theoretical charge for a full Cu monolayer ($480\,\mu\mathrm{C\,cm^{-2}}$) and the experimental Δf value at $-0.4\,\mathrm{V}$, the apparent molar weight for the adsorbate can be calculated to be around $66\,\mathrm{g\,mol^{-1}}$. This is close to the expected value of $63.5\,\mathrm{g\,mol^{-1}}$ for Cu.

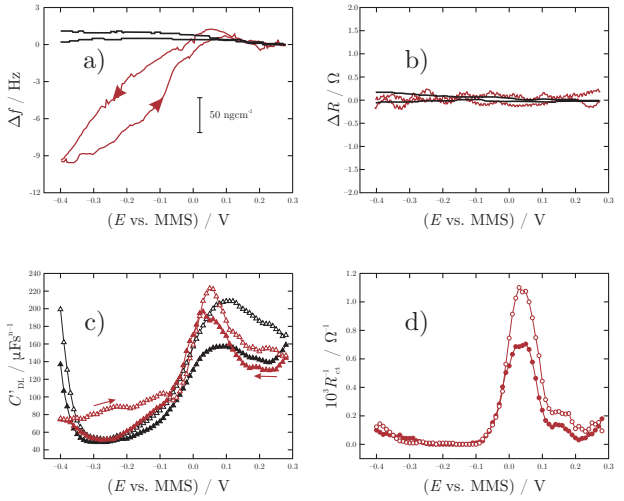

Figure 3.9: EIS-EQCN data for Cu UPD on Pt. The red and black curves show the results obtained for the measurements in 2 mmol dm^{-3} Cu^{2+} containing 0.1 mol dm^{-3} $HClO_4$ and in 0.1 mol dm^{-3} $HClO_4$ solutions, respectively. $dE/dt = 0.3\,mV\,s^{-1}$.

Therefore, in contrast to the previously considered Ag UPD on Au, we propose that significant coadsorption of perchlorate anions does not take place. However, more complex Cu–perchlorate interactions due to partial discharge of the Cu ad-atoms cannot be excluded.

Another difference between Ag UPD on Au and Cu UPD on Pt is that Cu deposition on Pt does not significantly change the surface resonance resistance ΔR (Figure 3.9b). This, in turn, suggests there is no significant surface alloying between Cu adatoms and the Pt surface. We also proved this hypothesis in a separate experiment using a Pt(111) single-crystal surface which is sensitive to surface defects [54, 55] (Figure 3.10). After the Cu UPD on Pt(111) and later anodic stripping of the deposited Cu monolayer followed by rinsing of the electrode under potential control, it was possible to restore the initial Pt(111) voltammogram. This provides evidence that the Cu UPD indeed leaves Pt(111) terraces unchanged.

Figure 3.9c,d shows the results of the EIS data analysis (for the complete set of data, see also Section 3.6). The EIS data for the Cu UPD on Pt can be described by the model shown in Figure 3.2c. More complex models which included parts related to a coadsorption of anions or diffusion did not improve the fitting and additionally increased the relative error of the individual parameters. However, the resulting best-fit model (Figure 3.2c) is consistent with the fact that the Cu UPD experiences kinetic difficulties. The elucidated model does not contain

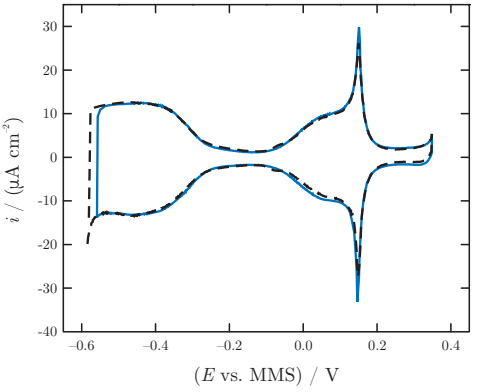

Figure 3.10: Cyclic voltammogram of Pt(111) in 0.1 mol dm^{-3} $HClO_4$ solution before (blue curve) and after (black curve) Cu UPD. $dE/dt = 20\,mV\,s^{-1}$.

pathways for perchlorate-anion coadsorption which is consistent with the EQCN data. However, possible coadsorption can be masked by slow Cu UPD kinetics (namely, Cu can potentially induce coadsorption).

Figure 3.9c compares the $C'_{DL}(E)$ curves for the Pt electrode in 0.1 mol dm^{-3} $HClO_4$ and in 2 mmol dm^{-3} Cu^{2+} containing 0.1 mol dm^{-3} $HClO_4$. Underpotential deposition of hydrogen and adsorption of OH on the bare Pt electrode increase the apparent C'_{DL} values in pure $HClO_4$ between −0.35 V and −0.4 V and between −0.1 V and 0.28 V, respectively. High apparent C'_{DL} values in the potential region between −0.1 V and 0.28 V are due to fast OH adsorption: EIS cannot distinguish the double-layer charging and OH adsorption within the selected frequency range [44]. The C'_{DL} curves for Pt are close to those reported for the polycrystalline samples in reference[56].

Early stages of Cu deposition slightly change the $C'_{DL}(E)$ profile between 0.28 V and 0.00 V (Figure 3.9c). Additional Cu deposition does not show pronounced differences in the $C'_{DL}(E)$ curves in comparison with the bare Pt surface until a potential of about −0.35 V. A more compact Cu layer formation blocks the H UPD in the potential between−0.35 V and 0.4 V. In the anodic scan, the $C'_{DL}(E)$ shows much higher values than in the cathodic scan up to a potential of −0.05 V. However, in general, Cu UPD on Pt is significantly affected by competitive OH adsorption on the bare Pt surface.

In contrast to Ag UPD on Au, kinetic information about Cu UPD on Pt can be derived only by the inverse charge transfer resistance $R_{ct}(E)^{-1} = \partial i/\partial E$ (Figure 3.9d). The $R_{ct}(E)^{-1}$ discloses a significant difference in the UPD rates at different stages. Early stages of the Cu UPD are much faster than the final ones. This is consistent with the voltammetric observations: 4 min deposition at −0.4 V is necessary to register a stable anodic current. Additionally, the rates change significantly in the cathodic and anodic scans. Considering that the value of $\Delta R(E)$

is constant within the experimental error during the whole investigated potential range (Figure 3.9b), we propose that this difference is due to changes in Cu–Cu and Cu–Cu–Pt interactions at high Cu coverages. These interactions can significantly alter the kinetics of the surface-limited process and be responsible for the apparent voltammetric irreversibility of the UPD. Contributions of different metal–metal and metal–substrate interactions on the UPD irreversibility were recently analyzed and confirmed using density functional theory calculations [57]. Nevertheless, the influence of OH adsorption may also play a significant role.

Direct comparison between the apparent rate coefficients for Ag UPD on Au and Cu UPD on Pt is difficult; however, a rough estimation suggests that the rate constant for Cu UPD is at least 5 orders of magnitude smaller than that for Ag UPD on Au.

3.5 CONCLUSIONS

Simultaneous acquisition and analysis of impedance and gravimetric data by EIS-EQCN in one cyclic potential scan can be advantageous for a detailed electrochemical characterization of nonstationary electrode | electrolyte interfaces. Both data sets complement each other in elucidating different aspects of the interfacial dynamics.

Two surface-limited UPD processes were characterized by EIS-EQCN: *i*) Ag UPD on Au and *ii*) Cu UPD on Pt. The EIS and gravimetric data appeared to be consistent with each other and with the data previously published in the literature. EIS physical models of the electrochemical interface during Ag and Cu UPD processes were elucidated in terms of equivalent circuits based on EQCN and EIS data recorded simultaneously.

Ag UPD on Au in $0.1\,\mathrm{mol\,dm^{-3}}$ $HClO_4$ is a complex process which is accompanied by changes of the electrode surface and perchlorate anion coadsorption. EIS-EQCN provided an opportunity to simultaneously monitor adsorption of anions and cations by $\Delta f(E)$ and the respective adsorption capacitance curves which are available from the impedance analysis. The latter shows that the anion coadsorption dynamics changes at different Ag UPD stages. Initial Ag deposition induces coadsorption of one ClO_4^- anion per about six Ag adatoms, while the later stages change this ratio to 1/4 at 0.2 V. Further perchlorate adsorption likely meets steric complications at the final stages of the Ag UPD.

New kinetic information on "intrinsically" nonstationary Ag UPD was obtained from EIS-EQCN through the evaluation of the apparent rate coefficients $k_a f_a(\theta)$. The $k_a f_a(\theta)$ values range from $0.15\,\mathrm{cm\,s^{-1}}$ to $0.45\,\mathrm{cm\,s^{-1}}$ which is between the standard rate constants k_0 of Ag bulk deposition on Ag for different Ag surfaces reported previously. The $k_a f_a$ values demonstrate a complex dependence on the electrode potential due to the occupancy related factor f_a and appeared to be different in the anodic and cathodic scans as a result of surface alloying.

Surface alloying between Ag and Au additionally contributes to the resonance resistance variation $\Delta R(E)$. The latter increases constantly in the presence of Ag adatoms in both cathodic and anodic scans.

Analysis of the EIS-EQCN data shows that in contrast to Ag UPD a specific adsorption of ClO_4^- does not contribute significantly to Cu UPD on Pt in 0.1 mol dm^{-3} $HClO_4$. Instead, the $C'_{DL}(E)$ dependencies demonstrate that a competitive OH adsorption influences the UPD process to a large extent, especially at the early stages of Cu deposition. Another difference between two UPD systems is that the Cu adsorption and desorption do not modify the Pt surface: $\Delta R(E)$ remains almost constant in the cyclic potential scan. In a wider context, EIS-EQCN appeared to be a promising tool for an in-depth characterization and understanding of nonstationary electrochemical interfaces.

3.6 APPENDIX

3.6.1 *The electric double layer capacitance*

The double layer capacitance, C_{DL} can be calculated from impedance measurements. Two interfacial parameters determine the actual C_{DL} values: the apparent dielectric constant of the inner H_2O layer and the apparent double layer thickness. Both parameters can change as a result of reorientations of the surface H_2O molecules or the specific adsorption and therefore affect the C_{DL}. Consequently, the dependence of the C_{DL} on the electrode potential can be used to monitor adsorption processes [58, 59].

However, fitting of the obtained EIS data demonstrates that the double layer exhibit so called "frequency dispersion" [42] in a wide range of electrode potentials. This means that the measured C_{DL} values change with the frequency. To describe this effect, a CPE is used [60] with the following equation for the impedance:

$$Z_{DL} = {C'_{DL}}^{-1}(j\omega)^{-n} \tag{3.5}$$

where C'_{DL} is the pre-exponential parameter of the CPE, which is proportional to the double layer capacitance of pure capacitive electrodes, the exponent n is the parameter ($0.5 \leq n \leq 1$) which is directly related to the dispersive behaviour. A CPE cannot be described by any finite number of electrical circuit elements [42].

The main hypotheses concerning the frequency dispersion are as follows [42]: *i*) the roughness effect, *ii*) effects of a fractal nature, *iii*) distortion of the electric double layer by Faradaic reactions . However, none of these theories can explain the complete variety of the experimental observations reported in literature.

Recently, the frequency dependence of the double layer was investigated using well defined single crystals [61–64]. The main results of these studies are: *i*) C'_{DL} and n, are strongly dependent on the electrode potential; and when $n = 1$ the interface presents pure capacitive behaviour, i.e. $C'_{DL} = C_{DL}$; *ii*) there is a strong relationship between the capacitance dispersion and the phase transition processes which take place at the interface, namely the reconstruction of the electrode surface, adsorption and phase transitions in the ordered adsorbed layers; *iii*) the value of n can be sometimes significantly lower than 1 if ordering in the adsorbate layer occurs; *iv*) in potential ranges where none of the above mentioned processes take place the interface presents almost pure capacitive behaviour.

There are reports [60] which show that rough electrodes can exhibit lower capacitance dispersion than smooth ones. Consequently, in some cases one might expect lower capacitance dispersion for polycrystalline electrodes than for single crystal surfaces.

In summary, information obtained from the potential dependencies of both C'_{DL} and n can contain valuable information on the interfacial behaviour, and can be used to evaluate the properties of the electrode | electrolyte boundary.

3.6.2 *EIS spectra analysis*

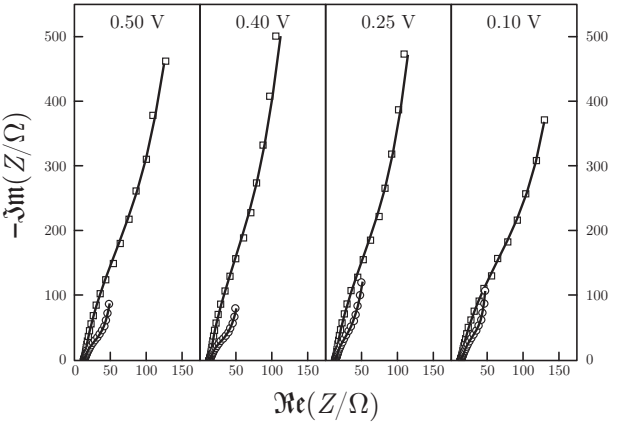

Figure 3.11: Comparison between impedance data taken for the Au electrode in presence and in absence of 1 mmol dm^{-3} Ag^+ in the electrolyte. Solid lines represent the best-fit to the corresponding physical models (cathodic scan).

For Ag UPD on Au in 1 mmol dm^{-3} Ag^+ containing 0.1 mol dm^{-3} $HClO_4$ solution, the model shown in Figure 3.2a demonstrated the best fit. The impedance of the double layer was initially treated as the CPE element. However, the actual fitting showed that the exponent n of the CPE element was equal to 1, except several potentials (randomly distributed points) where n was between 0.995 and 0.99. Therefore, we replaced the CPE element with a pure capacitance. In contrast, a Au electrode in pure $HClO_4$ showed pronounced frequency dispersion. Moreover, an additional RC branch should be added to account for the background OH adsorption at the Au electrode at higher potentials (Figure 3.2b). A specific adsorption on bare Au was found to contribute to the impedance response also at lower potentials. However, comparison of the data from the voltammograms, EQCN, and the corresponding adsorption capacitances showed that this contribution was about 3% of the total adsorption charge calculated from the voltammograms for weak perchlorate adsorption. Therefore, we spec-

ulate that this contribution is due to early OH adsorption; or it is an adsorption at defective Au-sites of the polycrystalline electrode.

Figure 3.11 compares examples of EIS taken at different potentials for a Au electrode in 1 mmol dm^{-3} Ag^+ containing 0.1 mol dm^{-3} $HClO_4$ solution. Solid lines represent the fitting to the respective models shown in Figure 3.2: *i*) shown in Figure 3.2b for the Au electrode in 0.1 mol dm^{-3} $HClO_4$, and *ii*) shown in Figure 3.2d in case of 1 mmol dm^{-3} Ag^+ containing 0.1 mol dm^{-3} $HClO_4$.

Figure 3.12 shows the dependencies of all the parameters of the model shown in Figure 3.2d on the electrode potential for Ag UPD on Au.

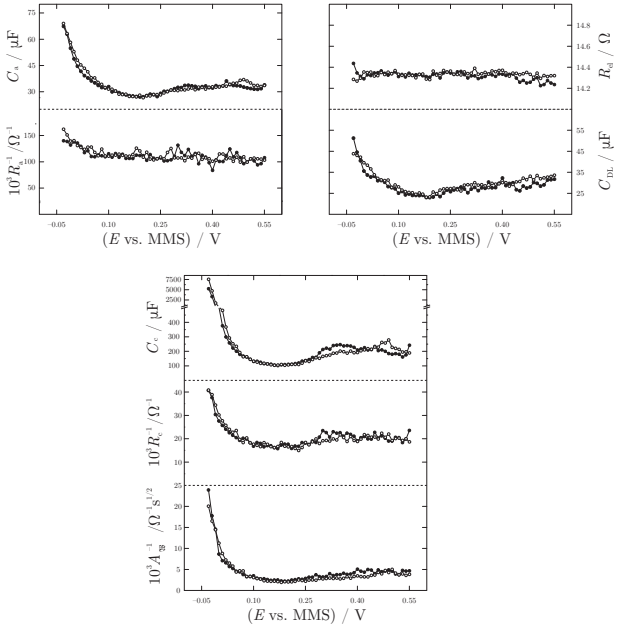

Figure 3.12: Dependencies on the electrode potential of all parameters of the model shown in Figure 3.2d.

For Cu UPD on Pt the simple adsorption model shown in Figure 3.2c was found to give the best fit to the impedance data. Figure 3.13 shows the dependencies of the two additional parameters of the model shown in Figure 3.2c on the electrode potential. For the sake of better visibility these two parameters were not plotted in Figure 3.9.

Figure 3.13b shows normalized deviations between measured and calculated EIS for Cu UPD on Pt at different electrode potentials. The deviations seem to be randomly distributed. This additionally suggests that the model was selected correctly and no additional elements are needed.

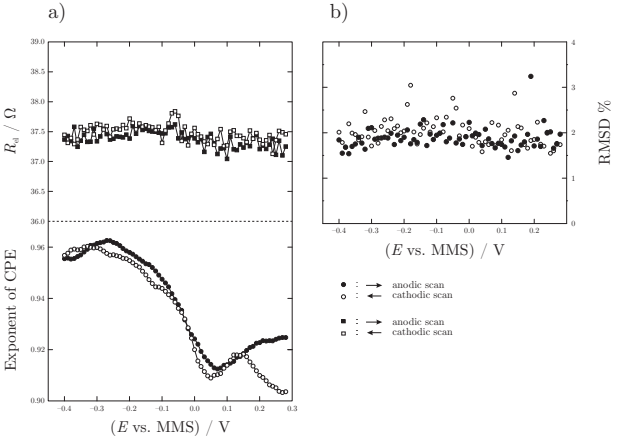

Figure 3.13: (a) Dependencies of the two additional parameters of the model shown in Figure 3.2c that were left out from the plots in Figure 3.9. 2 mmol dm^{-3} Cu^{2+} containing 0.1 mol dm^{-3} $HClO_4$. $dE/dt = 0.3\,mV\,s^{-1}$. The increased electrolyte resistance compared to that shown in case of Ag UPD on Au may be the result of the bigger reference- and working electrode separation. (b) Normalized deviations between measured and calculated EIS at different electrode potentials. Cu UPD on Pt.

[1] D. M. Kolb, Electrochemical surface science, Angewandte Chemie International Edition 40 (2001) 1162–1181.

[2] Z.-Q. Tian, B. Ren, Adsorption and reaction at electrochemical interfaces as probed by surface-enhanced Raman spectroscopy, Annual Review of Physical Chemistry 55 (2004) 197–229.

[3] M. Hugelmann, P. Hugelmann, W. J. Lorenz, W. Schindler, Nanoelectrochemistry and nanophysics at electrochemical interfaces, Surface Science 597 (2005) 156–172.

[4] B. E. Conway, Reflections on directions of electrochemical surface science as a leading edge of surface chemistry, Journal of Electroanalytical Chemistry 524-525 (2002) 4–19.

[5] C. G. Zoski (Ed.), Handbook of Electrochemistry, Elsevier, 1 edition, 2007.

[6] A. J. Bard, L. R. Faulkner, Electrochemical methods : fundamentals and applications, John Wiley & Sons, Inc, 2 edition.

[7] E. Herrero, L. J. Buller, H. D. Abruña, Underpotential deposition at single crystal surfaces of Au, Pt, Ag and other materials, Chemical Reviews 101 (2001) 1897–1930.

[8] C. M. Whelan, M. R. Smyth, C. J. Barnes, G. A. Attard, X. Yang, Surface structural transitions induced by repetitive underpotential deposition of Ag on Au(111) , Journal of Electroanalytical Chemistry 474 (1999) 138–146.

[9] J. D. Snyder, J. D. Erlebacher, Electrochemical measurement of the surface alloying kinetics of underpotentially deposited Ag on Au(111), Langmuir 25 (2009) 9596–9604.

[10] S. Garcia, D. Salinas, C. Mayer, E. Schmidt, G. Staikov, W. Lorenz, Ag UPD on Au(100) and Au(111), Electrochimica Acta 43 (1998) 3007–3019.

[11] M. C. Santos, L. H. Mascaro, S. A. S. Machado, Voltammetric and rotating ring-disk studies of underpotential deposition of Ag and Cu on polycrystalline Au electrodes in aqueous H_2SO_4, Electrochimica Acta 43 (1998) 2263–2272.

[12] D. Oyamatsu, S. Kuwabata, H. Yoneyama, Underpotential deposition behavior of metals onto gold electrodes coated with self-assembled monolayers of alkanethiols, Journal of Electroanalytical Chemistry 473 (1999) 59–67.

[13] J. W. Ndieyira, A. R. Ramadan, T. Rayment, In-situ and real time structural studies of underpotential deposition of silver on a gold (111) electrode using a transmission X-ray surface differential diffraction technique, Journal of Electroanalytical Chemistry 503 (2001) 28–35.

[14] T. Kondo, J. Morita, M. Okamura, T. Saito, K. Uosaki, In situ structural study on underpotential deposition of Ag on Au(111) electrode using surface X-ray scattering technique, Journal of Electroanalytical Chemistry 532 (2002) 201–205.

[15] M. J. Esplandiu, H. Hagenström, Functionalized self-assembled monolayers and their influence on silver electrodeposition, Solid State Ionics 150 (2002) 39–52.

[16] M. J. Esplandiu, M. A. Schneeweiss, D. M. Kolb, An insitu scanning tunneling microscopy study of Ag electrodeposition on Au(111), Physical Chemistry Chemical Physics 1 (1999) 4847–4854.

[17] S. G. Corcoran, G. S. Chakarova, K. Sieradzki, An in-situ STM investigation of the underpotential deposition of Ag on Au(111) electrodes, Journal of Electroanalytical Chemistry 377 (1994) 85–90.

[18] H. Uchida, M. Miura, M. Watanabe, Electrochemical quartz crystal microbalance study of silver ad-atoms on highly ordered Au(111) electrodes in sulfuric acid, Journal of Electroanalytical Chemistry 386 (1995) 261–265.

[19] L. B. Rogers, D. P. Krause, J. C. Griess, D. B. Ehrlinger, The electrodeposition behavior of traces of silver, Journal of The Electrochemical Society 95 (1949) 33–46.

[20] K. Ogaki, K. Itaya, In situ scanning tunneling microscopy of underpotential and bulk deposition of silver on gold (111) , Electrochimica Acta 40 (1995) 1249–1257.

[21] N. Markovic, P. N. Ross, Effect of anions on the underpotential deposition of copper on platinum(111) and platinum(100) surfaces, Langmuir 9 (1993) 580–590.

[22] N. M. Marković, H. A. Gasteiger, P. N. Ross, Jr, Copper electrodeposition on Pt(111) in the presence of chloride and (bi)sulfate: Rotating ring-Pt(111) disk electrode studies, Langmuir 11 (1995) 4098–4108.

[23] A. Aramata, Underpotential deposition on single-crystal metals, in: J. O'M. Bockris, B. E. Conway, R. E. White (Eds.), Modern Aspects of Electrochemistry, volume 31, Kluwer Academic / Plenum Publishers, New York, 2002, p. 181.

[24] C. L. Green, A. Kucernak, Determination of the platinum and ruthenium surface areas in platinum-ruthenium alloy electrocatalysts by underpotential deposition of copper. I. Unsupported catalysts, The Journal of Physical Chemistry B 106 (2002) 1036–1047.

[25] P. N. Ross, Jr, N. Markovic, Comment on "Electrochemical and ultrahigh vacuum characterization of ultrathin Cu films on Pt(111)", Langmuir 10 (1994) 976–977.

[26] L.-W. H. Leung, T. W. Gregg, D. W. Goodman, Coverage-dependent behavior of ultrathin Cu films on Pt(111): UHV and electrochemical studies, Chemical Physics Letters 188 (1992) 467–470.

[27] A. S. Bondarenko, G. A. Ragoisha, N. P. Osipovich, E. A. Streltsov, Multiparametric electrochemical characterisation of Te-Cu-Pb atomic three-layer structure deposition on polycrystalline gold, Electrochemistry Communications 8 (2006) 921–926.

[28] G. A. Ragoisha, A. S. Bondarenko, Potentiodynamic electrochemical impedance spectroscopy of silver on platinum in underpotential and overpotential deposition, Surface Science 566-568, Part 1 (2004) 315–320.

[29] C. M. Pettit, P. C. Goonetilleke, C. M. Sulyma, D. Roy, Combining impedance spectroscopy with cyclic voltammetry: Measurement and analysis of kinetic parameters for faradaic and nonfaradaic reactions on thin-film gold, Analytical Chemistry 78 (2006) 3723–3729.

[30] A. Sabot, S. Krause, Simultaneous quartz crystal microbalance impedance and electrochemical impedance measurements. Investigation into the degradation of thin polymer films, Analytical Chemistry 74 (2002) 3304–3311.

[31] J. Házi, D. M. Elton, W. A. Czerwinski, J. Schiewe, V. A. Vicente-Beckett, A. M. Bond, Microcomputer-based instrumentation for multi-frequency Fourier transform alternating current (admittance and impedance) voltammetry, Journal of Electroanalytical Chemistry 437 (1997) 1–15.

[32] J. Schiewe, J. Házi, V. A. Vicente-Beckett, A. M. Bond, A unified approach to trace analysis and evaluation of electrode kinetics with fast Fourier transform electrochemical instrumentation, Journal of Electroanalytical Chemistry 451 (1998) 129–138.

[33] K. Darowicki, P. Ślepski, Dynamic electrochemical impedance spectroscopy of the first order electrode reaction, Journal of Electroanalytical Chemistry 547 (2003) 1–8.

[34] O. L. Blajiev, T. Breugelmans, R. Pintelon, H. Terryn, A. Hubin, Potentiodynamic EIS investigation of the 2-methyl-5-mercapto-1,3,4-thiadiazole adsorption on copper, Electrochimica Acta 53 (2008) 7451–7459.

[35] G. S. Popkirov, E. Barsoukov, R. N. Schindler, Investigation of conducting polymer electrodes by impedance spectroscopy during electropolymerization under galvanostatic conditions, Journal of Electroanalytical Chemistry 425 (1997) 209–216.

[36] J. E. Garland, K. A. Assiongbon, C. M. Pettit, S. B. Emery, D. Roy, Kinetic analysis of electrosorption using fast Fourier transform electrochemical

impedance spectroscopy: underpotential deposition of Bi^{3+} in the presence of coadsorbing ClO_4^- on gold, Electrochimica Acta 47 (2002) 4113–4124.

[37] G. A. Ragoisha, A. S. Bondarenko, Potentiodynamic electrochemical impedance spectroscopy for solid state chemistry, Solid State Phenomena 90-91 (2003) 103–108.

[38] G. A. Ragoisha, A. S. Bondarenko, Potentiodynamic electrochemical impedance spectroscopy. Copper underpotential deposition on gold, Electrochemistry Communications 5 (2003) 392–395.

[39] G. A. Ragoisha, A. S. Bondarenko, Potentiodynamic electrochemical impedance spectroscopy, Electrochimica Acta 50 (2005) 1553–1563.

[40] A. S. Bondarenko, G. A. Ragoisha, Variable Mott-Schottky plots acquisition by potentiodynamic electrochemical impedance spectroscopy, Journal of Solid State Electrochemistry 9 (2005) 845–849.

[41] A. S. Bondarenko, G. A. Ragoisha, Inverse problem in potentiodynamic electrochemical impedance, in: A. L. Pomerantsev (Ed.), Progress in Chemometrics Research, Nova Science Publishers: New York, 2005, pp. 89–102.

[42] A. Lasia, Electrochemical impedance spectroscopy and its applications, in: B. E. Conway (Ed.), Modern Aspects of Electrochemistry, volume 32, Kluwer Academic Publishers, 2002, pp. 143–249.

[43] R. Durand, Extension de l'étude du système $H^+ \mid H \mid \frac{1}{2}H_2(Pt)$ vers les hautes fréquences, Electrochimica Acta 24 (1979) 1095–1100.

[44] E. Sibert, R. Faure, R. Durand, Pt(111) electrosorption impedance in mixed electrolyte, Journal of Electroanalytical Chemistry 528 (2002) 39–45.

[45] B. E. Conway, J. Barber, S. Morin, Comparative evaluation of surface structure specificity of kinetics of UPD and OPD of H at single-crystal Pt electrodes, Electrochimica Acta 44 (1998) 1109–1125.

[46] S. Morin, H. Dumont, B. E. Conway, Evaluation of the effect of two-dimensional geometry of Pt single-crystal faces on the kinetics of upd of H using impedance spectroscopy, Journal of Electroanalytical Chemistry 412 (1996) 39–52.

[47] Z. Kerner, T. Pajkossy, Measurement of adsorption rates of anions on Au(111) electrodes by impedance spectroscopy, Electrochimica Acta 47 (2002) 2055–2063.

[48] H. Uchida, M. Hiei, M. Watanabe, Electrochemical quartz crystal microbalance study of copper adatoms on Au(111) electrodes in solutions of perchloric and sulfuric acid, Journal of Electroanalytical Chemistry 452 (1998) 97–106.

[49] V. Rooryck, F. Reniers, C. Buess-Herman, G. A. Attard, X. Yang, The silver upd on gold(111) revisited, Journal of Electroanalytical Chemistry 482 (2000) 93–101.

[50] H.-G. Choi, P. E. Laibinis, Electrochemical detection of chloride by underpotentially deposited silver films on polycrystalline gold, Analytical Chemistry 76 (2004) 5911–5917.

[51] H. Uchida, N. Ikeda, M. Watanabe, Electrochemical quartz crystal microbalance study of copper adatoms on gold electrodes Part II. Further discussion on the specific adsorption of anions from solutions of perchloric and sulfuric acid, Journal of Electroanalytical Chemistry 424 (1997) 5–12.

[52] J. Sackmann, A. Bunk, R. Pötzschke, G. Staikov, W. Lorenz, Combined in situ SPM and EIS studies of Pb UPD on Ag(111) and Ag(100), Electrochimica Acta 43 (1998) 2863–2873.

[53] J. D. Porter, T. O. Robinson, Surface diffusion of silver at the silver (111) | liquid-water interface from electrocrystallization measurements, The Journal of Physical Chemistry 97 (1993) 6696–6709.

[54] A. Berná, V. Climent, J. M. Feliu, New understanding of the nature of OH adsorption on Pt(111) electrodes, Electrochemistry Communications 9 (2007) 2789–2794.

[55] J. Clavilier, A. Rodes, K. ElAchi, M. A. Zamakhchari, Electrochemistry at platinum single-crystal surfaces in acidic media - hydrogen and oxygen-adsorption, Journal de Chimie Physique et de Physico-Chimie Biologique 88 (1991) 1291–1337.

[56] G. A. Ragoisha, N. P. Osipovich, A. S. Bondarenko, J. Zhang, S. Kocha, A. Iiyama, Characterisation of the electrochemical redox behaviour of Pt electrodes by potentiodynamic electrochemical impedance spectroscopy, Journal of Solid State Electrochemistry 14 (2010) 531–542.

[57] J. Greeley, Structural effects on trends in the deposition and dissolution of metal-supported metal adstructures, Electrochimica Acta 55 (2010) 5545–5550.

[58] T. Pajkossy, D. M. Kolb, On the origin of the double layer capacitance maximum of Pt(111) single crystal electrodes, Electrochemistry Communications 5 (2003) 283–285.

[59] A. S. Bondarenko, G. A. Ragoisha, N. P. Osipovich, E. A. Streltsov, Potentiodynamic electrochemical impedance spectroscopy of lead upd on polycrystalline gold and on selenium atomic underlayer, Electrochemistry Communications 7 (2005) 631–636.

[60] T. Pajkossy, Impedance of rough capacitive electrodes, Journal of Electroanalytical Chemistry 364 (1994) 111–125.

[61] R. S. Neves, E. D. Robertis, A. J. Motheo, Capacitance dispersion in EIS measurements of halides adsorption on Au(210), Electrochimica Acta 51 (2006) 1215–1224.

[62] T. Pajkossy, Capacitance dispersion on solid electrodes: anion adsorption studies on gold single crystal electrodes, Solid State Ionics 94 (1997) 123–129.

[63] A. J. Motheo, J. R. Santos, Jr, A. Sadkowski, A. Hamelin, The gold (210) | perchloric acid interface: impedance spectroscopy, Journal of Electroanalytical Chemistry 397 (1995) 331–334.

[64] A. Sadkowski, A. J. Motheo, R. S. Neves, Characterisation of Au(111) and Au(210) | aqueous solution interfaces by electrochemical immittance spectroscopy, Journal of Electroanalytical Chemistry 455 (1998) 107–119.

Part IV

INFLUENCE OF CAESIUM AND SODIUM CATIONS ON THE ELECTROCHEMICAL BEHAVIOUR OF PLATINUM IN ACID MEDIA

Platinum electrodes have been investigated in sulfuric acid solutions in the presence and absence of Cs^+ and Na^+ ions by Electrochemical Impedance Spectroscopy (EIS) and Electrochemical Quartz Crystal Nanobalance (EQCN). First an unusual potential dependence of the quartz crystal frequency response has been observed in the presence of Cs^+ ions. The frequency decrease is more pronounced in the region of the underpotential deposition of hydrogen, and the frequency decrease in the double layer region diminishes as the concentration ratio of Cs^+ and H^+ ions increases. After immersion in Cs_2SO_4 solutions the frequency change was higher than that expected taking into account the effect of variation in density and viscosity. EIS, CV, and electrochemical nanogravimetry were used *i*) to elucidate the models of the interface between polycrystalline Pt and the electrolytes in a wide range of electrode potentials and, *ii*) to resolve contributions originating from adsorbed *H, (bi)sulfate, *OH, and *O as well as the cations to the overall interface status. Using impedance analysis it was possible to separate at least two adsorption processes: (bi)sulfate and hydrogen adsorption. The nanogravimetry additionally suggests specific adsorption of Cs^+ at Pt surface. Specifically adsorbed alkali cations, however, are desorbed by the onset of *OH(*O) adsorption at the Pt surface. Nevertheless, the cations likely remain in the close proximity to the surface, probably in the second H_2O layer, and largely contribute to the formation of the *OH and *O adsorbed species originating from the surface water.

The chapter is based on the following articles:

— B. B. Berkes, G. Inzelt, A. Székely, *Electrochemistry Communications* **12** (2010) 1095-1098.

— B. B. Berkes, G. Inzelt, W. Schuhmann, A. S. Bondarenko, *The Journal of Physical Chemistry C* **116** (2012) 10995-11003.

4

EFFECT OF ALKALI CATIONS ON PLATINUM ELECTRODES

4.1 INTRODUCTION

A phase boundary between platinum electrodes and liquid electrolytes plays a role of a model system in physical chemistry and electrochemistry [1]. The importance of these systems primarily originates from the fact that Pt demonstrates exceptionally good catalytic activity toward numerous technologically important reactions [2–4].

Adsorption energies for reaction intermediates at Pt surfaces are very close to the optima for oxygen reduction (ORR), hydrogen evolution (HER), and H_2 oxidation (HOR), making Pt highly active toward these catalytic processes vital for future energy production [5, 6]. From this point of view, understanding of adsorption phenomena at the Pt/electrolyte interface is of increasing importance. Particularly, characterization of adsorption dynamics for different adsorbates like *H, *OH, and *O (where * denotes adsorbed species) at Pt surfaces is critical as they are also intermediates in many important electrocatalytic reactions, including the ORR, HER, and HOR.

It is well-known that the presence of anions like SO_4^{2-} or Cl^- and their complex interactions with electrode surfaces strongly influences catalytic reactions at the interface [7–10]. Specific adsorption of (bi)sulfates significantly affects, for example, the ORR, if compared with acidic perchlorate solutions. However, not only specifically adsorbing anions can influence catalytic activities of the electrodes. It has been recently demonstrated that the nature of cations such as Li^+, Na^+, K^+, and Cs^+ also controls the activity of a number of reactions, particularly the ORR in alkaline solutions. It means that, to understand electrocatalytic trends in the ORR, HER, and HOR as well as some other reactions on Pt surfaces, noncovalent interactions at the interface should be considered as well [11].

Polycrystalline Pt electrodes in sulfate-containing media are widely used in many electrochemical and electrocatalytical studies to perform "blank" and model experiments. Therefore, it is critical to understand the contribution of both (bi)sulfates and alkali cations to the overall interface status in a wide range of electrode potentials covering *i*) the hydrogen adsorption region, *ii*) the so-called double layer region, and *iii*) *OH and *O adsorption region.

Platinum is one of the most thoroughly studied and used electrode materials [12–32]. In these studies several techniques such as EQCN [13, 15–21, 23–25], radiotracer method [12, 26, 27, 33], FTIR [28] and Raman [29] spectroscopies, sum frequency generation [30], and contact electric resistance [22] have been used. Significant progress has been made to understand the nature of adsorbing species at different potentials, highlighting that the phenomena which take place at the Pt surface are very complex [16, 17, 22, 34–37]. Nonetheless there are still numerous open questions concerning the properties of this precious

metal, for instance even the problem of the nature of the strongly and weakly adsorbed hydrogen has not been solved entirely, yet [38, 39]. The diversity of the ideas is partially due to the fact that the behaviour of the platinum electrode in the hydrogen UPD region strongly depends on the prehistory of the platinum sample, especially the previous oxide formation [12, 13, 16, 24].

Figure 4.1 shows a typical cyclic voltammogram and frequency change curve of a platinum electrode.

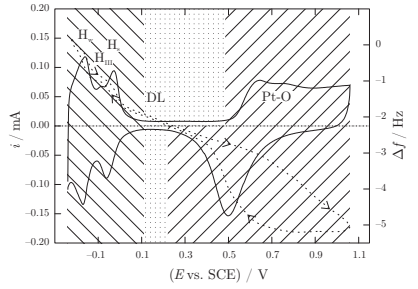

Figure 4.1: A typical cyclic voltammogram and frequency change curve of a platinum electrode in $1\,\mathrm{mol\,dm^{-3}}$ H_2SO_4, scan rate: $50\,\mathrm{mV\,s^{-1}}$.

On the basis of these curves supplemented by results from the literature a concise and comprehensive summary will be given in the following concerning the electrochemical behaviour of Pt in acid sulphuric media. In some works [24, 40, 41] peculiarities of the frequency response of the electrode have been observed which were assigned to different reasons, e.g. to the extensive use of the electrode and consequently the changes of the electrode structure; however, the explanations are contradictory, especially when completely opposite EQCN response has been reported [40]. In the course of our rather extensive studies none of these effects have been observed for a well-working electrode. Irregular behaviour has been observed only as an experimental artefact, e.g. when the contact between the platinum layer and the quartz became poor. Therefore, we restrict our discussion to the regular behaviour. Three distinct regions can be identified on the cyclic voltammograms. These are denoted with the differently striped areas.

The first one between ca. -0.24 V - 0.1 V is the hydrogen adsorption-desorption region. Starting at -0.24 V and going to the positive potentials oxidative desorption of hydrogen takes place. This results in two characteristic peaks, connected to weakly and strongly bonded hydrogens. These peaks are marked with H_w and H_s, respectively, in the figure. Often also a so-called third anodic hydrogen peak (H_{III}), is observed at a potential between the strongly and weakly bonded hydrogen peaks. It is well known that on polycrystalline platinum, multiple adsorption states are possible due to the adsorption on different crystal planes (e.g. (100), (110) and (111)). The voltammetric profile of the polycrystalline platinum electrode contains the contributions from all the sites present on the surface According to Solla-Gullón et al. [42] it is possible in principle to deconvolute the voltammetric profile to the contributions from the different crystal sites. It is accepted that the different peak potentials are related to the different bonding energies. Along with the desorption of hydrogen adsorption of water

and anions occurs, which process is manifested in the decreasing branch of the frequency curve. This frequency decrease could not be assigned to the removal of adsorbed hydrogen since it would cause a frequency increase, even though a small one due to the small molar mass of the hydrogen [14]. So the only reasonable explanation found so far is the mentioned anion and water adsorption to the places / surface sites becoming vacant when hydrogen gets removed.

Specific adsorption of (bi)sulfates also takes place. However, the nature of the adsorbed anion, either sulfate or bisulfate, still remains unclear as it is difficult to distinguish experimentally between these two possible adsorbed species. Density Functional Theory (DFT) calculations using the (111) model surfaces indicate, however, that at lower potentials bisulfate dominates, while at higher potentials there is a conformational change – deprotonation of the adsorbed HSO_4^- leads to a strong binding of the sulfate ion to a 3-fold site on the Pt(111) [43]. Other studies refine that the sulfate ion loses ca. 0.4 electron toward the metal and most of that charge comes from the noncoordinated oxygen atoms. However, the exact value would also depend on the electrode potential [27, 44].

The results of the radiotracer experiments [26, 33] showed that adsorption of (bi)sulfate at polycrystalline Pt starts almost simultaneously with the oxidation of the adsorbed hydrogen and continues after all adsorbed hydrogen is oxidized. Moreover, the positions of the peaks of anion and hydrogen adsorption/desorption are close to each other as monitored using ^{35}S-labeled H_2SO_4 [26]. At the Pt(111), this technique detects the anion adsorption at more positive potentials compared to the polycrystalline samples [27]. Water adsorption has also been considered simultaneously with or without the adsorption of anions [15, 16, 19–21, 23, 24, 31].

In the cathodic part of the region underpotential deposition of hydrogen to the platinum surface takes place. This is a spontaneous dissociation (dissociative chemisorption) of H_2 molecule at Pt resulting in the formation of Pt−H species.

$$Pt + H_2 \rightleftharpoons 2\,Pt{-}H \tag{4.1}$$

Owing to the not too high Pt−H bond energy, the exchange current of the following electrode reaction

$$H_2 + H_2O \rightleftharpoons 2\,H_3O^+ + 2\,e^- \qquad E^\ominus = 0\,V \tag{4.2}$$

is high and the electrode process is electrochemically reversible. It is the very reason why the hydrogen electrode is widely used as a reference electrode, and the standard hydrogen electrode (SHE) has been chosen as the primary standard in electrochemistry [45, 46]. The standard potential of an electrode reaction (standard electrode potential) is defined as the value of the standard potential of a cell reaction when that involves the oxidation of molecular hydrogen to solvated (hydrated) protons (hydrogen ions) according to Equation 4.2. The standard state is the hypothetical ideal solution of molality $1\,mol\,kg^{-1}$ (or the relative activity of H_3O^+, $a_{H_3O^+} = 1$) at standard pressure. The standard pressure is 1 bar (earlier it was 1 atm which is 1.013 25 bar, however, the shift is only 0.000 26 V at the potential scale). By definition, the potential of this electrode is zero.

No third peak could be ever observed in between the two underpotential deposition peaks. There are indications in the literature for the presence of an unusual peak in this region; however, it is connected to the overlap of the current responses of a certain type of platinum oxide reduction and hydrogen regions [47]. With respect to the EQCN curve mass decrease is the characteristic process to this region. From the structure of the frequency curve a subsequent hydrogen adsorption and anion / water desorption can be deduced [48].

In respect of the double layer region the adsorption of anions and water molecules (or OH species), reorientation of the water molecules and local viscosity effect have also been discussed [32].

At least two ordered (bi)sulfate adsorbate superstructures appear just before the onset of *OH and *O adsorption, as evaluated recently by electrochemical scanning tunneling microscopy using Pt(111) single crystals [49]. Finally, three adsorbed species, namely, (bi)sulfate, *OH, and *O, can coexist in a wide anodic potential range at polycrystalline Pt in acidic media. However, electrochemical STM measurements could not resolve ordered structures in this region, suggesting that the interface is very dynamic [49].

While the effect of anions have been intensively studied [15, 16, 18, 21, 23, 25], less attention has been paid to the effect of cations. Influence of the nature of alkali cations such as Li^+, Na^+, K^+, and Cs^+ on voltammetric response and infrared spectra of adsorbed (bi)sulfates at Pt(111) electrodes was studied by Feliu and co-workers [50, 51]. Using these measurements, it was proven that cations participate in the formation of the adlayer adsorbed at the Pt surface along with (bi)sulfate anions. It was additionally proposed that the cations have a stabilizing effect to decrease electrostatic repulsion between partially charged (bi)sulfates [51].

However, the behaviour of polycrystalline Pt electrodes in solutions containing different alkali cations shows only a minor variation. The only exception is the Cs^+ ion whose adsorption was revealed by the radiotracer method [33, 52, 53]. In this work we present and interpret the significant deviation from the usual behaviour of platinum that was observed in the presence of Cs^+ ions. First of all we give insight into the deviations from the normal behaviour of Pt in the hydrogen adsorption / desorption region observed by using merely the EQCN technique. Furthermore we compare the influence of two cations, Na^+ and Cs^+, on the adsorption of *H, *OH, and *O at polycrystalline Pt in acidic sulfuric media. To this end we use EIS, cyclic voltammetry, and electrochemical nanogravimetry *i*) to elucidate the models of the interface between polycrystalline Pt and the electrolytes in a wide potential range and *ii*) to resolve contributions originating from adsorbed *H, (bi)sulfate, *OH, and *O as well as the cations to the overall interface status. EIS itself is known as a sensitive electrochemical technique for the in situ investigation of the solid/liquid interface, which enables the resolution of processes taking place simultaneously. We demonstrate that a combination of voltammetry, electrochemical quartz crystal nanobalance, and impedance measurements can provide improved physical insight into the interfacial properties of these systems.

4.2 EXPERIMENTAL

The experimental conditions are described in Chapter 2 in more details. Here only some crucial points are summarized.

Either a Biologic SP-300 or an EF453 potentiostat was used to the measurements. The impedance analysis was carried out with the Biologic potentiostat, the experimental protocol was the same as previously demonstrated (Chapter 3). The potential was scanned stepwise, from -0.65 V to 0.35 V vs a mercury/mercury sulfate electrode. The AC probing frequency range was 30 kHz - 5 Hz (amplitude 10 mV). A capacitive shunt was connected between the reference and counter electrodes to minimize artefacts caused by the potentiostat at high frequencies. The impedance spectra analysis including Kramers-Kronig tests was performed with the EIS Spectrum Analyzer software written by Aliaksandr Bandarenka.

Either the QCM 100 or the QCM 200 quartz crystal microbalance system was used. For some experiments (indicated at the figure caption) platinized platinum electrode was used. Its roughness factor was 19.4. The platinization was carried out by using the usual galvanostatic protocol, i.e. after applying 30 mA cm^{-2} for a short period of time, the platinum deposition was continued with 3 mA cm^{-2} current density. The integral sensitivity of that crystal was $C_f = 3.43 \times 10^7$ Hz cm^2 g^{-1}. The reference electrode was a sodium chloride saturated calomel electrode (SCE) or a potassium sulfate saturated mercury – mercury sulfate electrode (MMS). This is always shown in the figures. Platinum foil was used as counter electrode. The experimental setup for the impedance measurements is shown in Figure 2.5. The cleaning of the electrodes and the glassware is described in Chapter 2.

Cs_2SO_4 was dissolved in H_2SO_4 solution, and these solutions were used to increase the concentration of Cs^+ ions in order to keep the pH more or less constant, except at high Cs^+/H^+ ratios when the Cs_2SO_4 solution was not previously acidified. The density and the viscosity of the solutions were measured by using a Mohr–Westphal balance and an Ostwald viscometer at 25 °C. The values obtained for sulfuric acid of different concentrations were similar to those can be found in the literature [54].

4.3 RESULTS AND DISCUSSIONS

4.3.1 *Effect of Cs^+ on the H adsorption/desorption region*

The effect of the concentration of sulfuric acid is illustrated in Figure 4.2. The cyclic voltammograms shifted along the potential axis due to the variation of the activity of the H^+ ions in the solution (Figure 4.2a). At not too high sulfuric acid concentrations the shift is 59 mV/pH, at high concentrations a deviation of several millivolts was observed due to the change of the junction potential and the activity effect. A slight variation in the amount of the weakly and strongly bonded hydrogen can also be seen. The frequency shifts due to the variation in the density and viscosity (Figure 4.2b) were in accordance with the expected values. The frequency change as a function of potential (Figure 4.2c) reveals

that the mass increase during the oxidative removal of adsorbed hydrogen also occurs in two steps, and continues in the double layer region. The similar curves have been elucidated by the adsorption of water in the hydrogen UPD region and the adsorption of hydrated anions in the double layer region [15]; however, according to the radiotracer results [26, 33] the anion adsorption already starts as the adsorbed hydrogen being oxidized, therefore adsorption of anions should also be considered even in this potential range.

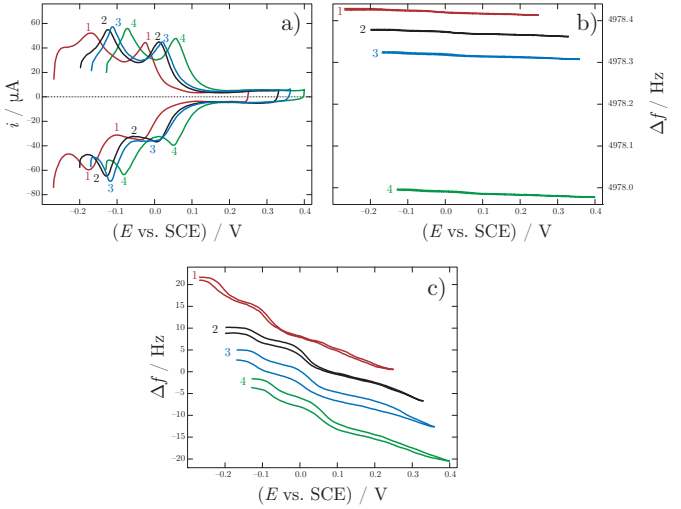

Figure 4.2: The effect of the concentration of sulfuric acid on the cyclic voltammetric (a) and the simultaneously detected EQCN frequency (b) responses at a platinized platinum electrode in contact with (1) 0.1 (2) 0.5 (3) 1 and (4) 4 mol dm^{-3} H_2SO_4. (c) The respective Δf vs. E plots. Scan rate: 2 mV s^{-1}.

The increasing concentration of Cs^+ ions induces several observable changes (Figure 4.3). First, the potential (energy) difference between the weakly and strongly bonded hydrogen decreases. Second, the total amount of the adsorbed hydrogen (i.e. the charge under the voltammetric waves) decreases. While these changes can only be discovered after a closer inspection of the curves, the drastic variation of the EQCN response is striking. The mass change is much higher in the hydrogen UPD region than that is in sulfuric acid solutions, while in the double layer region practically no frequency decrease can be detected at high enough Cs^+ ion concentrations. At low concentration of Cs^+ ions an intermediate response develops and the EQCN curves show a hysteresis. This phenomenon can be explained by the increased H^+ ion concentration at the electrode surface during the oxidation of the adsorbed hydrogen, while during the cathodic scan there is no such effect. After immersion of the Pt electrode in Cs_2SO_4 containing solution the frequency change is higher than that expected taking into account

the change in the density and viscosity of the solutions. From the difference between the expected and the measured frequencies at −0.28 V vs. SCE, assuming that the excess is due to the adsorption of Cs^+ ions, a surface coverage of $\theta = 0.16$ was obtained in the case of the 0.136 mol dm^{-3} Cs_2SO_4 solution. At the lowest concentration, i.e. at 0.029 mol dm^{-3} Cs_2SO_4 $\theta = 0.05$ was calculated, which is in good accordance with the results of the radiotracer experiments [33]. Such a plot is displayed in Figure 4.4.

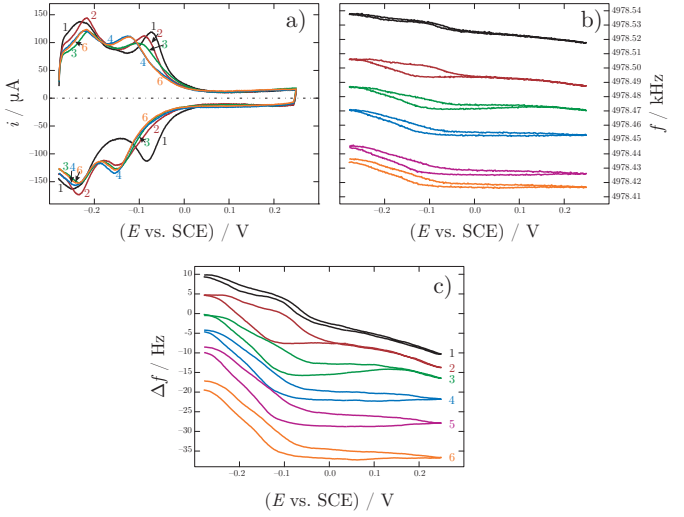

Figure 4.3: The effect of the concentration of Cs_2SO_4 on the cyclic voltammetric (a) and the simultaneously detected EQCN frequency (b) responses for the electrode used in the experiments shown in Figure 4.2 in contact with (1) 0.0 (2) 0.029 (3) 0.056 (4) 0.1 (5) 0.12 and (6) 0.136 mol dm^{-3} Cs_2SO_4; (c) The respective Δf vs. E plots. Scan rate: 5 mV s^{-1}. Sulfuric acid concentrations and the pH values were as follows: (1) 0.05 (2) 0.0765 (3) 0.1 (4) 0.14 (5) 0.133 and (6) 0.127 mol dm^{-3}; pH: (1) 1.56 (2) 1.21 (3) 1.18 (4) 1.16 (5) 1.27 and (6) 1.38. For the sake of clarity curve (5) is not shown in figures (a) and (c).

The deviation at high concentrations (last two values) can be assigned to the higher Cs^+/H^+ ratios since in these cases the concentration was increased by unacidified Cs_2SO_4 solutions. The effect of the pH change plays a minor role, only. The effect observed is certainly depends on the ratio of the concentrations of Cs^+ and H^+ ions, since at high concentrations of sulfuric acid the addition of Cs_2SO_4 results in a minor effect, if any. It follows that the adsorption of these two ions are competitive.

In the presence of Cs^+ ions the charge consumed during the oxidation of adsorbed hydrogen also somewhat decreases with the increasing concentration. The differences between the charges measured for the oxidative removal of ad-

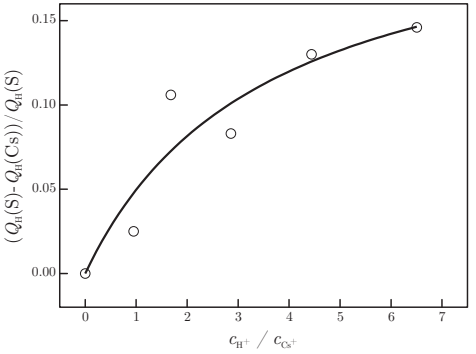

Figure 4.4: The excess frequency difference (Δf) as a function of the concentration of Cs^+ ions. Δf is the difference of the frequencies measured at $-0.28\,\mathrm{V}$ vs. SCE and those calculated from the density and the viscosity of the respective solutions.

sorbed hydrogen in the absence and presence of Cs^+ ions, respectively, in H_2SO_4 solutions divided by the charge observed in sulfuric acid solution in the absence of Cs^+ ions as a function of the concentration ratio of Cs^+ and H^+ are shown in Figure 4.5. At the maximum concentration of Cs^+ ions applied $\theta = 0.12$ can be calculated, which is in good accordance with the value derived from the EQCN frequency change.

From the plots of the mass change vs. charge consumed in the hydrogen UPD region and double layer region the calculated values of the apparent molar masses of the adsorbed species (M) were practically the same in the case of $0.05 - 1\,\mathrm{mol\,dm^{-3}}$ sulfuric acid solutions ($M = 5 - 6\,\mathrm{g\,mol^{-1}}$), however, substantial difference was observed when Cs^+ ions were present in a concentration of $0.136\,\mathrm{mol\,dm^{-3}}$ ($M = 15 - 16\,\mathrm{g\,mol^{-1}}$). The higher M value that was calculated in the case of Cs^+ ion containing solutions indicates that less water molecules and more HSO_4^- ions were adsorbed during the oxidation of the adsorbed hydrogen. In the literature very diverse values have been reported depending on the experimental conditions [15, 16, 24, 25, 32]. It is a consequence of the fact that the charge used in this calculation is related to the oxidation of adsorbed hydrogen while water adsorption occurs. The adsorption of a neutral species is only indirectly related to the oxidative removal of the hydrogen from the surface, and the number of water molecules adsorbed may be substantially less than the number of hydrogen atoms desorbed. Furthermore, there are experimental evidences that water molecules adsorb even on the hydrogen-covered electrode [24, 30, 31], therefore the one to one replacement of H atoms by H_2O molecules cannot be considered. In the double layer region in sulfuric acid solutions the M value obtained is close to the molar mass of HSO_4^- ions; however, in this case the experimental error is rather high since the charge is small.

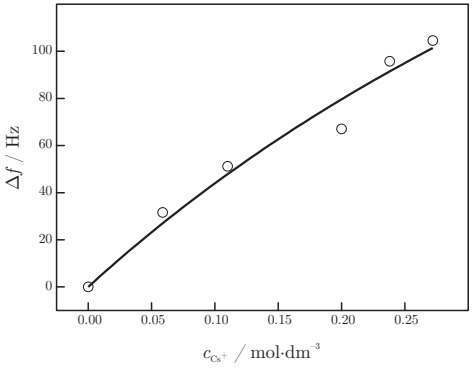

Figure 4.5: The difference between the charges measured for the oxidative removal of adsorbed hydrogen in the absence (S) and presence of Cs^+ ions (Cs) in H_2SO_4 solutions related to the charge observed in the sulfuric acid solution (S) as a function of the concentration ratio of Cs^+ and H^+ ions. The continuous lines are fitting curves by using a Langmuir-type equation: $y = a \times b \times x/(1 + b \times x)$.

4.3.2 *Influence of Cs^+ and Na^+ on specific adsorption of *OH, *O, and *H*

It was found that the increase in Cs^+ ion concentration has a significant effect on Pt in a wider potential range, too. A typical example is shown in Figure 4.6 for the case of Pt electrodes in solutions of $0.05\,\mathrm{mol\,dm^{-3}}$ H_2SO_4 containing $0.05\,\mathrm{mol\,dm^{-3}}$ of either Na_2SO_4 or Cs_2SO_4, respectively. Voltammograms and massograms are significantly affected by the nature of alkali cations. Large differences are noticeable in the voltammograms in the potential region between around -0.55 and $-0.4\,\mathrm{V}$ and between around 0.0 and 0.25 V. In the presence of Cs^+, the onsets of *H and *OH(*O) adsorption are shifted toward more negative and more positive potentials, respectively. However, only in the former case, this shift corresponds to the prominent differences in the deposited mass between the Cs^+- and Na^+-containing electrolytes, with the maximum difference between the $\Delta f(E)$ values at around $-0.4\,\mathrm{V}$. No significant differences between the two $\Delta f(E)$ dependences are seen in the potential region of *OH and *O adsorption/desorption between about 0.0 and 0.35 V.

The effects of Cs+ on *H adsorption/desorption dynamics were investigated in the previous section. It was found that the increase in Cs^+ concentration resulted in a more pronounced shift in the onset of *H adsorption and larger differences in the $\Delta f(E)$ dependences compared to pure H_2SO_4 solutions. The effects were explained by the specific adsorption of Cs^+ ions on the Pt surface. At more positive potentials, however, desorption of the Cs^+ ions starts and the mass change caused by the desorption of Cs^+ ions and the adsorption of (bi)sulfate ions compensate each other. The differences in the voltammetry and electrogravimetric data between the Cs^+- and Na^+-containing electrolytes (Fig-

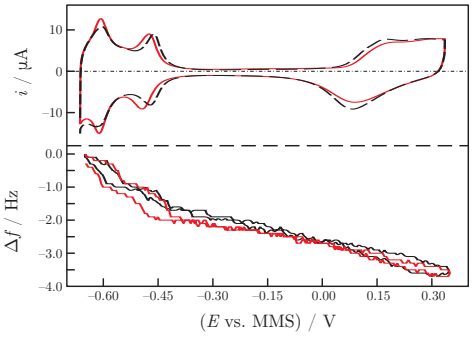

Figure 4.6: Cyclic voltammograms and corresponding electrogravimetric data of the polycrystalline Pt electrode in the 0.05 mol dm^{-3} H_2SO_4 electrolyte containing 0.05 mol dm^{-3} of either Na_2SO_4 or Cs_2SO_4. $dE/dt = 5\,mV\,s^{-1}$.

ure 4.6) can be explained analogously. However, in the following, our primary goal is to distinguish different constituents of the adsorption processes using the EIS measurements and to monitor the interface status in more detail.

4.3.3 *Modelling of Specific Adsorption at Pt Electrodes*

In the following, theoretical background will be presented which is necessary for the impedance data analysis and elucidation of the Pt/electrolyte interface model in terms of equivalent electrical circuits (EECs). In the electrode potential region that is of interest for this study (see Figure 4.6), several adsorption/desorption processes can take place: namely, adsorption of *H, (bi)sulfates, *OH, and *O, as well as some alkali cations. High concentrations of all the electrolyte components used in this work (0.05 mol dm^{-3} H_2SO_4 containing 0.05 mol dm^{-3} of either Na_2SO_4 or Cs_2SO_4) allow one to neglect possible contributions of diffusional mass transport.

When small AC perturbation signals are applied to a system where reversible single-stage surface limited adsorption occurs, the Faradaic current, i, and the adatom coverage, θ, oscillate around quasi-steady-state values. The linear part of the response assigned to the adsorption process can be written as [55–58]

$$\Delta i = \left(\frac{\partial i}{\partial E}\right)\Delta E + \left(\frac{\partial i}{\partial \theta}\right)\Delta\theta \tag{4.3}$$

where Δ corresponds to parameters that oscillate during AC probing. If the current due to specific adsorption and the current of double layer charging are assumed to be additive, then the solution of Equation 4.3 leads to the classical model of reversible adsorption (see related examples in for example refs [55–59]) with interfacial impedance, Z, given by

$$Z(j\omega) = R_s + \left((j\omega)^n C'_{DL} + \frac{1}{R_{ct} + (j\omega C_a)^{-1}}\right)^{-1} \tag{4.4}$$

where ω is the angular frequency, C'_{DL} and the exponent n describe the response of the double layer (discussed in Section 4.3.4), $R_{ct} = 1/(\partial i/\partial E)$ is the charge transfer resistance, $C_a = -q_a(\partial\theta/\partial E)$ is the adsorption capacitance, q_a is the charge necessary to form an adsorbate layer, R_s is the electrolyte resistance, and j is the imaginary unit. The adsorption model described by the Equation 4.4 does not show any continuous pathways for the DC current at $\omega \to 0$. This is in agreement with the fact that the DC current of the surface limited adsorption (like *H or anion adsorption) in the steady state is zero. This model; however, accepts a DC current to flow at non-steady-state conditions, for example, in a potentiodynamic scan, enabling the adsorption capacitance to charge. In classical impedance experiments, the ability to distinguish between contributions of the double layer and the adsorption capacitance C_a will depend on the R_{ct}. For a very fast adsorption, R_{ct} is small and the double layer response will effectively incorporate C_a.

If two adsorption processes with significantly different time constants occur simultaneously [56, 57], the interfacial impedance can be described by the following equation:

$$Z(j\omega) = R_s + \left((j\omega)^n C'_{DL} + \frac{1}{R_{ct,1} + (j\omega C_{a,1})^{-1}} + \frac{1}{R_{ct,2} + (j\omega C_{a,2})^{-1}} \right)^{-1} \quad (4.5)$$

where parameters $R_{ct,1}$ and $C_{a,1}$ and, correspondingly, the parameters $R_{ct,2}$ and $C_{a,2}$ apply to the two different adsorption processes.

All of the above-mentioned situations can be met in the case of polycrystalline Pt electrode in sulfate electrolytes. Figure 4.7 summarizes physical models in terms of equivalent electrical circuits that have been used in the literature for the Pt | electrolyte interface at different electrode potentials [56–58, 60].

The model shown in Figure 4.7a was found [56] to describe the electrochemical interface in the presence of *H and (bi)sulfate specific adsorption at Pt electrodes, as both adsorption processes have significantly different time constants (the impedance of the model is described by Equation 4.5). The model shown in Figure 4.7b mainly accounts for the (bi)sulfate adsorption/desorption in the potential region prior to the onset of *OH and *O adsorption (the impedance of the model is described by Equation 4.4). This is especially important to be taken into account in the case of polycrystalline Pt electrodes as, for example, the completion of the (bi)sulfate adsorption is systematically shifted toward more positive potentials with the increase of (111)-step density at the Pt surface [1, 61]. Separation of the responses of the double layer and fast *OH adsorption/desorption in classical EIS experiments is questionable: the measurements using the common frequency ranges and electrodes cannot distinguish those constituents. In this case, the double layer impedance apparently incorporates the major part of the *OH adsorption response, as discussed above. On the other hand, the major part of the Faradaic response of the "irreversible" *O adsorption will be lost in a relatively slow EIS experiment [62]. Therefore, application of the model shown in Figure 4.7c (i.e. appearance of the $R_{ct} - Z_f$ combination in parallel to the double layer impedance) depends on many factors, including electrolyte composition, electrode surface status, and time required to record the EIS data.

From the analysis of models presented in Figure 4.7, it is evident that the model shown in Figure 4.7a is formally applicable in the whole potential range

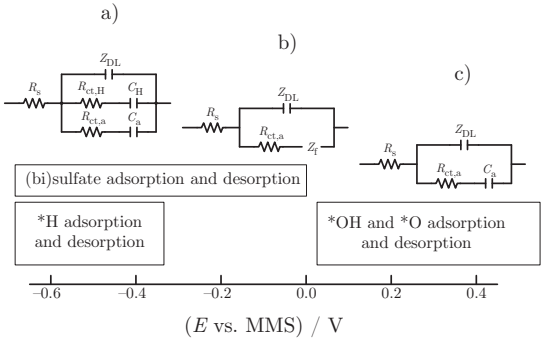

Figure 4.7: Physical models (in terms of equivalent electrical circuits) of the Pt/electrolyte interface in sulfate media proposed in the literature for different electrode potential regions [56–58, 60]. R_s, electrolyte resistance; Z_{DL}, impedance of the double layer; C_H and C_a, adsorption capacitances; R_{ct}, $R_{ct,\,H}$, and $R_{ct,\,a}$, charge transfer resistances; Z_f, an additional impedance depending on system reversibility and the mechanism of adsorption (in the simplest case, it is equivalent to the adsorption capacitance impedance)[60].

of interest. If the electrode potential is more positive than the *H adsorption region, the corresponding $R_{ct,\,H}$ and C_H values would increase the total impedance of the corresponding branch to infinity ($R_{ct,\,H} \rightarrow 0$, $C_H \longrightarrow 0$). The latter situation would be equivalent to the model depicted in Figure 4.7b. Consequently, if the (bi)sulfates form a "saturated" adlayer at the surface at higher potentials, the $-q_a(\partial\theta/\partial E)$ term determining the adsorption capacitance would approach 0 and the model in Figure 4.7a would be equivalent to a simple series combination of the electrolyte resistance R_s and the double layer impedance Z_{DL}. Implementation of a stable fitting algorithm [63] can provide an opportunity to use only one model to adequately fit large sets of EIS data in an automatic mode in the whole potential range of interest.

4.3.4 *Impedance Response of the Double Layer in Presence of Specific Adsorption*

Two interfacial parameters determine the double layer capacitance: the apparent dielectric constant of the structured H_2O layer close to the electrode surface and the apparent double layer thickness. Both parameters can change as a result of reorientations of the surface water molecules or the specific adsorption and, therefore, affect the capacitance values.

EIS data of solid electrodes; however, demonstrate that the double layer can exhibit so-called "frequency dispersion" [55] in a wide range of electrode potentials. This means that the measured values of the double layer capacitance

change with the probing AC frequency. To describe this effect, a constant phase element (CPE) is used with the following equation for the impedance [64, 65]

$$Z_{DL} = C_{DL}^{'\,-1}(j\omega)^{-n} \tag{4.6}$$

where $C_{DL}^{'}$ is the pre-exponential parameter of the CPE, which is proportional to the double layer capacitance of pure capacitive electrodes, and the exponent n is the parameter $(0.5 \leq n \leq 1)$ which is directly related to the dispersive behaviour.

The existence of the CPE indicates a time-constant dispersion at the electrode surface. This dispersion can be attributed to distributions of time constants along either the surface of the electrode (2D distribution) or along the axis normal to the electrode surface (3D distribution). A 2D distribution could arise from many factors like geometry-induced non-uniform current and potential distributions, distortion of the double layer by Faradaic reactions, grain boundaries, different crystal faces on a polycrystalline electrode, or other local variations in surface properties [66].

Recently, the frequency dependence of the double layer was investigated using metal single crystals [62, 67–71]. The main results of these studies are *i*) the parameters of the CPE are dependent on the electrode potential, *ii*) there is a strong correlation between the capacitance dispersion and 2D phase transitions in the adsorbed layers, and *iii*) the value of n can be significantly lower than 1 if ordering in the adsorbate layer occurs .

Taking into account the above-mentioned findings, one can expect a 2D time-constant distribution at the Pt surface. The latter can be caused e.g. by a formation of ordered layers of (bi)sulfates or other anions (cations). One example is given in Figure 4.8 showing a model of the sulfate adlayer superstructure $(\sqrt{3} \times \sqrt{7})R19.1^{\circ}$ with coadsorbed H_2O formed at Pt(111) facets in H_2SO_4 electrolytes [49].

A closer look at the Figure 4.8a can identify at least three local nonequivalent sites where frequency dispersion can originate from inseparable coupling of the local electrolyte resistances with the capacitances and charge transfer resistances periodically distributed along the surface. Taking into account that different ordered structures can coexist at the same electrode potential (see Section 4.1), the situation can be schematically illustrated with Figure 4.8b in terms of localized equivalent circuits. Similar sequences of the localized equivalent circuits were shown to explain the CPE behavior (see, e.g. references [64, 66]).

An alternative qualitative explanation of the situation in the case of specific adsorption is as follows. Specific adsorption, apart from purely electrostatic forces, result in additional structuring and restructuring of the solvent near the interface with hydrogen bond breaking. This structuring can affect not only the first water layer but at least three layers of H_2O molecules, as has been probed experimentally [72]. This causes nonuniform potential and current distribution at the surface (either 2D or in some cases 3D) as discussed above. Moreover, it is less likely that the interfacial double layer would respond to the AC probing completely reversibly if ordered adsorbate structures appear at the surface. Surface ordering would cause a relatively slow exchange of ions between the outer and inner Helmholtz planes and slow reorientation of H_2O molecules [67], as

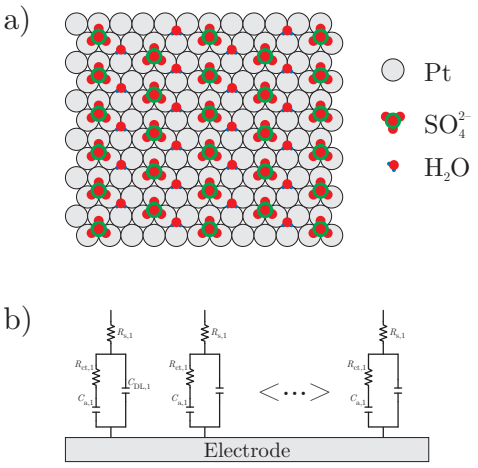

Figure 4.8: (a) Model of the sulfate adlayer superstructure ($(\sqrt{3} \times \sqrt{7})R19.1°$) with coadsorbed H_2O formed at Pt(111) facets in H_2SO_4 electrolytes as proposed in reference [49]. (b) Schematic representation of a 2D impedance distribution (in terms of localized equivalent circuits) that can arise from variations in local electrode surface properties [64, 66].

the system is at a local energy minimum. The latter fact will lead to dissipation of the energy of the probing signal and will be responsible for the CPE behavior. There is a simple relationship that links the fraction of the dissipated energy, $\mathrm{Diss}_{\mathrm{CPE}}$, in one harmonic cycle and the CPE exponent n [71]:

$$\mathrm{Diss}_{\mathrm{CPE}}(\%) = \cos(n\pi/2) \times 100\% \tag{4.7}$$

Taking into account common rules applicable to phase transitions, one can expect higher energy losses and, consequently, lower n values close to the disorder/order phase transitions.

It is evident that regularly (structured) or randomly distributed local surface nonuniformities would differently change the exponent of the CPE. Monitoring both C'_{DL} and n as a function of the electrode potential can give additional important information about the interfacial dynamics at Pt electrodes.

4.3.5 *Analysis of Experimental Impedance Data*

A set of impedance data characterizing the electrochemical interface in presence of Cs^+ is shown in Figure 4.9. A similar data set was obtained for the Na^+-containing electrolyte (data are not shown). As discussed in Section 4.3.3, the model depicted in Figure 4.7a with the overall impedance described by Equation 4.5 was tested as a general model of the interface in the whole investigated

potential region. Some of the fitting results at the selected electrode potentials are presented in Figure 4.10a-c.

a) EIS spectra: H-UPD region

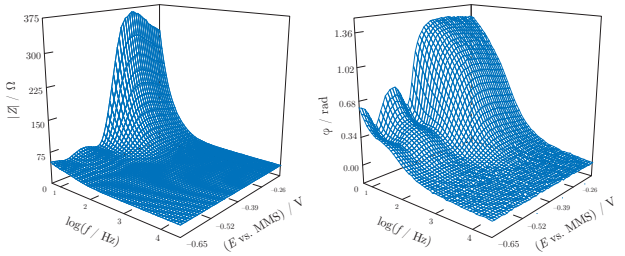

b) EIS spectra: *OH and *O adsorption region

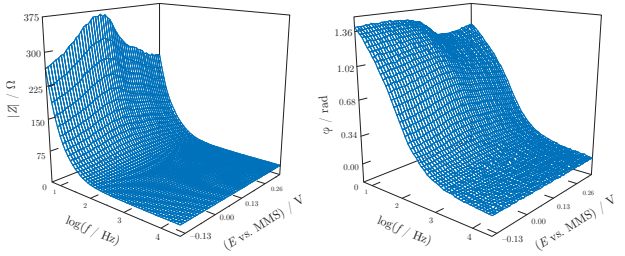

Figure 4.9: Extended Bode plots of the impedance spectra ($|Z|$) and the phase shift φ as a function of frequency f and the electrode potential E) characterizing the polycrystalline Pt electrode in (a) the *H-adsorption region and (b) the *OH and *O adsorption regions. $dE/dt = 0.3\,mV\,s^{-1}$ (anodic scans). Electrolyte: $0.05\,mol\,dm^{-3}$ H_2SO_4 + $0.05\,mol\,dm^{-3}$ Cs_2SO_4.

The model in Figure 4.7a fits well to the experimental data with appropriately low estimated individual parameter errors in the regions where the corresponding parameters have physical meaning. In the *H adsorption region, the EIS data fitting does distinguish two simultaneous adsorption/desorption processes with low estimated individual parameter errors.

To independently verify that it is indeed possible to distinguish at least two adsorption processes and it is not an artifact from the fitting procedure, time-constant distribution functions were obtained from the spectra using differential impedance analysis [73]. The latter does not require any assumptions about the model and gives a distribution of the effective time constants. Figure 4.10d show examples of thus obtained time-constant distribution functions at the potentials where *H and (bi)sulfate adsorption is proven to be possible [26]. At least three fairly separated time constants (related to the double layer and two adsorption

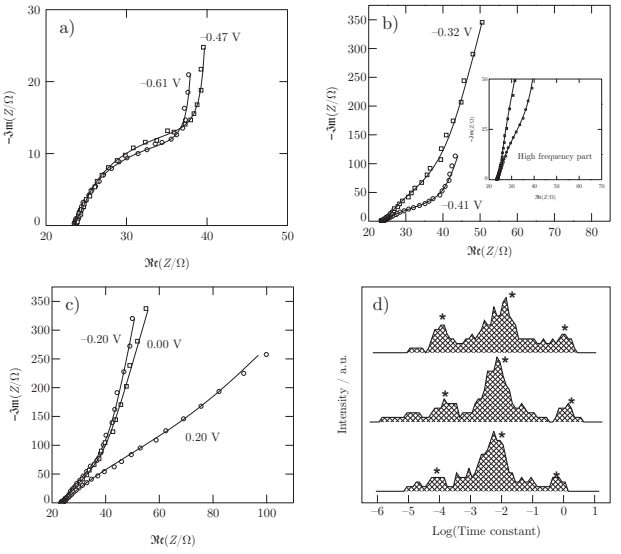

Figure 4.10: (a-c) Examples of the experimental impedance data (open symbols) and the fitting results (solid lines, the equivalent circuit is shown in Figure 4.7a) at some selected electrode potentials, as indicated in the figure. (d) Examples of the effective time-constant distribution functions obtained from the EIS spectra according to the procedure described in ref [73] (*H adsorption potential region).

processes) are distinguishable from the corresponding plots in Figure 4.10d, providing additional evidence that the EEC analysis and the fitting are correct.

Figure 4.11 compares the dependences of the EEC parameters as a function of the electrode potential obtained in $0.05\,\mathrm{mol\,dm^{-3}}$ H_2SO_4 containing either $0.05\,\mathrm{mol\,dm^{-3}}$ Na_2SO_4 or Cs_2SO_4 (electrolyte resistances and charge transfer resistances are not shown to keep simplicity; the $R_s(E)$ values remain essentially constant with the maximum deviations of about $0.15\,\Omega\,\mathrm{cm^2}$, while the charge transfer resistances correlate with the corresponding adsorption capacitances).

Figure 4.11a,b represent the adsorption capacitance dependences, $C_H(E)$ and $C_a(E)$. In the potential region where *H adsorption is possible, the C_H values are more than 1 order of magnitude larger than the corresponding C_a values. Outside the *H adsorption region, the calculated C_H values are very small and basically constant, while the $C_a(E)$ shows a complex dynamics and reveals some adsorption process until about 0.1 V. Such a behavior enables the assignment of the $C_H(E)$ to the *H adsorption/desorption while of the $C_a(E)$ to the (bi)sulfate adsorption/desorption. It is worth noting that features of the $C_a(E)$ dependences between around and -0.3 V and 0.1 V are somehow characteristic for (bi)sulfate adsorption at the stepped Pt electrodes in sulfuric media [1, 61]. However, these

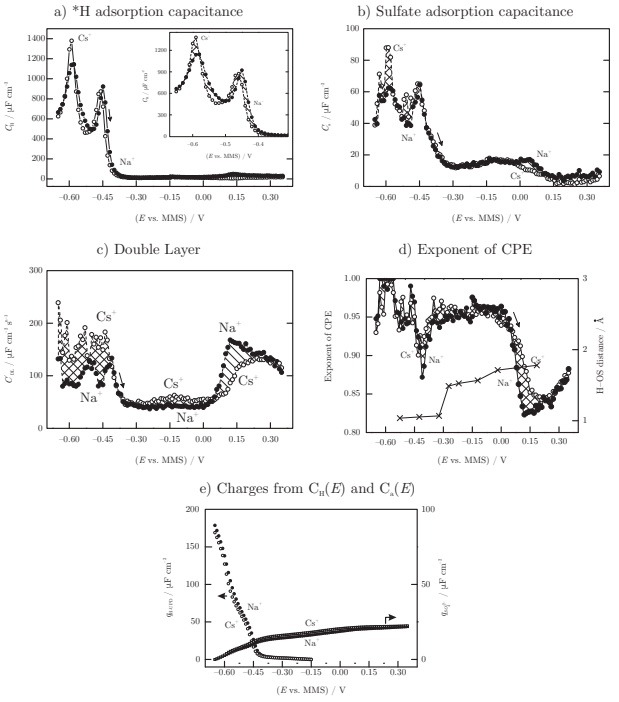

Figure 4.11: (a-d) Equivalent circuit parameter dependences on the electrode potential characterizing the polycrystalline Pt electrode in 0.05 mol dm^{-3} H_2SO_4 containing 0.05 mol dm^{-3} of either Na_2SO_4 or Cs_2SO_4. Plot (d) additionally shows DFT-calculated changes in the H-OS bond distance in the adsorbed (bi)sulfate as reported in ref [43]. (e) Amounts of the adsorbed *H and (bi)sulfates in terms of charges as a function of the potential as calculated from the corresponding adsorption capacitance dependences shown in parts (a) and (b). $dE/dt = 0.3\,\mathrm{mV\,s^{-1}}$ (anodic scans).

features do not clearly appear in the corresponding voltammograms shown in Figure 4.6.

As can be seen from Figure 4.11a, the $C_H(E)$ dependences are significantly affected by the nature of the alkali cation: there is a shift toward more negative potentials in the presence of Cs^+ in a wide potential range between about -0.4 V and -0.6 V, analogous to the voltammograms shown in Figure 4.6. In contrast to that, the $C_a(E)$ dependences (Figure 4.11b) look similar, with the exception of narrow potential regions around -0.6 V and -0.5 V.

Formal integration of the $C_H(E)$ and $C_a(E)$ dependences gives the charges and, hence, the amount of the adsorbed *H and (bi)sulfates, as shown in Fig-

ure 4.11e. While the integration gives almost identical charges for the (bi)sulfate adsorption (the charge difference is less than $2\,\mu C\,cm^{-2}$ at $-0.2\,V$), there is a noticeable mismatch of about $10\,\mu C\,cm^{-2}$ in the case of *H adsorption. As both processes (desorption of *H and adsorption of sulfates) contribute to the anodic charge in the positive potential scan, one can calculate the total anodic charges in the *H adsorption region for the Na^+- and Cs^+-containing electrolytes and compare them with the charges obtained from the corresponding cyclic voltammograms. The resulted charges obtained using adsorption capacitance dependences were around $200\,\mu C\,cm^{-2}$ for the Na^+-containing electrolyte and around $190\,\mu C\,cm^{-2}$ for the Cs^+-containing electrolyte. On the other hand, integration of the cyclic voltammograms (Figure 4.6) between $-0.3\,V$ and $-0.65\,V$ gives the charge of roughly $230\,\mu C\,cm^{-2}$, performing a usual correction to the double layer background charge. Obviously, there is a mismatch in the total charge balance.

However, closer analysis of Figure 4.11c in the potential range between $-0.3\,V$ and $-0.65\,V$ suggests that the above-mentioned mismatch between the voltammetric charges and the charges obtained from the adsorption capacitances originates from the fact that some of the adsorption responses are incorporated into the double layer response. There is a fast constituent of the adsorption (no more than $10-15\%$ of the total adsorption charge) that is not possible to separate from the double layer response using the conditions of the current work.

Estimation of the corresponding interfacial capacitances $C_{DL}(E)$ from the $C'_{DL}(E)$ using the approach summarized in ref [66] eliminates the mismatch in the total charge balance between the EIS and voltammetric experiments for both Cs_2SO_4 and Na_2SO_4 solutions. However, much higher $C'_{DL}(E)$ values in the potential region between $-0.4\,V$ and $-0.65\,V$ for the Cs_2SO_4 solution compared to the Na_2SO_4 one are worth noting.

As was discussed above, the EIS analysis gives roughly the same amount of (bi)sulfates adsorbed at the Pt surface in the anodic scan in both electrolytes. This fact additionally proves that the bigger apparent mass change in the presence of Cs^+ at around $-0.44\,V$ (Figure 4.6) originates from a specific adsorption of Cs^+ cations. Summarizing the data from Figure 4.11 and Figure 4.6, we hypothesize that the differences between the two $C'_{DL}(E)$ dependences in the potential region between $-0.4\,V$ and $-0.65\,V$ (Figure 4.11c) and differences between the *H-charges calculated using the $C_H(E)$ dependences are due to an additional contribution from the fast specific adsorption of Cs^+ competing with the *H adsorption. Accepting this hypothesis, the charge that is associated with the adsorption of Cs^+ is approximately $10\,\mu C\,cm^{-2}$. This charge difference, however, can originate from either the charge transfer to the Cs^+ itself or from the *H, which is largely affected by the specifically adsorbed Cs^+. Considering that the maximal mass difference between two massograms is $\sim 12\,ng\,cm^{-2}$ at $-0.44\,V$ (Figure 4.6), the apparent molar weight of the adsorbing cation is approximately $115\,g\,mol^{-1}$, which is reasonably close to the expected $133\,g\,mol^{-1}$ for Cs^+. The lower apparent molar weight can be either due to the measurement/estimation accuracy or due to Na^+, which might be also involved in the mass balance. The electrogravimetric data shown in Figure 4.6 can also be used to estimate the mass change due to (bi)sulfate adsorption solely. Close to the onset of *OH(*O)

adsorption at around 0.1 V, the overall mass change of about 50 ng cm^{-2} is due to (bi)sulfate adsorption, and it is roughly the same in the case of Cs^+- andNa^+-containing electrolytes. This corresponds to an approximately 0.2 ML coverage, assuming that the (111) facets dominate at the surface of the polycrystalline Pt. The resulting coverage is reasonably close to the one expected for the sulfate adlayer superstructure ($(\sqrt{3} \times \sqrt{7})R19.1°$) with coadsorbed H_2O formed at Pt(111) facets and shown in Figure 4.8a. Taking into account the charge obtained after integration of the $C_a(E)$ dependences (Figure 4.11e), one can estimate that each (bi)sulfate apparently loses about 0.44 electron toward the metal. This fractional electron transfer is in quantitative agreement with the theoretical results and the results obtained using the radioactive labeling method [27, 44], giving 0.4 and 0.3 electron transfer per (bi)sulfate anion, respectively.

One should additionally assign around 30 μC cm^{-2} of the charge that is not possible to separate from the double layer response in *H adsorption region for both Cs_2SO_4 and Na_2SO_4 electrolytes. This charge can originate either from "fast" (bi)sulfate or from "fast" *H adsorption. The former assumption would, however, correct the apparent charge transferred per one adsorbed (bi)sulfate to be ca. 1.04 of the electron charge. If the charge comes from a fast *H, it might likely interact with (bi)sulfates, too. However, this requires additional studies using other in situ techniques.

*OH adsorption/desorption cannot be separated from the double layer response (Figure 4.11a–c). Comparing Figure 4.6 and Figure 4.11c, it is evident that the nature of the alkali cation controls the dynamics of the interface also in the *OH and *O region between around 0.0 V and 0.3 V. However, there is no evidence for a specific adsorption of the cations in this region neither from electrogravimetric measurements nor from EIS analysis. Therefore, it is reasonable to assume that the cation, once desorbed in the anodic scan between around −0.3 V and 0.0 V, remains in the close proximity to the surface, participating in polarization of surface H_2O molecules at higher anodic potentials.

Additional information can be provided by the dependence of the CPE exponent n on the electrode potential, as discussed in Section 4.3.4. Figure 4.11d shows the $n(E)$ dependences for the electrolytes containing Cs^+ and Na^+. Both $n(E)$ dependences correlate with the corresponding $C'_{DL}(E)$ curves in the *OH(*O) adsorption region, while there are no obvious correlations where *H adsorption takes place.

At very cathodic potentials (about −0.65 V), where ordered *H-adsorbed superstructures with the surface H_2O are stable according to DFT calculations [74], the values of the exponent are around 0.95 in Cs^+- and Na^+-containing electrolytes. Surprisingly, between around −0.63 V and 0.56 V, where the most intensive anodic current is observed in the voltammograms, the double layer demonstrates almost ideal capacitive behaviour with n values being very close or equal to 1. There is a pronounced minimum in both $n(E)$ dependences at around −0.41 V, where the values of the exponents are as low as 0.88. This corresponds to about 18.7% of the dissipated energy of the AC probing signal (Equation 4.7). According to Figure 4.11e, the adsorbed (bi)sulfates already dominate at this potential if compared to the other adsorbates. This potential is also very close to the potential where restructuring in the (bi)sulfate layer

occurs, according to DFT calculations [43] (see Figure 4.11d, where the calculated H-OS bond distance of the adsorbed (bi)sulfate is shown as a function of the potential) and electrochemical STM measurements performed using (111) model surfaces [49]. A shift of about 50 mV toward more negative potentials compared to the Pt(111) can be explained by the change in the potential of zero charge of the polycrystalline electrode. It was found using well-defined Pt$[n(111) \times (111)]$ and Pt$[n(111) \times (100)]$ electrodes that the potential of zero charge of the stepped electrodes is systematically shifted toward more negative potentials with increasing the step density [75]. Taking into account theoretical considerations as presented in Section 4.3.4, we attribute the minima of the $n(E)$ curves (Figure 4.11d) at around -0.41 V to the 2D phase transition in the surface (bi)sulfate layer, particularly upon (111) facets of the polycrystalline electrode. Notably, both $n(E)$ curves (Figure 4.11d) remain constant between -0.3 V and 0.0 V with relatively low values of around 0.95. If there would be no effects of additional interface structuring due to adsorbed sulfates, the double layer should have exhibited the ideal capacitive behaviour, like in the potential region between around -0.63 V and 0.56 V.

In the *OH(*O) adsorption region, another fast decrease of the CPE exponent values is observed (Figure 4.11d). At the minima of the $n(E)$ curves at around 0.2 V, almost 25% of the energy of the probing signal is dissipated. Similar to ref [62], we attribute this behaviour to the formation of superstructures involving *OH, *O, sulfates, and, indirectly, alkali cations.

Figure 4.12 schematically summarizes the results of the combined voltammetric, electrogravimetric, and impedance study. This picture uses an assumption that the (111) facets dominate at the surface of the polycrystalline Pt. Therefore, the model in Figure 4.12 is a first approximation, and additional investigations will be necessary using well-defined stepped single crystals to further test this model.

At the potential of about -0.65 V, the existence of ordered superstructures consisting of surface water and adsorbed hydrogen species is probable, as supported by DFT calculations (Figure 4.12a) [74]. When the potential is shifted toward more positive potentials, specific adsorption of both (bi)sulfates and the alkali cations starts playing an important role in the surface dynamics (Figure 4.12b). There is a 2D phase transition in the adsorbed (bi)sulfate layer forming ordered structures similar to that shown in Figure 4.8a upon (111) facets by the potential of approximately -0.3 V. Specifically adsorbed alkali cations are desorbed by the onset of *OH(*O) adsorption. However, they are likely remaining in close proximity to the surface, probably in the second H_2O layer (Figure 4.12c) and contribute to the formation of the *OH and *O adsorbed species from the surface water, as shown in Figure 4.12d.

4.4 CONCLUSIONS

Alone the results of the electrochemical quartz crystal nanobalance experiments furnish evidences that a competitive adsorption of Cs^+ ions and H^+ ions exists in the hydrogen UPD region. The unusual EQCN frequency change in the double layer region can be explained by the desorption of Cs^+ ions, and the simultane-

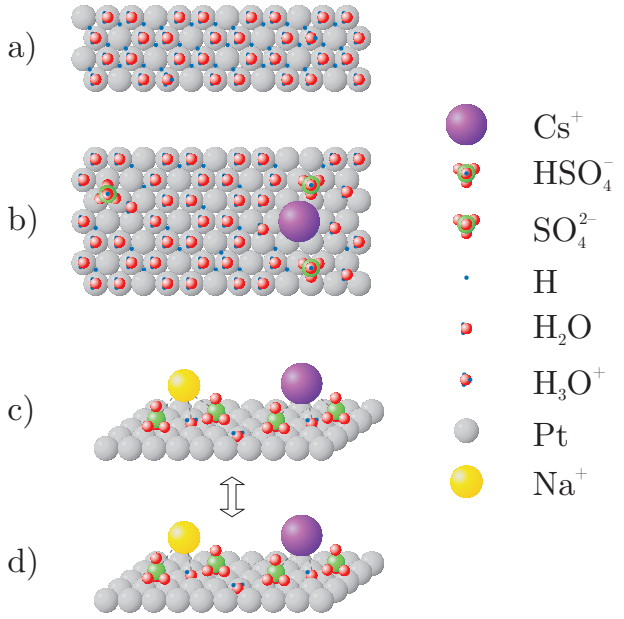

Figure 4.12: Schematic representation of possible adsorbate superstructures formed at (111) facets of Pt electrodes in (a, b) *H adsorption and (c, d) *OH and *O adsorption regions.

ous adsorption of bisulfate and/or sulfate ions as well as water molecules. The cation adsorption on platinum electrode depends on the adsorption ability of the ions, which is the highest in the case of Cs^+, and it is the very reason why this effect cannot be detected in the presence of other alkali metal ions.

The influence of two cations, Na^+ and Cs^+, on the adsorption of *H, *OH, and *O at polycrystalline Pt in acidic sulfuric media has been further investigated. Noncovalent interactions at the interface caused by alkali cations change drastically the interface status, which should be taken into account while model electrocatalytic experiments are performed.

Using impedance analysis it was possible to separate at least two adsorption processes: (bi)sulfate and hydrogen adsorption. Nanogravimetry additionally resolves the contribution from Cs^+. Specific adsorption of Cs^+ at Pt surface significantly affects hydrogen adsorption, while it has almost no effect on the dynamics of sulfate ion adsorption. Specifically adsorbed alkali cations, however, are desorbed by the onset of *OH(*O) adsorption. Nevertheless, they likely remain in close proximity to the surface, probably in the second H_2O layer, and largely contribute to the formation of the *OH and *O adsorbed species from

the surface water. This can be important for the catalytic processes that involve these species as the reaction intermediates.

Additional information is provided by the dependence of the exponent $n(E)$ of the constant phase element, which describes the response of the double electric layer. 2D phase transitions in the adsorbate layer decrease the exponent values, significantly confirming the general observations reported earlier in the literature.

[1] V. Climent, J. M. Feliu, Thirty years of platinum single crystal electrochemistry, Journal of Solid State Electrochemistry 15 (2011) 1297–1315.

[2] J. K. Nørskov, T. Bligaard, J. Rossmeisl, C. H. Christensen, Towards the computational design of solid catalysts, Nature Chemistry 1 (2009) 37–46.

[3] J. P. Meyers, Getting back into gear: Fuel cell development after the hype, Interface 17 (2008) 36–39.

[4] S. Srinivasan, Fuel cells, Springer: New York, 2006.

[5] J. Greeley, T. F. Jaramillo, J. Bonde, I. Chorkendorff, J. K. Nørskov, Computational high-throughput screening of electrocatalytic materials for hydrogen evolution, Nature Materials 5 (2006) 909–913.

[6] G. Hoogers, Fuel Cell Technology Handbook, CRC Press: Boca Raton, FL, 2002.

[7] J. X. Wang, N. M. Markovic, R. R. Adzic, Kinetic analysis of oxygen reduction on Pt(111) in acid solutions: Intrinsic kinetic parameters and anion adsorption effects, The Journal of Physical Chemistry B 108 (2004) 4127–4133.

[8] G. Horányi, State of Art: Present Knowledge and Understanding, volume 1, Wiley-VCH: Weinheim, pp. 349–382.

[9] G. Horányi, G. Inzelt, Study of the adsorption of chloride ions on platinum electrodes from concentrated solutions of H_2SO_4, H_3PO_4 and $HClO_4$, Journal of Electroanalytical Chemistry and Interfacial Electrochemistry 86 (1978) 215–218.

[10] A. Wieckowski, Encyclopedia of Electrochemistry, Plenum: New York London, pp. 65–119.

[11] D. Strmcnik, K. Kodama, D. van der Vliet, J. Greeley, V. R. Stamenkovic, N. M. Marković, The role of non-covalent interactions in electrocatalytic fuel-cell reactions on platinum, Nature Chemistry 1 (2009) 466–472.

[12] G. Horányi, G. Inzelt, The Nickel Group (Nickel, Palladium, and Platinum), in: F. Scholz, C. J. Pickett, A. J. Bard, M. Strattmann (Eds.), Encyclopedia of Electrochemistry, volume 7a, Wiley-VCH, Weinheim, 2006, pp. 497–528.

[13] G. Inzelt, B. B. Berkes, Á. Kriston, Temperature dependence of two types of dissolution of platinum in acid media. an electrochemical nanogravimetric study, Electrochimica Acta 55 (2010) 4742–4749.

[14] G. Inzelt, B. B. Berkes, Á. Kriston, Electrochemical nanogravimetric studies of adsorption, deposition, and dissolution processes occurring at platinum electrodes in acid media, Pure and Applied Chemistry 83 (2011) 269–279.

[15] M. C. Santos, D. W. Miwa, S. A. S. Machado, Study of anion adsorption on polycrystalline Pt by electrochemical quartz crystal microbalance, Electrochemistry Communications 2 (2000) 692–696.

[16] F. Gloaguen, J.-M. Léger, C. Lamy, An electrochemical quartz crystal microbalance study of the hydrogen underpotential deposition at a Pt electrode, Journal of Electroanalytical Chemistry 467 (1999) 186–192.

[17] B. Gollas, J. M. Elliott, P. N. Bartlett, Electrodeposition and properties of nanostructured platinum films studied by quartz crystal impedance measurements at 10 MHz, Electrochimica Acta 45 (2000) 3711–3724.

[18] Z. X. Shu, S. Bruckenstein, Iodine adsorption studies at platinum, Journal of Electroanalytical Chemistry and Interfacial Electrochemistry 317 (1991) 263–277.

[19] K. Shimazu, H. Kita, In situ measurements of water adsorption on a platinum electrode by an electrochemical quartz crystal microbalance, Journal of Electroanalytical Chemistry 341 (1992) 361–367.

[20] V. I. Birss, M. Chang, J. Segal, Platinum oxide film formation-reduction: an in-situ mass measurement study, Journal of Electroanalytical Chemistry 355 (1993) 181–191.

[21] M. Watanabe, H. Uchida, N. Ikeda, Electrochemical quartz crystal microbalance study of copper ad-atoms on gold and platinum electrodes Part I. Adsorption of anions in sulfuric acid, Journal of Electroanalytical Chemistry 380 (1995) 255–260.

[22] V. A. Marichev, Reversibility of platinum voltammograms in aqueous electrolytes, ionic product and dissociative adsorption of water, Electrochemistry Communications 10 (2008) 643–646.

[23] B. E. Conway, A. Zolfaghari, W. G. Pell, G. Jerkiewicz, Voltammetry, nanogravimetry and double-layer capacitance studies on chemisorption of Cl^- and Br^-, competitive with potentialdependent electrosorption of O species at Pt electrodes, Electrochimica Acta 48 (2003) 3775–3778.

[24] C. P. Wilde, S. V. D. Cliff, K. C. A. Hui, D. J. L. Brett, The influence of adsorbed hydrogen and extended cycling on the EQCM response of electrodeposited Pt electrodes, Electrochimica Acta 45 (2000) 3649–3658.

[25] W. Visscher, J. F. E. Gootzen, A. P. Cox, J. A. R. van Veen, Electrochemical quartz crystal microbalance measurements of CO adsorption and oxidation on Pt in various electrolytes, Electrochimica Acta 43 (1997) 533–547.

[26] G. Horányi, E. M. Rizmayer, A coupled voltammetric and radiometric (voltradiometric) study of the simultaneous adsorption of hydrogen

and anions at platinized platinum electrodes, Journal of Electroanalytical Chemistry and Interfacial Electrochemistry 218 (1987) 337–340.

[27] A. Kolics, A. Wieckowski, Adsorption of bisulfate and sulfate anions on a Pt(111) electrode, The Journal of Physical Chemistry B 105 (2001) 2588–2595.

[28] D.-M. Zeng, Y.-X. Jiang, Z.-Y. Zhou, Z.-F. Su, S.-G. Sun, In situ FTIR spectroscopic studies of (bi)sulfate adsorption on electrodes of Pt nanoparticles supported on different substrates, Electrochimica Acta 55 (2010) 2065–2072.

[29] B. Ren, X. Xu, X. Q. Li, W. B. Cai, Z. Q. Tian, Extending surface Raman spectroscopic studies to transition metals for practical applications II. Hydrogen adsorption at platinum electrodes, Surface Science 427-428 (1999) 157–161.

[30] H. Noguchi, T. Okada, K. Uosaki, SFG study on potential-dependent structure of water at Pt electrode | electrolyte solution interface, Electrochimica Acta 53 (2008) 6841–6844.

[31] P. A. Christensen, A. Hamnett, Techniques and Mechanisms in Electrochemistry, Blackie Academic Professional, London, 1994.

[32] V. Tsionsky, L. Daikhin, M. Urbakh, E. Gileadi, Looking at the metal/solution interface with the electrochemical quartz-crystal microbalance: Theory and experiment, in: A. J. Bard, I. Rubinstein (Eds.), Electroanalytical Chemistry, volume 22, Marcel Dekker, New York, 2004, pp. 1–99.

[33] Т. Я. Колотыркина, О. А. Петрий, Б. Е. Казаринов, Определение зависимости потенциала нулевого свободного заряда платины от pH раствора методом радиоактивных индикаторов, Электрохимия 10 (1974) 1352–1355.

[34] S. J. Xia, V. I. Birss, In situ mass and ellipsometric study of hydrous oxide film growth on Pt in alkaline solutions, Electrochimica Acta 45 (2000) 3659–3673.

[35] E. Sitta, A. L. Santos, R. Nagao, H. Varela, Nanogravimetric study of the complex voltammetric response in the electro-oxidation of methanol on platinum, Electrochimica Acta 55 (2009) 404–409.

[36] G. Jerkiewicz, G. Vatankhah, J. Lessard, M. P. Soriaga, Y.-S. Park, Surface-oxide growth at platinum electrodes in aqueous H_2SO_4 Reexamination of its mechanism through combined cyclic-voltammetry, electrochemical quartz-crystal nanobalance, and Auger electron spectroscopy measurements, Electrochimica Acta 49 (2004) 1451–1459.

[37] M. Tian, B. E. Conway, Electrocatalysis in oscillatory kinetics of anodic oxidation of formic acid: At Pt; nanogravimetry and voltammetry studies on the role of reactive surface oxide, Journal of Electroanalytical Chemistry 616 (2008) 45–56.

[38] M. P. Sumino, S. Shibata, Specific adsorption of hydrogen on polycrystalline platinum electrode, Electrochimica Acta 37 (1992) 2629–2635.

[39] T. Frelink, W. Visscher, J. A. R. van Veen, The third anodic hydrogen peak on platinum; Subsurface H_2 adsorption, Electrochimica Acta 40 (1995) 545–549.

[40] R. Schumacher, The quartz microbalance: A novel approach to the in-situ investigation of interfacial phenomena at the solid | liquid junction [new analytical methods (40)], Angewandte Chemie International Edition in English 29 (1990) 329–343.

[41] R. Raudonis, D. Plausinaitis, V. Daujotis, On the frequency response of a quartz supported platinum electrode: dependence on pretreatment, Journal of Electroanalytical Chemistry 358 (1993) 351–356.

[42] J. Solla-Gullón, P. Rodríguez, E. Herrero, A. Aldaz, J. M. Feliu, Surface characterization of platinum electrodes, Physical Chemistry Chemical Physics 10 (2008) 1359–1373.

[43] J. A. Santana, C. R. Cabrera, Y. Ishikawa, A density-functional theory study of electrochemical adsorption of sulfuric acid anions on Pt(111), Physical Chemistry Chemical Physics 12 (2010) 9526–9534.

[44] P. P. Olivera, M. Patrito, H. Sellers, Interfacial Electrochemistry: Experimental, Theory and Applications, Marcel Dekker: New York, p. 63.

[45] R. Parsons, Electrochemical nomenclature, Pure and Applied Chemistry 37 (1974) 499–516.

[46] IUPAC, Quantities, Units and Symbols in Physical Chemistry, RSC Publishing, 3rd edition, pp. 70–76.

[47] D. L. Burke, A. J. Ahern, Overlap of the oxide and hydrogen regions of platinum electrodes in aqueous acid solution, Journal of Solid State Electrochemistry 5 (2001) 553–561.

[48] G. Inzelt, B. B. Berkes, Á. Kriston, A. Székely, Electrochemical nanogravimetric studies of platinum in acid media, Journal of Solid State Electrochemistry 15 (2011) 901–915.

[49] B. Braunschweig, W. Daum, Superstructures and order-disorder transition of sulfate adlayers on Pt(111) in sulfuric acid solution, Langmuir 25 (2009) 11112–11120.

[50] N. García, V. Climent, J. M. Orts, J. M. Feliu, A. Aldaz, Effect of pH and alkaline metal cations on the voltammetry of Pt(111) single crystal electrodes in sulfuric acid solution, ChemPhysChem 5 (2004) 1221–1227.

[51] V. Climent, N. García-Araez, J. M. Feliu, Influence of alkali cations on the infrared spectra of adsorbed (bi)sulphate on Pt(111) electrodes, Electrochemistry Communications 8 (2006) 1577–1582.

[52] A. N. Frumkin, O. A. Petrii, I. G. Schchigorev, V. A. Safonov, Beeinflussung der Wasserstoffadsorption an Platin durch anorganische Katione, Zeitschrift für Physikalische Chemie (Leipzig) 243 (1970) 261–266.

[53] A. Wieckowski, In situ surface electrochemistry: Radioactive labeling, in: J. O. Bockris, B. E. Conway, R. E. White (Eds.), Modern Aspects of Electrochemistry, volume 21, Plenum, New York, 1990, pp. 65–119.

[54] L. Andrussow, B. Schramm, K. Schäfer (Eds.), Landolt-Börnstein, Zahlenwerte und Functionen aus Physik und Chemie, volume 2nd, Springer, 1969.

[55] A. Lasia, Electrochemical impedance spectroscopy and its applications, in: B. E. Conway (Ed.), Modern Aspects of Electrochemistry, volume 32, Kluwer Academic Publishers New York, Boston, Dordrecht, London, Moscow, 2002, pp. 143–249.

[56] B. E. Conway, J. Barber, S. Morin, Comparative evaluation of surface structure specificity of kinetics of UPD and OPD of H at single-crystal Pt electrodes, Electrochimica Acta 44 (1998) 1109–1125.

[57] S. Morin, H. Dumont, B. E. Conway, Evaluation of the effect of two-dimensional geometry of Pt single-crystal faces on the kinetics of upd of H using impedance spectroscopy, Journal of Electroanalytical Chemistry 412 (1996) 39–52.

[58] E. Sibert, R. Faure, R. Durand, High frequency impedance measurements on Pt(111) in sulphuric and perchloric acids, Journal of Electroanalytical Chemistry 515 (2001) 71–81.

[59] R. Durand, Extension de l'étude du système $H^+ \mid H \mid \frac{1}{2}H_2(Pt)$ vers les hautes fréquences, Electrochimica Acta 24 (1979) 1095–1100.

[60] G. A. Ragoisha, N. P. Osipovich, A. S. Bondarenko, J. Zhang, S. Kocha, A. Iiyama, Characterisation of the electrochemical redox behaviour of Pt electrodes by potentiodynamic electrochemical impedance spectroscopy, Journal of Solid State Electrochemistry 14 (2010) 531–542.

[61] N. P. Lebedeva, M. T. M. Koper, E. Herrero, J. M. Feliu, R. A. van Santen, Cooxidation on stepped Pt[n(111)×(111)] electrodes, Journal of Electroanalytical Chemistry 487 (2000) 37–44.

[62] A. S. Bondarenko, I. E. L. Stephens, H. A. Hansen, F. J. Pérez-Alonso, V. Tripkovic, T. P. Johansson, J. Rossmeisl, J. K. Norskov, I. Chorkendorff, The Pt(111) | electrolyte interface under oxygen reduction reaction conditions: An electrochemical impedance spectroscopy study, Langmuir 27 (2011) 2058–2066.

[63] A. S. Bondarenko, G. A. Ragoisha, Inverse problem in potentiodynamic electrochemical impedance, in: A. L. Pomerantsev (Ed.), Progress in Chemometrics Research, Nova Science Publishers: New York, 2005, pp. 89–102.

[64] G. J. Brug, A. L. G. van den Eeden, M. Sluyters-Rehbach, J. H. Sluyters, The analysis of electrode impedances complicated by the presence of a constant phase element, Journal of Electroanalytical Chemistry and Interfacial Electrochemistry 176 (1984) 275–295.

[65] T. Pajkossy, Impedance of rough capacitive electrodes, Journal of Electroanalytical Chemistry 364 (1994) 111–125.

[66] V. M.-W. Huang, V. Vivier, M. E. Orazem, N. Pébère, B. Tribollet, The apparent constant-phase-element behavior of an ideally polarized blocking electrode, Journal of The Electrochemical Society 154 (2007) C81–C88.

[67] T. Pajkossy, D. M. Kolb, Anion-adsorption-related frequency-dependent double layer capacitance of the platinum-group metals in the double layer region, Electrochimica Acta 53 (2008) 7403–7409.

[68] R. S. Neves, E. D. Robertis, A. J. Motheo, Capacitance dispersion in EIS measurements of halides adsorption on Au(210), Electrochimica Acta 51 (2006) 1215–1224.

[69] T. Pajkossy, Capacitance dispersion on solid electrodes: anion adsorption studies on gold single crystal electrodes, Solid State Ionics 94 (1997) 123–129.

[70] A. J. Motheo, J. R. Santos Jr, A. Sadkowski, A. Hamelin, The gold (210) | perchloric acid interface: impedance spectroscopy, Journal of Electroanalytical Chemistry 397 (1995) 331–334.

[71] A. Sadkowski, A. J. Motheo, R. S. Neves, Characterisation of Au(111) and Au(210) | aqueous solution interfaces by electrochemical immittance spectroscopy, Journal of Electroanalytical Chemistry 455 (1998) 107–119.

[72] M. Hugelmann, W. Schindler, Tunnel barrier height oscillations at the solid | liquid interface, Surface Science 541 (2003) L643–L648.

[73] D. Vladikova, Z. Stoynov, Secondary differential impedance analysis – a tool for recognition of CPE behavior, Journal of Electroanalytical Chemistry 572 (2004) 377–387.

[74] E. Skúlason, V. Tripkovic, M. E. Björketun, S. Gudmundsdóttir, G. Karlberg, J. Rossmeisl, T. Bligaard, H. Jónsson, J. K. Nørskov, Modeling the electrochemical hydrogen oxidation and evolution reactions on the basis of density functional theory calculations, The Journal of Physical Chemistry C 114 (2010) 18182–18197.

[75] R. Gómez, V. Clíment, J. M. Feliu, M. J. Weaver, Dependence of the potential of zero charge of stepped platinum (111) electrodes on the oriented step-edge density: Electrochemical implications and comparison with work function behavior, The Journal of Physical Chemistry B 104 (2000) 597–605.

Part V

ELECTROCHEMICAL NANOGRAVIMETRIC STUDY OF THE ADSORPTION AND ELECTROPOLYMERIZATION OF INDOLE AND 4-AMINOINDOLE

The Electrochemical Quartz Crystal Nanobalance (EQCN) was employed to study the adsorption and electropolymerization of indole and 4-aminoindole at different electrodes in acid media. It was found that a spontaneous deposition of an electrochemically active layer occurs for both molecules at oxidised platinum which is accelerated in the presence of oxygen, while no such effect was observed at gold. Electrooxidation of 4-aminoindole by potential cycling up to 0.6 V leads to the formation of multilayer films at both Pt and Au electrodes. The electrogravimetric responses of these polymeric films are similar to those of the spontaneously formed adsorbed multilayer. Electropolymerization of indole is much slower, even at higher positive potentials. The charge compensation reactions differ for the two types of polymer as well. In case of polyindole the ingress and egress of anions while in case of poly(4-aminoindole) most probably partial deprotonation of the film maintains the electroneutrality. These features are readily distinguishable with the EQCN.

The chapter is based on the following articles:

— B. B. Berkes, G. Inzelt, E. Vass, *Electrochimica Acta* **96** (2013) 51-60.

— B. B. Berkes, G. Inzelt, Electrochemical nanogravimetric studies on the electropolymerization of indole and on polyindole, *Electrochimica Acta* – submitted

5

ADSORPTION AND ELECTROCHEMICAL BEHAVIOUR OF INDOLE AND 4-AMINOINDOLE

5.1 INTRODUCTION

This chapter discusses the results of electrochemical and nanogravimetric studies of indole and 4-aminoindole starting with the description of their adsorption phenomena and analysis of the formed layer. The role of oxygen in assisting the adsorption–polymerisation will be demonstrated too. This process results in a material which characteristics do not fall far from that of the electrochemically produced polymer modified electrode. For the sake of their comparison finally the polymerization reactions will be explicated. However the study of the reaction mechanisms and the properties of the polymer films is beyond the scope of adsorption studies, therefore they will not be discussed here.

5.1.1 *Molecular adsorption of organic compounds on electrodes*

Adsorption of organic molecules on metal surfaces is a thoroughly studied field of electrochemistry. The earliest research in the field was carried out with the use of liquid electrodes. In the past over one hundred years several metal electrodes were investigated and they are usually classified according to the strength of adsorption of the organic molecules [1–3]. To the platinum group the strong interaction between the electrode and the adsorbates is characteristic, commonly an irreversible, dissociative chemisorption. Elements of the IB group are prone to less strong adsorption that is usually even reversible. Our interest in the present study is on a particular member of the group: on gold. The interaction between the metals and the adsorbed molecules is weaker than in the case of platinum. As we will see later the forming oxide layer on a platinum electrode may show significant effects. This layer forms relatively easily: presence of oxygen in the electrolyte is enough for the formation in the case of an electrode without potential control. Surface oxides of gold play also a role in these type of studies; however, they are only present at higher potentials. Typical onset potential of oxide formation is between 1.0 V and 1.1 V vs. SCE in 1 mol dm^{-3} H_2SO_4 [4, 5]. The monomers concerned here undergo irreversible overoxidation at such high potentials, therefore oxides of gold are out of our interest.

Surface crystallography of the metal electrode, the structure of the electrode | electrolyte interface and the nature of the solvent molecules, i.e. the interaction between solvent molecules and surface atoms have the highest impact on the adsorption of organic molecules. Adsorbate-adsorbate interactions might not be negligible too. The last three effects were studied as early as the first part of the 20th century by Gouy [6], Chapman [7], Stern [8], Фрýмкин [9] and Butler

[10]. Later their theory was further developed and new, widely used classical models and descriptions appeared [11, 12].

To be able to pay more attention to the effects of surface structure on adsorption the appearance of sophisticated techniques was required. After the discovery of low-energy electron diffraction in 1927 by Davisson and Germer more than 30 years elapsed until it began to be widely applied for surface adsorption studies. Ultrahigh vacuum systems were developed, Auger spectroscopy and electron energy-loss spectroscopy appeared to serve as complementary techniques to the detailed characterisation and an in-depth analysis of surfaces, surface processes. Surface electrochemistry started to expand in a rapid manner simultaneously. The appearance of a cheap and convenient preparation method of single crystal electrodes [13] was beneficial to the widespread use of well defined surfaces.

5.1.2 *Conducting polymers from the indole family*

The preparation, characterization and application of electrochemically active, electronically conducting polymeric systems are still in the foreground of research activity in electrochemistry. This intense interest is due to wide range of promising applications of these compounds in the fields of energy storage, electrocatalysis, organic electrochemistry, bioelectrochemistry, photoelectrochemistry, electroanalysis, sensors, electrochromic displays, microsystem technologies, electronic devices, microwave screening and corrosion protection, etc. [14]. During the first three decades the researchers took all the possible aromatic compounds from the shelves, and tried to polymerize those. Especially in the cases of aromatic amines and heterocyclic compounds their efforts were crowned with success. Electropolymerization of indole and its derivatives has also been studied [15–24], and a wide range of applications for these polymers from corrosion protection via Li-ion batteries to ion sensors and electrochromic devices has been suggested [25–31]. However, there are still controversial issues in the literature concerning the structure and the behaviour of the formed polymers. Not only the position of the couplings between the monomers has been disputed, but even the formation of a real polymer has been questioned [32]. In the case of indole monomers substituted at different positions different suggestions have been made for the linkages [16, 22]. Theoretical considerations about the polymer structure support the C2–C3, C2–C7 connections [20, 33]. On the basis of spectroscopic data measured in the case of derivatives rather the C2–C3 coupling seems to be more likely [34]. The formation of cyclic forms was not excluded, either [32, 33, 35].

Substituent effects may have interesting influence on the polymerization. Jennings et al.[23] claimed, that amino or hydroxyl substituted indole derivatives (5-aminoindole and 5 hydroxyindole) adsorbing on the surface of a platinum electrode via the substituents inhibit the redox active film formation. However, according to their findings, the appropriate polymers could be produced if the electropolymerization was carried out onto a predeposited layer of other polymers. Recently Yue et al. [24] reported the electropolymerization of 5-aminoindole in aqueous sulphuric acid solution. It was found that the elec-

tropolymerization mainly occurred at C2 and C3 positions, while the amino group remained intact.

While the 5-substituted derivatives have thoroughly been studied [23, 24, 34, 36–40] much less attention has been paid to the 4-substituted derivatives. The paper by Kokkinidis and Kelaidopoulou [35] can be mentioned where electrochemical behaviour of 4-nitroindole, and the polymer formation can be assigned to the oxidation of the reduction product of the parent compound. Preparation of the polymers from compounds in the indole family has been carried out mainly in acetonitrile [21, 22, 27] or in organic solvents like dichloromethane [18] or boron trifluoride diethyl etherate [34]. Polyindole has an electric conductivity $\sim 1 \times 10^{-2}\,\mathrm{S\,cm^{-1}}$ [22], it is highly stable; however, above 0.9 V vs. SCE an irreversible degradation of the polymer occurs and results in the decrease of the electrical conductivity [27].

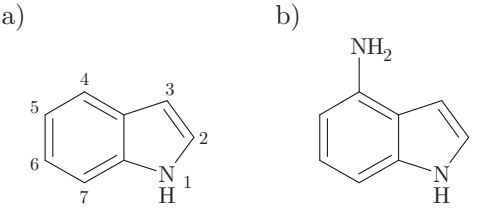

Figure 5.1: The formula of indole (a) and 4-aminoindole (b) and the numbering of atoms on the indole ring.

Our attention turned to indole and 4-aminoindole (Figure 5.1) for several reasons. First, the electrochemical behaviour of 4-aminoindole has not been studied yet, albeit due to its structure, the free site in the para position to the amino group, the formation of a polyaniline-like polymer might also be expected. Second, it was hoped that by using EQCN technique, the application of which has been neglected in these studies, several controversies that can be found in the electrochemical literature of the indole compounds including their adsorption and electropolymerization could be resolved.

We report herein the results obtained and their possible explanation concerning the adsorption and electrooxidation of indole and 4-aminoindole as well as the characterization of the resulting surface films in different aqueous acid solutions by EQCN technique. Attention is paid to the crucial role of the oxygen and the positive potential limit.

5.2 EXPERIMENTAL

Analytical grade chemicals such as $HClO_4$ (Merck), H_2SO_4 (Merck), Na_2SO_4 (Merck), HCl (Sigma–Aldrich) and 4-aminoindole (Sigma–Aldrich) were used as received. The solutions from 4-aminoindole were always freshly prepared. The solutions were deaerated before the monomer was dissolved. To fasten the dissolution process an ultrasonic bath was applied. All solutions were purged

with oxygen-free argon (purity: 5.0, Linde Gas Hungary Co. Cltd.) and an inert gas blanket was maintained throughout the experiments. The glass cell set-up, shown in Figure 2.6 was used to the measurements.

The concentration of the monomer solutions was 1 mmol dm^{-3}. Polymerization was carried out by potentiodynamic cycling at a scan rate of 10 mV s^{-1} in acid media. The applied potential ranges are indicated at the discussion of the experiments. The cycling of the potential as a pretreatment of the electrode was carried out before each experiment in the supporting electrolyte, until a stable voltammogram characteristic to the clean Pt or Au surface was obtained.

5.3 RESULTS AND DISCUSSION

5.3.1 *Adsorption of 4-aminoindole at platinum and gold. Effect of oxygen*

The adsorption was examined in the case of platinum and gold covered EQCN electrodes. Two different methods have been applied. Either 4-aminoindole was added into the supporting electrolyte or the nanobalance was immersed into a monomer containing solution.

By using platinum electrodes in both cases a decrease of the frequency (Δf), i.e. an increase in the surface mass can be detected, consequently adsorption of 4-aminoindole takes place. Figure 5.2 shows the results of a typical experiment, where the supporting electrolyte was a deaerated 1:1 mixture of 0.05 mol dm^{-3} H_2SO_4 and 0.05 mol dm^{-3} Na_2SO_4 ($\sim$ pH = 2). Immersion of the EQCN into this solution results in -830 Hz frequency decrease, while in the presence of 1 mmol dm^{-3} 4-aminoindole after the completion of the adsorption process -916 Hz was detected (see section I of Figure 5.2).

Presuming that the low concentration of the monomer has no effect on the viscosity and density of the solution, the difference between the frequency decreases (86 Hz) is due to adsorption of 4-aminoindole. The open circuit potential (OCP) of the system was also monitored during the adsorption. With the stabilization of the frequency the electrode potential also reached a steady-state value of 0.222 V vs. SCE. It dropped from 0.67 V corresponding to an oxidized Pt surface.

At the end of section I cyclic voltammograms of the adsorbed layer were measured. The graph on the left side of Figure 5.3 shows the resulted curves. The adsorbate can be oxidized and reduced reversibly in the potential range shown. This is reflected by the formation of a pair of surface waves. With increasing scan rate the peak currents increase linearly (diamond symbols in Figure 5.3b).

Oxygen has a great influence on the deposition process of 4- aminoindole. Purging the cell with air the frequency decreased further with a constant rate (the rate is defined here as the slope of the frequency change, see Figure 5.2, section II). The OCP of the electrode rapidly reached its stable value at 0.357 V. When Ar purging was applied again (section III) the rate of frequency change first slowly decreased, and finally frequency reached again a steady state. The total frequency decrease was -291 Hz, the characteristics of the cyclic voltammograms taken after section III have not changed in comparison with that of the layer obtained after section I.

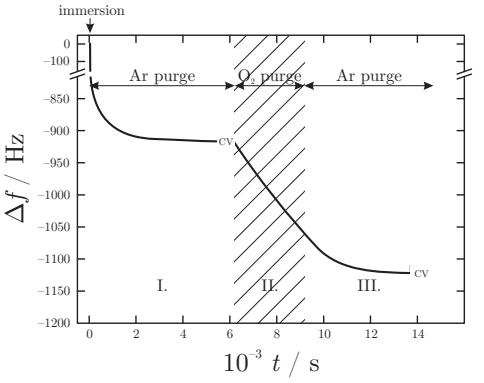

Figure 5.2: Frequency change of a Pt EQCN electrode during the immersion into a $1\,\mathrm{mmol\,dm^{-3}}$ 4-aminoindole containing $0.05\,\mathrm{mol\,dm^{-3}}$ H_2SO_4/$0.05\,\mathrm{mol\,dm^{-3}}$ Na_2SO_4 ($\sim$ pH = 2) supporting electrolyte. The labels CV indicate the periods where cyclic voltammograms shown in Figure 5.3 were measured. The part of the curve corresponding to immersion related frequency change (from $-100\,\mathrm{Hz}$ to $-800\,\mathrm{Hz}$) was skipped for the sake of better visibility of the adsorption related changes.

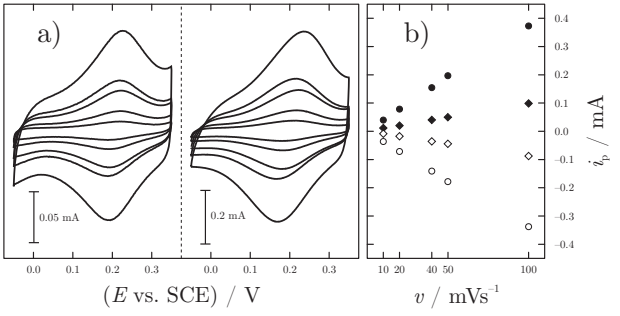

Figure 5.3: (a) Cyclic voltammograms measured at two different layer thicknesses (see Figure 5.2). (b) The corresponding peak current vs. scan rate diagram. The scan rates were $10\,\mathrm{mV\,s^{-1}}$, $20\,\mathrm{mV\,s^{-1}}$, $40\,\mathrm{mV\,s^{-1}}$, $50\,\mathrm{mV\,s^{-1}}$ and $100\,\mathrm{mV\,s^{-1}}$, respectively.

We carried out the adsorption experiment also in a closed system when the oxygen had been removed as perfectly as possible (Figure 5.4). Pt was reduced at $-0.24\,\mathrm{V}$, and was left at its open-circuit potential in its reduced state. In this case after addition of 4-aminoindole the frequency decrease, i.e. the adsorbed amount was minor. Both the electrolyte and the solution containing 4-aminoindole had been purged carefully with argon. 4-aminoindole solution was

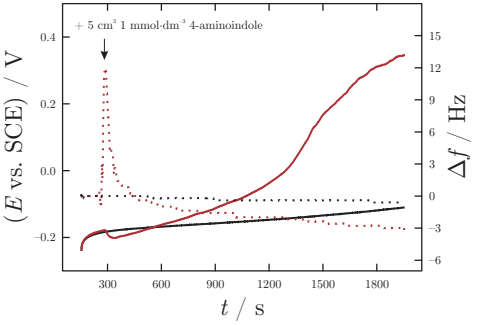

Figure 5.4: Open circuit potentials (solid lines) and the corresponding frequency change curves (dotted lines) of a platinum EQCN electrode in oxygen free 0.1 mol dm^{-3} H_2SO_4 solutions. The black curves serve as references when the system contained only clean sulfuric acid. The red lines show the results of the experiment when 4-aminoindole was added to the solution. The final concentration of 4-aminoindole was 3.2×10^{-4} mol dm^{-3}.

added to the system with the help of a syringe with a needle through a septum. It follows that the presence of very minor amount of oxygen can cause this oxidative adsorption process. It is most likely due to the formation of PtOH or PtO, which reacts with the 4-aminoindole. Under similar conditions no such effect can be observed at a gold electrode, where the oxide formation occurs at much higher potentials (see below).

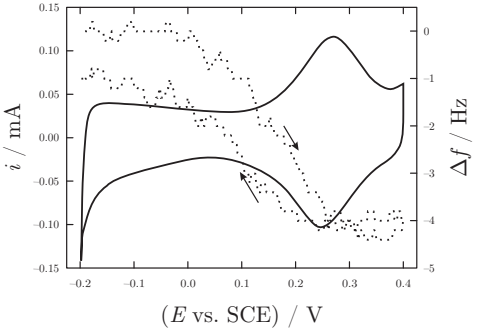

Figure 5.5: Cyclic voltammogram and the corresponding frequency excursion of an adsorbed layer of 4-aminoindole. Concentration of 4-aminoindole was 1 mmol dm^{-3} in 1 mol dm^{-3} $HClO_4$. Electrode: platinized platinum, adsorbed layer: 300 Hz and $dE/dt = 10$ mV s^{-1}.

Figure 5.5 shows a cylic voltammogram and the corresponding frequency change curve of the adsorbed layer of 4-aminoindole on Pt in 1 mol dm^{-3} $HClO_4$ solution. The frequency variation during the redox transformation of the adsorbed layer is small and reversible. The highest apparent molar mass (M) value that can be calculated from the $\Delta f(Q)$ curve is only 9 g mol^{-1}. To calculate the apparent molar mass the frequency change (Δf) is plotted versus the charge (Q). From the slope of the curve ($\mathrm{d}\Delta f/\mathrm{d}Q$) M can be calculated at each value of Q using the following formula: $M(Q) = nF/C_\mathrm{f} \times \mathrm{d}\Delta f/\mathrm{d}Q$, where n is the number of electrons involved in the electrochemical reaction and F is the Faraday constant.

From the rather low molar mass value determined it is rather difficult to draw a conclusion on the nature of the exchanged species. The frequency change is in the order of magnitude that can be observed for the double layer charging. However, because it nicely follows the redox transformation of the electrochemically active layer, it is reasonable to assume that more than one species enter and leave the surface film simultaneously. Because oxidation occurs, i.e. positive charges are generated, if only deprotonation would occur a slight mass loss could be expected. The incorporation of counterions would cause a much higher mass increase. Therefore, it can be assumed that amino groups are protonated, and the positive charges are compensated by the presence of the counterions in the reduced film. It follows that the excess positive charges in the film due to the oxidation are not compensated by the incorporation of the counterions but the oxidation is mostly accompanied by partial deprotonation and only a small amount of anions enter the surface layer, i.e. the molar mass calculated is related to a counterflux of ions. We will return to this issue later.

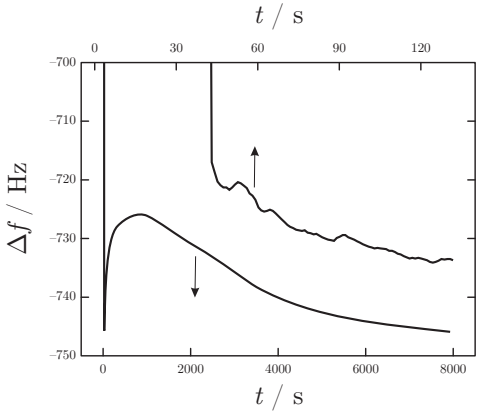

Figure 5.6: Frequency change obtained for a Pt EQCN electrode during the immersion into a 1 mol dm^{-3} HCl containing 1 mmol dm^{-3} 4-aminoindole (1) and in 1 mol dm^{-3} HCl (2), respectively. For the sake of the better visibility the immersion related frequency changes were skipped from the curves.

The adsorption phenomena has been studied also in HCl solutions. In this way, the strength and the nature of the adsorption can be tested. After the immersion of the Pt electrode into the 1 mmol dm^{-3} 4-aminoindole containing 1 mol dm^{-3} HCl electrolyte a fast frequency decrease which is related to the viscosity and density of the liquid occurred (Figure 5.6, curve 1). There was an increase of the frequency, and after a maximum it decreased again to a steady state value. This transient response is due to the perturbation of the system which can be observed also in other cases during such type of EQCN experiments. Both the chloride ions and the 4-aminoindole molecules adsorb on the platinum surface, therefore a competitive adsorption occurs. First, the adsorption of chloride ions prevails which is a much faster process due to their three orders of magnitude higher concentration; however, simultaneously the adsorption of 4-aminoindole also takes place. The 4-aminoindole molecules slowly replace the chloride ions forming a more stably attached layer. Due to the competitive nature of the adsorption, the population of the more strongly adsorbed species will be higher at the surface. However, the other species (chloride ions in this case) still occupy surface places, the amount of the adsorbed 4-aminoindole will be eventually less than in sulphate media due to the higher adsorption ability of the chloride than that of the sulphate ions.

As can be seen in pure 1 mol dm^{-3} HCl after a fast frequency decrease a low change for a relatively long time occurs due to the adsorption of the chloride ions; however, the total frequency decrease is smaller than in the presence of 4-aminoindole (Figure 5.6, curve 2).

In the case of gold electrodes no adsorption phenomena – even in the presence of oxygen – were observed, since the frequency did not change upon addition of 4-aminoindole in the supporting electrolyte, or no excess frequency decrease was observed immersing the electrode into the solution contained 4-aminoindole. During the potential cycling between −0.2 V and 0.4 V in 1 mol dm^{-3} $HClO_4$ electrolyte no oxidation–reduction waves appeared, and the simultaneously detected frequency change was insignificant, too (Figure 5.8, curves 1 and 1′).

In all cases oxygen was carefully removed from the solution, therefore the substrate effect can be explained by a spontaneous reaction between the Pt–OH or PtO layer still present at OCP (and/or the very small amount of oxygen that was still dissolved in the electrolyte) and the 4-aminoindole in the beginning of the adsorption process. Alternatively, a chemisorption at Pt can also be assumed; however, it would contradict to the effect observed in the presence of chloride ions, which admittedly strongly adsorb on Pt (more strongly than sulphate ions) but cannot remove chemisorbed species.

5.3.2 *Effect of oxygen on the adsorption of indole on platinum*

In connection with the polymerization of indole first the adsorption of the monomer was studied. Figure 5.7 shows the results of an experiment in which the frequency and potential change of a platinum EQCN electrode was monitored. For the sake of clarity the immersion related frequency change and the

initially established stable frequency and potential responses in the deaereted solution are not shown in the figure.

Purging oxygen into the monomer containing solution results in a continuous frequency decrease. The rate of the change remains approximately constant for relatively long times (for hours) and the same for the two sections when oxygen was bubbled. Comparing this rate (i.e. the slope of the $\Delta f(t)$ curve) with that of obtained from the very similar experiment done with 4-aminoindole, it can be concluded that there is one order of magnitude difference in the rate of the two processes. In the case of indole the rate is $\sim 14\,\mathrm{Hz\,h^{-1}}$ while that is $\sim 172\,\mathrm{Hz\,h^{-1}}$ in the case of 4-aminoindole with the same concentration. Even though the pH of the supporting electrolytes was different (the difference in the two pH values is ~ 0.3) it seems that 4-aminoindole is more prone to adsorption / polymer formation due to oxidation than indole. The same conclusion will be drawn from the electropolymerization experiments too.

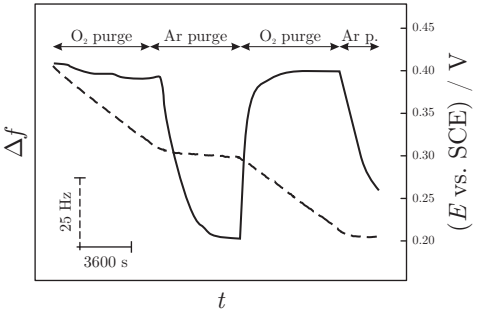

Figure 5.7: Part of a frequency change curve obtained for a Pt EQCN electrode in an experiment where the 1 mmol dm^{-3} indole containing electrolyte was purged with oxygen and argon repeatedly. Electrolyte: 0.1 mol dm^{-3} H_2SO_4.

Deoxygenating the solution with high purity argon gradually stops the decrease of the frequency. Both the potential and the frequency reaches a steady state value. The potential stabilizes at 0.2 V. The stabilization is relatively long in time and it requires the complete removal of oxygen, since even the traces of oxygen in the solution induce the deposition of the monomer. This reveals in the abrupt changes when purging the solution with oxygen again. The deposition occurs with the same rate as in the previous section.

The ability to generate conducting polymers on a platinum surface in this simple however controlled way, even without the use of a potentiostat may open new vistas in the production of polymer modified electrodes.

5.3.3 *Electropolymerization of 4-aminoindole*

In the case of gold electrodes at potentials higher than 0.4 V a huge anodic current appears and simultaneously the resonant frequency suddenly decreases

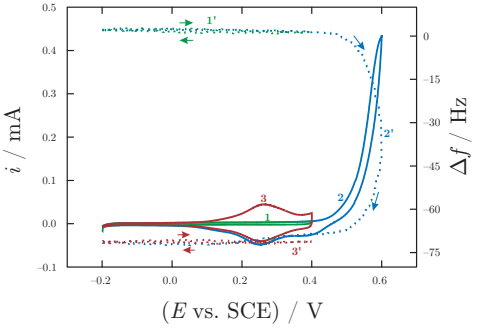

Figure 5.8: Three consecutive cyclic voltammograms (1–3) and the corresponding frequency changes (1′–3′) in the case of a Au EQCN electrode at different positive potential limits in 1 mol dm^{-3} $HClO_4$ solution containing 1 mmol dm^{-3} monomer. $dE/dt = 10\,mV\,s^{-1}$. The positive potential limits were as follows: (1) 0.4 V, (2) 0.6 V and (3) 0.4 V.

(Figure 5.8, curves 2 and 2′). This indicates the occurrence of the deposition of a polymer film. The −70 Hz frequency decrease corresponds to a 10 nm thin film, assuming 1.2 g cm^{-3} for the density of the film. The layer formed was investigated setting the positive potential limit to 0.4 V again. A pair of current peaks appears (Figure 5.8, curves 3 and 3′), the characteristics of which resemble the layer formed after the spontaneous deposition at Pt. During continuous cycling by applying 0.6 V as positive potential limit an increase of this pair of waves can be detected, which is accompanied with the continuous increase of the surface mass. A substantial frequency decrease (mass increase) occurring in the potential region between 0.4 V and 0.6 V clearly indicates the place where the oxidation of the monomers, i.e. the electropolymerization takes place. During cycling a second anodic current peak also develops.

While more and more material was deposited, the mass change due to the ingress and egress of the charge compensating ions, respectively, during the redox response remains minor, and does not increase as usually expected with increasing film thickness (Figure 5.9a).

Figure 5.9b shows the cyclic voltammetric and the EQCN frequency curves detected in the course of a single (20th) cycle of polymerization. While the mass change related to the formation of new polymeric layer dominates, simultaneously with the anodic voltammetric wave a small frequency decrease followed by a small frequency increase occurs, while in the course of the cathodic scan only a small frequency decrease can be detected. It indicates a complex nature of the redox mechanism which may involve protonation/deprotonation, a limited anion exchange but such phenomena as the double layer charging, water uptake or the stress due to the structural change of the surface layer cannot be excluded, either.

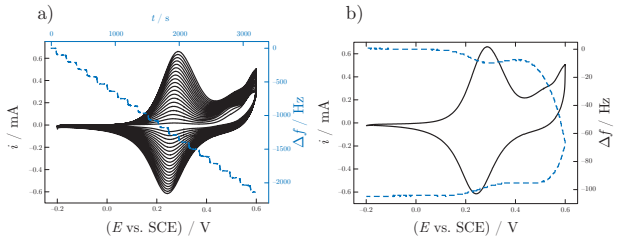

Figure 5.9: Polymerization of 4-aminoindole on Au electrode. (a) The subsequent cyclic voltammograms and the simultaneously detected EQCN curves from the 2nd to the 21st cycles. The 1st cycle is shown in Figure 5.8. Frequency change curves are plotted as a function of time. (b) The 20th cycle. Electrolyte: $1\,\mathrm{mol\,dm^{-3}}$ $HClO_4$ solution containing $1\,\mathrm{mmol\,dm^{-3}}$ monomer. $\mathrm{d}E/\mathrm{d}t = 10\,\mathrm{mV\,s^{-1}}$.

The electropolymerization process takes place similarly in the case of platinum electrodes. The main difference is the appearance of an oxidation peak in the 1st cycle due to the layer that has already been deposited in the course of the adsorption. While this oxidation peak can be observed when sulphuric acid or perchloric acid were applied, no such phenomenon occurs in hydrochloric acid (see Figure 5.10), the reason of which is the competitive adsorption with chloride ions. The growth of the layer seems to be independent of the electrode material. The increase of the first anodic peak with the increase of the deposited amount of polymer clearly suggests that the process is the oxidation of the polymer. The constant remaining frequency changes (same height and shape of the steps in Figure 5.9a) during the deposition suggest that there is practically no population change of anions or water molecules in the film. It follows that anions are already present in the polymer film even in reduced state, therefore no substantial exchange of anions between the polymer and electrolyte occurs. It is a consequence that the amino groups are protonated, and the positive charges are compensated by the presence of the counterions in the reduced film. It follows that the excess positive charges in the film due to the oxidation are not compensated by the incorporation of the counterions but the oxidation is accompanied by partial deprotonation which causes only a minor mass change. Similar findings and explanation have been reported by Skompska and Tarajko-Wazny [41] in the case of poly(1,8-diaminocarbazole) in contact with aqueous solutions of $HClO_4$. This view is supported by the fact that in the case of unsubstituted indole a mass change can be observed during the redox processes the magnitude of which is proportional to the molar mass of the counterions, i.e. an expected ingress/egress of ions occurs in the course of the oxidation and reduction, respectively [42]. In less acidic solutions (above pH = 2) where the amino groups become unprotonated the mass changes are getting higher; however, the electroactivity of the polymer decreases considerably, therefore a reliable comparison cannot be made.

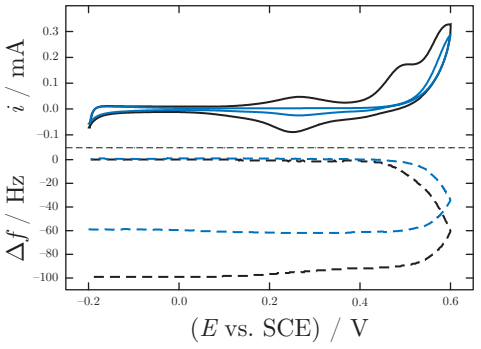

Figure 5.10: Cyclic voltammograms and simultaneously detected frequency change curves during the 1st cycle of the electropolymerization of 4-aminoindole from 1 mmol dm^{-3} monomer containing 1 mol dm^{-3} HCl (blue lines) and 1 mol dm^{-3} $HClO_4$ (black lines) solutions.

The electropolymerization has been carried out using different acids. In this way information can be obtained concerning the nature of the incorporation of anions that was discussed above. Furthermore, conclusions can be drawn on the efficiency of the electropolymerization, and even the effect of the electrolyte on the morphology of the films [14]. Representative results obtained by using 1 mol dm^{-3} $HClO_4$ and HCl, respectively, are presented in Figure 5.10 and Figure 5.11.

The current vs. potential curves clearly indicate the absence of oxidation peak characteristic to adsorbed layer of 4-aminoindole during the first cycle in chloride containing solution. From the frequency change (Δf) vs. charge (Q) plots (Figure 5.11) the apparent molar masses of the exchanged (incorporated) species were determined as follows. In the course of each cycle the following sections can be distinguished: *i*) in the beginning – albeit an increasing amount of charge is injected – the frequency practically remains constant, *ii*) in the region of the electropolymerization the surface mass proportionally increases with the charge consumed, *iii*) during reduction ($-Q$) no frequency change can be seen. In order to calculate an average of apparent molar masses specific to the deposition, the charge and frequency values at the end of each cycle, i.e. at the neutral state of the polymer were used. These values are plotted in the inset of the figures. Two linear sections with different slopes can be clearly identified in both experiments executed in different electrolytes. The regression lines fit the data very well: $R^2 \geq 0.999$ in all cases. The first section includes the first 8 cycles, the second one is related to the remaining cycles. The linear dependence of the frequency change on the charge consumed by the deposition indicates, that the film is rigidly attached to the surface. Thus the Sauerbrey equation can be really used for calculations of the mass. The molar mass of 4-aminoindole is 132.16 g mol^{-1}. The apparent molar masses calculated from

the slopes of the $\Delta f(Q)$ curves were M =151 g mol^{-1} and 131 g mol^{-1} (perchloric acid) and 122 g mol^{-1} and 96 g mol^{-1} (hydrochloric acid), respectively. This result is in accordance with difference of the molar mass of the anions. Assuming 1:1 codeposition of the monomer (protonated) and anions apparent molar masses of 232 g mol^{-1} (132.16 + 99.45) and 168 g mol^{-1} (132.16 + 35.45) could be expected. The somewhat lower M values obtained can be explained with the lower polymerization efficiency than 100%. Furthermore, in the case of partial deprotonation less anions remain in the film which decreases the value of the apparent molar mass calculated. Even in this case the difference in the molar mass of anions manifests itself. The decrease of the polymerization efficiency may also be related to the overoxidation of the polymer. Despite the fact that below 0.6 V 'well-behaving' polymer films are formed, the overoxidation – albeit with a slow rate – can start at 0.6 V.

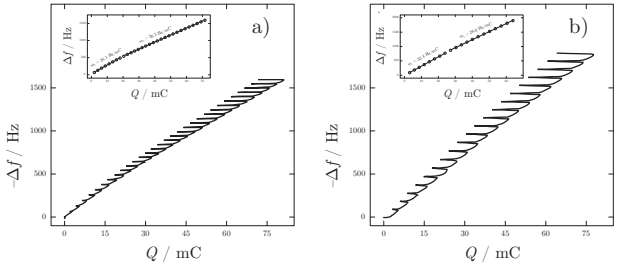

Figure 5.11: Frequency change vs. charge plots for the polymerization of 1 mmol dm^{-3} 4-aminoindole in (a) 1 mol dm^{-3} HCl and (b) 1 mol dm^{-3} $HClO_4$. 30 and 20 potential cycles were measured respectively. Insets show the slopes of the Δf vs. Q curves where Δf and Q values belonging to the end of each cycle are plotted.

5.3.4 *Electropolymerization of indole*

Figure 5.12 shows the cyclic voltammetric and the corresponding frequency change curves during 40 consecutive cycles of polymerization. During the first cycles oxidation of the adsorbed hydrogen and the underpotential deposition of hydrogen can be observed which were suppressed in the subsequent cycles by the growth of polyindole layer. Based on this observation it can be concluded, that the adsorption ability of indole is comparable with that of the hydrogen.

Possible overoxidation of the film was reported [27]. To avoid this phenomenon the positive potential limit was kept at 0.7 V during the deposition. Oxidation of indole in the first cycle starts at 0.52 V. The anodic current corresponding to the oxidation of the monomer increases in the course of further cycles. The frequency decrease caused by the deposition is uniform from cycle to cycle. The total frequency change within one cycle increases with the increase of film thickness. This refers to the movement of ions between the solution and the

film, i.e. in the case of thicker films more and more counterions are needed to compensate the charge on the polymer chains.

Under these circumstances two pairs of peaks corresponding to the redox transformations of the forming polyindole develop gradually. The resulting layer is uniform and has a gold color.

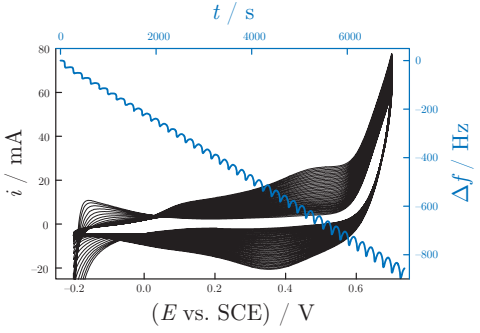

Figure 5.12: Cyclic voltammograms and the simultaneous change of the frequency during the polymerization of indole ($1\,\mathrm{mmol\,dm^{-3}}$), in 40 consecutive cycles, in $1\,\mathrm{mol\,dm^{-3}}$ $HClO_4$, $\mathrm{d}E/\mathrm{d}t = 10\,\mathrm{mV\,s^{-1}}$.

Figure 5.13 shows a typical frequency vs. charge plot. The total charge was calculated integrating the current obtained from the cyclic voltammograms (CVs). The plot contains the charge values belonging to the reduced state of the film ($E = -0.2\,\mathrm{V}$) and the corresponding frequency change values (an ordered pair from every CV). In this way the charges and frequency changes related to the redox processes of the film are neglected, i.e. only the charge and frequency decrease belonging to the film growth are taken into account. A function $\Delta f = (13.49 \pm 0.30) + (25.298 \pm 0.074) \times 10^3 \times Q^{0.92617 \pm 0.00084}$ perfectly fits the measured points. Taking the first derivative of this function $\mathrm{d}\Delta f/\mathrm{d}Q$ the variation of the apparent molar mass during the deposition can be determined. It was calculated from the following equation: $M = -\mathrm{d}\Delta f/\mathrm{d}Q \times nFA/C_\mathrm{f}$, where n is the number of electrons transferred in the reaction, F is the Faraday constant, A is the electrode surface area, C_f is the integral sensitivity of the quartz crystal used. This curve is plotted in Figure 5.13 as well. Assuming that the apparent molar mass value should be constant, its decrease can be the result of the decrease of the efficiency of the deposition. The apparent molar mass value is calculated for $n = 2$, and it falls from $194\,\mathrm{g\,mol^{-1}}$ to $144\,\mathrm{g\,mol^{-1}}$ assuming 100% charge efficiency. Since the molar mass of indole is $M_\mathrm{indole} = 117.15\,\mathrm{g\,mol^{-1}}$ it can be assumed that certain amount of solvent and counterions also remain in the film at the end of each cycle.

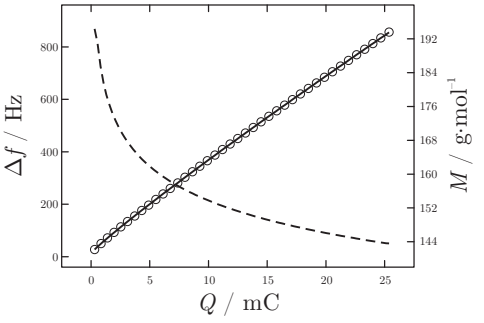

Figure 5.13: Frequency change vs. charge curve together with its derivative. The charge values were obtained from the cyclic voltammograms, and they correspond to the end of each cycle, i.e. to the reduced, neutral state of the polymer. A power function was fitted to the points, from whose derivative the apparent molar mass values were calculated.

5.3.5 *Comparing the electropolymerization of indole and 4-aminoindole*

The case of these two molecules, which only differ in an amino-group from each other, is a salient example, how largely a small change in structure may influence the polymerization process. The presence of adsorbed 4-aminoindole on Pt surface is already noticeable in the first cycle of polymerization [43]. Comparing Figure 5.9a andFigure 5.12 it can be seen that 4-aminoindole is much more prone to deposition via potential cycling than indole itself even when applying a narrower potential window; the frequency decrease in each cycle is almost five times higher. At the end of the experiments 856 Hz and 1903 Hz were the total frequency decreases, respectively, in the reduced states of the films. The peaks characteristic to the redox transformation of the film are separated on the CV of polyindole, while the symmetric redox peak pair, appearing in case of poly(4-aminoindole) encompasses several processes. In the case of indole at the beginning the frequency vs. time curve is staircase-like; however, as more and more material is deposited the shape transforms to a line resembling a stretched conical helix (Figure 5.12). This type of transformation is connected to the increasing effect of ion migration on the EQCN response during the film growth. In the case of 4-aminoindole the frequency vs. time curve resembles a staircase (Figure 5.9a). This dependence reflects that the deposition occurs with the same rate from cycle-to-cycle and that the frequency variation is independent of the film thickness. It is only possible if there is no movement of ions of remarkable mass, i.e. anions between the film and the solution. Therefore, it is evident that amino groups are responsible for the completely different behaviour.

5.4 CONCLUSIONS

The results of electrochemical quartz crystal nanobalance experiments reveal several interesting features on the adsorption and electropolymerization of indole and 4-aminoindole in acid media. These compounds undergo a strong oxidative adsorption at platinum electrode, which does not occur at gold. The presence of the amino-group on the molecule even strengthens this effect. The adsorption is due to the hydroxide–oxide layer on the Pt surface. When the oxygen had been carefully removed and the experiment was started with reduced Pt the adsorption phenomenon could not be observed. However, the adsorbed layer does not inhibit the electropolymerization at higher positive potentials, which has been reported for amino-substituted indoles [23]. The presence of molecular oxygen in the system leads to the overoxidation of the deposited polymer therefore, even the traces of oxygen should be removed in order to have good quality polymer. This effect might be responsible for the contradictory findings that have been reported so far for polyindoles and indole derivatives. Despite the effect of the substrates on the adsorption behaviour, the electropolymerization process occurs unhindered and in a similar manner at both Pt and Au electrodes.

The relatively small difference in structure has a huge effect on the nanogravimetric response of the deposited materials. While in the case of indole the charge compensating processes during the redox transformations are the ingression or egression of anions, in the case of 4-aminoindole most probably a partial deprotonation of the film compensates the excess charges. These are readily detectable with the EQCN, and reveal already during the polymerizations: the shape of $\Delta f(t)$ function serves as evidence for these statements.

[1] A. T. Hubbard, Electrochemistry at well-characterized surfaces, Chemical Reviews 88 (1988) 633–656.

[2] R. Parsons, Inner layer structure and the adsorption of organic compounds at metal electrodes, Electrochimica Acta 29 (1984) 1563–1567.

[3] J. Lipkowski, L. Stolberg, D.-F. Yang, B. Pettinger, S. Mirwald, F. Henglein, D. M. Kolb, Molecular adsorption at metal electrodes, Electrochimica Acta 39 (1994) 1045–1056.

[4] L. D. Burke, P. F. Nugent, The electrochemistry of gold: I the redox behaviour of the metal in aqueous media, Gold Bulletin 30 (1997) 43–53.

[5] S. Bruckenstein, M. Shay, An in situ weighing study of the mechanism for the formation of the adsorbed oxygen monolayer at a gold electrode, Journal of Electroanalytical Chemistry and Interfacial Electrochemistry 188 (1985) 131–136.

[6] L. G. Gouy, Sur la constitution de la charge électrique à la surface d'un électrolyte, Journal de Physique Théorique et Appliquée 9 (1910) 457–468.

[7] D. L. Chapman, A contribution to the theory of electrocapillarity, The London, Edinburgh, and Dublin Philosophical Magazine and Journal of Science 25 (1913) 475–481.

[8] O. Stern, Zur Theorie der Elektrolytischen Doppelschicht, Zeitschrift für Elektrochemie und angewandte physikalische Chemie 30 (1924) 508–516.

[9] A. Frumkin, Über die Beeinflussung der Adsorption von Neutralmolekülen durch ein elektrisches Feld, Zeitschrift für Physik 35 (1926) 792–802.

[10] J. A. V. Butler, The equilibrium of heterogeneous systems including electrolytes. Part III. The effect of an electric field on the adsorption of organic molecules, and the interpretation of electrocapillary curves, Proceedings of the Royal Society of London 122 (1929) 399–416.

[11] J. O'M. Bockris, M. A. V. Devanathan, K. Müller, On the structure of charged interfaces, Proceedings of the Royal Society of London. Series A. Mathematical and Physical Sciences 274 (1963) 55–79.

[12] J. O'M. Bockris, E. Gileadi, K. Müller, A molecular theory of the charge dependence of competitive adsorption, Electrochimica Acta 12 (1967) 1301–1321.

[13] J. Clavilier, R. Faure, G. Guinet, R. Durand, Preparation of monocrystalline Pt microelectrodes and electrochemical study of the plane surfaces cut in

the direction of the {111} and {110} planes, Journal of Electroanalytical Chemistry and Interfacial Electrochemistry 107 (1979) 205–209.

[14] G. Inzelt, Conducting Polymers: A New Era in Electrochemistry, Monographs in electrochemistry, Springer, 2nd edition, 2012.

[15] D. Billaud, E. B. Maarouf, E. Hannecart, Chemical oxidation and polymerization of indole, Synthetic Metals 69 (1995) 571–572.

[16] R. Holze, C. H. Hamann, Electrosynthetic aspects of anodic reactions of anilines and indoles, Tetrahedron 47 (1991) 737–746.

[17] K. Jackowska, A. Kudelski, J. Bukowska, Spectroelectrochemical and EPR determination of the number of electrons transferred in redox processes in electroactive polymers. Polyindole films, Electrochimica Acta 39 (1994) 1365–1368.

[18] P. C. Pandey, R. Prakash, Characterization of electropolymerized polyindole, Journal of The Electrochemical Society 145 (1998) 4103–4107.

[19] M. Saraji, A. Bagheri, Electropolymerization of indole and study of electrochemical behavior of the polymer in aqueous solutions, Synthetic Metals 98 (1998) 57–63.

[20] H. Talbi, G. Monard, M. Loos, D. Billaud, Theoretical study of indole polymerization, Journal of Molecular Structure: THEOCHEM 434 (1998) 129–134.

[21] G. Tourillon, F. Garnier, New electrochemically generated organic conducting polymers, Journal of Electroanalytical Chemistry and Interfacial Electrochemistry 135 (1982) 173–178.

[22] R. J. Waltman, A. F. Diaz, J. Bargon, Substituent effects in the electropolymerization of aromatic heterocyclic compounds, The Journal of Physical Chemistry 88 (1984) 4343–4346.

[23] P. Jennings, A. C. Jones, A. R. Mount, A. D. Thomson, Electrooxidation of 5-substituted indoles, Journal of the Chemical Society, Faraday Transactions 93 (1997) 3791–3797.

[24] R. Yue, F. Jiang, Y. Du, J. Xu, P. Yang, Electrosynthesis of a novel polyindole derivative from 5-aminoindole and its use as catalyst support for formic acid electrooxidation, Electrochimica Acta 77 (2012) 29–38.

[25] Z. Cai, G. Yang, Synthesis of polyindole and its evaluation for Li-ion battery applications, Synthetic Metals 160 (2010) 1902–1905.

[26] L. Fornarini, F. Stirpe, B. Scrosati, Electrochemical solar cells with layer-type semiconductor anodes, Journal of The Electrochemical Society 130 (1983) 2184–2187.

[27] E. B. Maarouf, D. Billaud, E. Hannecart, Electrochemical cycling and electrochromic properties of polyindole, Materials Research Bulletin 29 (1994) 637–643.

[28] G. Nie, L. Zhou, Q. Guo, S. Zhang, A new electrochromic material from an indole derivative and its application in high-quality electrochromic devices, Electrochemistry Communications 12 (2010) 160–163.

[29] P. C. Pandey, Copper (II) ion sensor based on electropolymerized undoped-polyindole modified electrode, Sensors and Actuators B: Chemical 54 (1999) 210–214.

[30] P. C. Pandey, R. Prakash, Electrochemical synthesis of polyindole and its evaluation for rechargeable battery applications, Journal of The Electrochemical Society 145 (1998) 999–1003.

[31] T. Tüken, B. Yazıcı, M. Erbil, The use of polyindole for prevention of copper corrosion, Surface and Coatings Technology 200 (2006) 4802–4809.

[32] J. B. Henry, A. R. Mount, Calculation of the redox properties of aromatics and prediction of their coupling mechanism and oligomer redox properties, The Journal of Physical Chemistry A 113 (2009) 13023–13028.

[33] M. Yurtsever, E. Yurtsever, A DFT study of polymerization mechanisms of indole, Polymer 43 (2002) 6019–6025.

[34] G. Nie, T. Cai, S. Zhang, Q. Bao, J. Xu, Electrodeposition of poly(indole-5-carboxylic acid) in boron trifluoride diethyl etherate containing additional diethyl ether, Electrochimica Acta 52 (2007) 7097–7106.

[35] G. Kokkinidis, A. Kelaidopoulou, Electrochemical behaviour of nitroindoles: oxidative electropolymerization and reduction of the nitro group of polymerized and non-polymerized 4-nitro and 5-nitroindole, Journal of Electroanalytical Chemistry 414 (1996) 197–208.

[36] D. Billaud, B. Humbert, L. Thevenot, P. Thomas, H. Talbi, Electrochemical properties and Fourier transform-infrared spectroscopic investigations of the redox behaviour of poly(indole-5-carboxylic acid) in $LiClO_4$–acetonitrile solutions, Spectrochimica Acta Part A: Molecular and Biomolecular Spectroscopy 59 (2003) 163–168.

[37] J. G. Mackintosh, A. R. Mount, Electropolymerisation of indole-5-carboxylic acid, Journal of the Chemical Society, Faraday Transactions 90 (1994) 1121–1125.

[38] J. G. Mackintosh, C. R. Redpath, A. C. Jones, P. R. R. Langridge-Smith, A. R. Mount, The electropolymerization and characterization of 5-cyanoindole, Journal of Electroanalytical Chemistry 388 (1995) 179–185.

[39] G. Moretti, G. Quartarone, A. Tassan, A. Zingales, 5-amino- and 5-chloroindole as mild steel corrosion inhibitors in 1 N sulphuric acid, Electrochimica Acta 41 (1996) 1971–1980.

[40] H. Talbi, D. Billaud, Oxidative electropolymerization of 5-nitroindole, Synthetic Metals 97 (1998) 239–244.

[41] M. Skompska, A. Tarajko-Wazny, Electrochemical quartz crystal microbalance studies of polymerization and redox process of poly(1,8-diaminocarbazole) in protic and aprotic solutions, Electrochimica Acta 56 (2011) 3494–3499.

[42] E. H. Rodd, Chemistry of Carbon Compounds: A Modern Comprehensive Treatise, Elsevier Pub. Co. Amsterdam, New York, 1957.

[43] B. B. Berkes, G. Inzelt, E. Vass, Electrochemical nanogravimetric study of the adsorption of 4-aminoindole and the surface layer formed by electrooxidation in aqueous acid media, Electrochimica Acta 96 (2013) 51–60.

Part VI

APPENDIX

ABSTRACT

The research problems described in the dissertation are connected through the use of the electrochemical quartz crystal nanobalance (EQCN). Adsorption, underpotential deposition (UPD) and film formation processes were investigated with its help. These phenomena are discussed in the dissertation in three separate chapters.

In the 3rd part of the work we show how the simultaneous acquisition of electrochemical impedance spectroscopy (EIS) and gravimetric data in cyclic electrode potential scans was used to characterize nonstationary UPD of atomic layers of Ag on Au and Cu on Pt. Both EIS and EQCN data sets complemented each other in the elucidation of interface models and the investigation of different aspects of the interfacial dynamics. EIS-EQCN provided an opportunity to monitor coadsorption and competitive adsorption of anions during the Ag and Cu UPD using *i*) the electrode mass change, *ii*) adsorption capacitances, and *iii*) double-layer capacitances. Kinetic information is available in the EIS-EQCN through the charge transfer resistances and apparent rate coefficients. The EIS-EQCN appeared to be a promising tool for an improved characterization and understanding of nonstationary electrochemical interfaces.

In the 4th part the influence of caesium and sodium cations on the electrochemical behaviour of platinum in sulfuric acid media is described. First an unusual potential dependence of the quartz crystal frequency response in the presence of Cs^+ ions is reported. Further studies with the help of EIS, cyclic voltammetry and EQCN were carried out *i*) to elucidate the models of the interface between polycrystalline Pt and the electrolytes in a wide range of electrode potentials and, *ii*) to resolve contributions originating from adsorbed *H, (bi)sulfate, *OH, and *O as well as the cations to the overall interface status. Using impedance analysis it was possible to separate at least two adsorption processes: (bi)sulfate and hydrogen adsorption. The nanogravimetry additionally suggests specific adsorption of Cs^+ at Pt surface.

Finally the 5th part discusses the adsorption and electropolymerization of indole and 4-aminoindole at different electrodes in acid media. It was found that a spontaneous deposition of an electrochemically active layer occurs for both molecules at oxidised platinum which is accelerated in the presence of oxygen, while no such effect was observed at gold. Electrooxidation of 4-aminoindole by potential cycling up to 0.6 V leads to the formation of multilayer films at both Pt and Au electrodes. The electrogravimetric responses of these polymeric films are similar to those of the spontaneously formed adsorbed multilayer. Electropolymerization of indole is much slower, even at higher positive potentials. The charge compensation reactions differ for the two types of polymer as well. In case of polyindole the ingress and egress of anions while in case of poly(4-aminoindole) most probably partial deprotonation of the film maintains the electroneutrality. These features are readily distinguishable with the EQCN.

ÖSSZEFOGLALÁS

A dolgozatban tárgyalt kutatási témaköröket az elektrokémiai kvarckristály nanomérleg (EQCN) használata köti össze. Segítségével adszorpciós, előleválási (UPD) és filmképződési folyamatokat vizsgáltunk. Ezeket a jelenségeket három külön fejezetben tárgyaljuk.

A harmadik fejezetben bemutatjuk, miként alkalmaztuk egyidejűleg, egy potenciálcikluson belül az elektrokémiai impedanciaspektroszkópiával (EIS) kapcsolt nanogravimetriát nemstacionárius előleválási folyamatok tanulmányozására. Ilyen folyamatok az ezüst előleválása arany és a réz előleválása platina felületeken. A két technika jól kiegészítette egymást a határfelületi folyamatok modellezése és feltérképezése terén. A kapcsolt EIS-EQCN módszer lehetőséget biztosított anionok egyidejű és kompetitív adszorpciójának tanulmányozására *i*) az elektród tömegváltozásának nyomonkövetése, *ii*) az adszorpciós kapacitások és *iii*) a kettősréteg kapacitás meghatározása révén. A folyamatok kinetikájáról a töltésátlépési ellenállás és a közvetve meghatározható sebességi állandók biztosítanak információt. A kapcsolt EIS-EQCN módszer igéretesnek bizonyult a nemstacionárius elektromémiai folyamatok mélyebb megértésében.

A negyedik fejezetben a cézium és nátrium ionok kénsavas közegben való, platina elektródokra gyakorolt hatását mutatjuk be. Először a cézium ionok okozta, a rendszer által demonstrált szokatlan frekvenciaválaszról lesz szó. Majd a folyamat megértése érdekében tett további vizsgálatokról, melyhez az (EIS), ciklikus voltammetria és EQCN technikákat használtuk. Célunk volt *i*) a platina elektród | elektrolit határfelületre javasolt modelleink tanulmányozása egy széles potenciáltartományban és *ii*) az adszorbeált *H, (bi)szulfát, *OH, *O specieszek valamint a kationok határfelületen betöltött szerepének felkutatása, ezek járulékainak megfejtése. Az impedancia analízis segítségével kétféle adszorpciós folyamatot különítettünk el: a (bi)szulfátét és a hidrogénét. A nanogravimetriás mérések pedig a cézium ionok specifikus adszorpciójának meglétét támasztják alá.

Végül, az ötödik fejezetben az indol és 4-aminoindol molekulák savas közegben való, különböző elektródokon történő adszorpciós viselkedését és elektropolimerizációját mutatjuk be. Azt találtuk, hogy mindkét molekula képes oxidált platina elektródokon való spontán rétegképzésre, melyet az oldatban jelenlévő oxigén még inkább elősegít. Ugyanez a jelenség arany elektródokon nem figyelhető meg. 4-aminoindol potenciálciklizálással, 0.6 V-ig történő elektrooxidációja többrétegű film képződéséhez vezet mind arany, mind platina elektródokon. A képződött réteg tulajdonságai nagyban hasonlítanak az adszorpcióval, spontán levált réteg tulajdonságaihoz. Az indol elektropolimerizációja sokkal lassabb, még nagyobb pozitív potenciálokon is. A töltés kompenzációs folyamatok a kétféle polimer esetén különböznek. Poliindol filmben anionok ki-és bevándorlása, míg poli(4-aminoindol) filmben legvalószínűbben részleges deprotonálódás által valósul meg az elektroneutralitás. Ezek a különböző módok jól elkülöníthetőek az EQCN-nel.

PUBLICATIONS

RESEARCH ARTICLES

1. B. B. Berkes, G. Inzelt, Generation and electrochemical nanogravimetric response of the third anodic hydrogen peak on a platinum electrode in sulfuric acid media, *Journal of Solid State Electrochemistry* – submitted

2. B. B. Berkes, Á. Nemes, C. E. Moore, F. Szabó, G. Inzelt, Electrochemical nanogravimetric study of the electropolymerization of 6-aminoindole and the redox transformations of the polymer formed in aqueous media, *Journal of Solid State Electrochemistry* – submitted

3. B. B. Berkes, G. Inzelt, Electrochemical nanogravimetric studies on the electropolymerization of indole and on polyindole, *Electrochimica Acta* – submitted

4. B. B. Berkes, G. Inzelt, E. Vass, Electrochemical nanogravimetric study of the adsorption of 4-aminoindole and the surface layer formed by electrooxidation in aqueous acid media, *Electrochimica Acta* **96** (2013) 51-60.

5. B. B. Berkes, The 2012 Joseph W. Richards summer research fellowship - Summary report Catalytic activity for ORR of a platinum-free electrocatalyst in phosphoric acid, *The Electrochemical Society Interface* **21** (2012) 93-94.

6. B. B. Berkes, J. B. Henry, M. H. Huang, A. S. Bondarenko, Electrochemical Characterisation of Copper Thin-Film Formation on Polycrystalline Platinum, *ChemPhysChem* **13** (2012) 3210-3217.

7. B. B. Berkes, G. Inzelt, W. Schuhmann, A. S. Bondarenko, Influence of Cs^+ and Na^+ on Specific Adsorption of *OH, *O, and *H at Platinum in Acidic Sulfuric Media, *Journal of Physical Chemistry C* **116** (2012) 10995-11003.

8. M. H. Huang, J. B. Henry, B. B. Berkes, A. Maljusch, W. Schuhmann, A. S. Bondarenko, Towards a detailed in situ characterization of non-stationary electrocatalytic systems, *Analyst* **137** (2012) 631-640.

9. Á. Kriston, B. B. Berkes, P. Simon, G. Inzelt, K. Dobos, Á. Nemes, Unusual surface mass changes in the course of the oxygen reduction reaction on platinum and their explanation by using a kinetic model, *Journal of Solid State Electrochemistry* **16** (2012) 1723-1732.

10. B. B. Berkes, A. Maljusch, A. S. Bondarenko, W. Schuhmann, Simultaneous acquisition of impedance and gravimetric data in a cyclic potential scan for the characterization of non-stationary electrode/electrolyte interfaces, *Journal of Physical Chemistry C* **115** (2011) 9122-9130.

11. G. Inzelt, B. B. Berkes, Á. Kriston, Electrochemical nanogravimetric studies of adsorption, deposition and dissolution processes occurring at platinum electrodes in acid media, *Pure and Applied Chemistry* **83** (2011) 269-279.

12. G. Inzelt, B. B. Berkes, Á. Kriston, A. Székely, Electrochemical nanogravimetric studies of platinum in acid media, *Journal of Solid State Electrochemistry* **15** (2011) 901-915.

13. G. Inzelt, B. B. Berkes, Á. Kriston, Temperature dependence of two types of dissolution of platinum in acid media. An electrochemical nanogravimetric study, *Electrochimica Acta* **55** (2010) 4742-4749.

14. G. Inzelt, B. B. Berkes, Á. Kriston, Two Types Dissolution of Platinum in Acid Media. An Electrochemical Nanogravimetric Study, *ECS Transactions* **25** (2010) 137-156.

15. B. B. Berkes, A. Székely, G. Inzelt, Effect of Cs^+ ions on the electrochemical nanogravimetric response of platinum electrode in acid media, *Electrochemistry Communications* **12** (2010) 1095-1098.

BOOK CHAPTER

B1. M. Huang, J. B. Henry, B. B. Berkes, A. Maljusch, W. Schuhmann, A. S. Bondarenko, Simultaneous acquisition of impedance and gravimetric data for the characterization of the electrode | electrolyte interfaces, in: Lecture Notes on Impedance Spectroscopy. Measurement, Modeling and Applications, volume 3, (Ed.) O. Kanoun, CRC Press - Taylor and Francis Group, London, 2012, pp. 35-41.

PRESENTATIONS, CONFERENCE PARTICIPATIONS

E1. G. Inzelt, B. B. Berkes, Nanogravimetric Study on the Adsorption and Electropolymerization of Indole and Indole Derivatives and on the Redox Behavior of Polyindoles, *63rd ISE Meeting*, Prague, Czech Republic, August 19-24, 2012

E2. B. B. Berkes, G. Inzelt, Study of Formation and Redox Behaviour of Polyindoles by Electrochemical Quartz Crystal Microbalance, *International Workshop on the Electrochemistry of Electroactive Materials WEEM – 2012*, Hódmezővásárhely, Hungary, June 3-8, 2012

E3. B. B. Berkes, G. Inzelt, Adsorption and electropolymerization of indole and indole derivatives, *Third Regional Symposium on Electrochemistry*, Bucharest, Romania, May 13-17, 2012

E4. B. B. Berkes, G. Inzelt, Nanogravimetric Studies of Formation and Redox Behaviour of Polyindole and Its Derivatives, *International Workshop: Polymers at Electrodes A Quarter of a Century later*, Bad Schandau, Germany, November 6-9, 2011

E5. B. B. Berkes, A. Maljusch, A. S. Bondarenko, W. Schuhmann, Simultaneous acquisition of impedance and gravimetric data in a cylic potential scan. Characterization of UPD of Ag on Au and Cu on Pt, *EIRELEC 2011*, Adare, Ireland, May 16-18, 2011

E6. B. B. Berkes, Á. Kriston, P. Simon, G. Inzelt, Investigation of oxygen reduction reaction on Pt by using electrochemical quartz crystal nanobalance and numerical simulation, *Second Regional Symposium on Electrochemistry*, Belgrade, Serbia, June 6-10, 2010

E7. G. Inzelt, B. B. Berkes, Á. Kriston, Electrochemical nanogravimetric studies of platinum in acid and neutral media, *Second Regional Symposium on Electrochemistry*, Belgrade, Serbia, June 6-10, 2010

E8. B. B. Berkes, G. Inzelt, Á. Kriston, Electrochemical nanogravimetric studies of platinum in acid media, *61th ISE Meeting*, Nice, France, September 26-October 1, 2010

E9. G. Inzelt, B. B. Berkes, Á. Kriston, Two types of platinum dissolution in acid media, *216th ECS Meeting*, Vienna, Austria, October 4-9, 2009

POSTERS

P1. B. B. Berkes, A. Maljusch, A. S. Bondarenko, W. Schuhmann, Simultaneous acquisition of impedance and gravimetric data in a cyclic potential scan for the characterization of non-stationary electrode | electrolyte interfaces, *62th ISE Meeting*, Niigata, Japan, September 11-16, 2011, s13-P-015

P2. Á. Kriston, T. Szabó, Á. Nemes, S. Vesztergom, B. B. Berkes, T. Horváth, N. Molnár, K. Dobos, The application of multi-level simulation during the development of a hydrogen fuel cell vehicle, *61th ISE Meeting*, Nice, France, September 26-October 1, 2010, s15-P-030

P3. Á. Kriston, B. B. Berkes, P. Simon, G. Inzelt, Investigation of oxygen reduction reaction on Pt by using electrochemical quartz crystal nanobalance and numerical simulation, *61th ISE Meeting*, Nice, France, September 26-October 1, 2010, s15-P-005

INFORMATIVE

I1. B. B. Berkes, Tüzelőanyag-cellák (Hungarian), *Természet Világa*, **143** (2012) 63-65.

I2. Á. Kriston, T. Szabó, B. B. Berkes, Á. Nemes, Városi közlekedés hidrogénalapon, (Hungarian), *Környezetvédelem*, **17** (2010) 16-17.

COLOPHON

This document was typeset using the LaTeX document preparation system and is based on the typographical look-and-feel `classicthesis` developed by André Miede. The style was inspired by Robert Bringhurst's seminal book on typography *"The Elements of Typographic Style"*.

DECLARATION

I, Balázs B. Berkes, hereby certify that this thesis, entitled *Investigation of adsorption, underpotential deposition and film formation processes with the electrochemical quartz crystal nanobalance technique* and is approximately 43,000 words in length, has been compiled by me, that it is the record of work carried out by me and that it has not been submitted in any previous application for a higher degree.

The research activity on which the thesis is based was carried out

— at the Eötvös Loránd University, Budapest, Hungary during the period of 2010-2013, under the supervision of Professor György Inzelt, and

— at the Ruhr University, Bochum, Germany during the period 1 September 2010 – 1 February 2011 and 1 August 2011 – 15 September 2011, under the supervision of Dr. Aliaksandr Bandarenka and Professor Wolfgang Schuhmann.

The thesis was mainly compiled from the already published results. I undertake that all the material presented for examination is my own work and has not been written for me, in whole or in part, by any other person. I also undertake that any quotation or paraphrase from the published or unpublished work of another person has been clearly attributed in the work which I present for examination.

Budapest, May 2013

Balázs B. Berkes
May 23, 2013